Quarterly Reviews of Biophysics **38**, 2 (2005), pp. 167–219. © 2006 Cambridge University Press
doi:10.1017/S0033583506004161 Printed in the United Kingdom
First published online 4 May 2006

NMR structures of paramagnetic metalloproteins

Fabio Arnesano, Lucia Banci* and Mario Piccioli

Magnetic Resonance Center (CERM) and Department of Chemistry, University of Florence, Italy

Abstract. Metalloproteins represent a large share of the proteome and many of them contain paramagnetic metal ions. The knowledge, at atomic resolution, of their structure in solution is important to understand processes in which they are involved, such as electron transfer mechanisms, enzymatic reactions, metal homeostasis and metal trafficking, as well as interactions with their partners. Formerly considered as unfeasible, the first structure in solution by nuclear magnetic resonance (NMR) of a paramagnetic protein was obtained in 1994. Methodological and instrumental advancements pursued over the last decade are such that NMR structure of paramagnetic proteins may be now routinely obtained. We focus here on approaches and problems related to the structure determination of paramagnetic proteins in solution through NMR spectroscopy. After a survey of the background theory, we show how the effects produced by the presence of a paramagnetic metal ion on the NMR parameters, which are in many cases deleterious for the detection of NMR spectra, can be overcome and turned into an additional source of structural restraints. We also briefly address features and perspectives given by the use of ^{13}C-detected protonless NMR spectroscopy for proteins in solution. The structural information obtained through the exploitation of a paramagnetic center are discussed for some Cu^{2+}-binding proteins and for Ca^{2+}-binding proteins, where the replacement of a diamagnetic metal ion with suitable paramagnetic metal ions suggests novel approaches to the structural characterization of proteins containing diamagnetic and NMR-silent metal ions.

1. Introduction 168
- 1.1 Genomic annotation of metalloproteins 168
- 1.2 Why NMR structures? 168
- 1.3 Why paramagnetic metalloproteins? 169

2. General theory 170
- 2.1 Nuclear and electron spins 170
- 2.2 Hyperfine coupling 171
- 2.3 The effect of the hyperfine coupling on the NMR shift: the hyperfine shift 173
- 2.4 The effect of the hyperfine coupling on nuclear relaxation 174
- 2.5 Interplay between electron spin properties and features of the NMR spectra 178

3. Paramagnetism-based structural restraints 180
- 3.1 Contact shifts and relaxation rates as restraints 181
- 3.2 Locating the metal ion within the protein frame: pseudocontact shifts 184
- 3.3 Cross-correlation rates 186

* Address for correspondence: Professor Lucia Banci, Magnetic Resonance Center (CERM), University of Florence, Via L. Sacconi 6, 50019 Sesto Fiorentino, Italy.
Tel.: +39 055 4574263; Fax: +39 055 4574271; E-mail: banci@cerm.unifi.it

https://doi.org/10.1017/S0033583506004161 Published online by Cambridge University Press

3.4 Residual dipolar couplings 188
3.5 Interplay between different restraints 190

4. NMR without ^{1}H detection 191
4.1 The protocol for ^{13}C-detected protonless assignment of backbone and side-chains 194
4.2 Protonless heteronuclear NMR experiments tailored to paramagnetic systems 196

5. The use of lanthanides as paramagnetic probes 198

6. The case of Cu(II) proteins 202

7. Perspectives 208

8. Acknowledgments 209

9. References 209

1. Introduction

1.1 Genomic annotation of metalloproteins

The genomic revolution has dramatically changed the perspective of structural biology and the strategies to determine the structure of macromolecules. The massive number of proteins encoded into the genome of the various organisms requires different strategies for their characterization. High throughput approaches are needed, and indeed they have been developed, for protein cloning and expression, as well as for crystallization and structure determination by X-ray and by nuclear magnetic resonance (NMR). As a result of these efforts, a continuously increasing number of proteins is produced and structurally characterized. It is, however, evident that the genome sequences do not contain *per se* information on the metal-binding capabilities of proteins encoded by the genome. This type of information is essential for any project aimed at characterizing the products of the genomes, in order to work on proteins which are in a physiologically relevant state. Metalloproteins represent a large share of the genome products and their study is mandatory to have a complete characterization of several fundamental processes of life. In the various heterologous expression systems used for efficiently cloning and expressing proteins, they are produced in several cases without metal ions or bound to spurious ones. Therefore, this post-traslational modification needs to be defined prior to any structural and functional characterization. For this purpose, bioinformatic tools, which analyze a complete genome with respect to the presence of known metal-binding patterns or of domains known to bind a given metal ion, are being developed in order to evaluate the metal binding capability of the genome products (Degtyarenko *et al.* 1999; Degtyarenko, 2000; Andreini *et al.* 2004).

1.2 Why NMR structures?

The use of NMR for structure determination in solution is now a well established method, and the number of solution structures deposited in the Protein Data Bank (PDB) is annually increasing, from the first solution structure solved by Kurt Wuthrich in 1985 to now, in absolute number (4280 in 2004) and also as share of the total number of structures (15% in 2004).

https://doi.org/10.1017/S0033583506004161 Published online by Cambridge University Press

Structure determination through NMR spectroscopy has several advantages with respect to X-ray, even if in general it is more time consuming and has severe limitations in the size of the proteins and in resolution that can be afforded:

- NMR is able to provide both dynamic and structural information on proteins in a variety of different states in solution at atomic resolution;
- NMR is unique in characterizing internal mobility at atomic level over a large time range, as well as hydration properties, solvent accessibility, and exchange processes;
- NMR has the power to study transient complexes and weak protein–protein and protein–ligand interactions;
- NMR has the power to characterize proteins with some level of internal disorder or in non-completely folded states, to probe residual structure, and to study low-molecular-weight aggregates. This aspect is particularly relevant as it is becoming more and more evident that a relatively large number of proteins exist *in vivo* in partially unfolded states. This property allows the proteins a facile interaction with their partners, and also makes them more prone to aggregation.

The methods for solution structure determination are well standardized, and spectroscopic (e.g. Transverse Relaxation Optimized Spectroscopy (TROSY)-type experiments; Pervushin *et al.* 1997; Pervushin, 2000) and technological (e.g. cryo/cold probes; Kovacs *et al.* 2005) advances, coupled with sophisticated isotopic labeling strategies (Fiaux *et al.* 2002; Pervushin & Eletsky, 2003; Tugarinov *et al.* 2004, 2005; Schubert *et al.* 2005; Bertini *et al.* 2005b), are continuously expanding the limits of NMR applicability as a structural tool, now affording the solution structure determination of proteins with molecular weights above 50 000 (Kay, 2005) and of samples with protein concentrations as low as 100–200 μM. Also computational tools are being developed to automate the tedious steps of spectral assignment and structural calculations (Herrmann *et al.* 2002b; Hyberts & Wagner, 2003; Malmodin *et al.* 2003; Slupsky *et al.* 2003; Ried *et al.* 2004; Altieri & Byrd, 2004; Atreya & Szyperski, 2004; Guntert, 2004; Jung & Zweckstetter, 2004; Bailey-Kellogg *et al.* 2005; Eghbalnia *et al.* 2005; Fossi *et al.* 2005; Grishaev & Llinas, 2005; Vranken *et al.* 2005). However, problems and challenges need to be overcome when dealing with metalloproteins, i.e. proteins binding a metal or a metal-containing cofactor. Indeed, the metal ion, which in most cases has no NMR accessible nucleus, constitutes a point of discontinuity in the network of inter-nuclear dipolar and scalar couplings (which provide distance and angle restraints for structure calculations). Even more severe effects need to be taken into account when the metal ion is paramagnetic, i.e. it contains one or more unpaired electrons.

1.3 Why paramagnetic metalloproteins?

Metalloproteins represent a large share of the proteome, being predicted to be ∼30% of the total in humans (Chance *et al.* 2004; Hasnain, 2004; Szupnar, 2004), but, despite their high number and their involvement in a large variety of processes essential for life, they are not characterized as extensively as the other proteins. Furthermore, some of their structures do not contain the native, or any, metal ion, or contain spurious metal ions instead, and therefore they do not represent the active form of the protein.

Among metalloproteins, a large number of them contain paramagnetic metal ions which possess unpaired electrons, or metal ions which cycle between different oxidation states, one of which is paramagnetic. The presence of a paramagnetic center not only affects the NMR

https://doi.org/10.1017/S0033583506004161 Published online by Cambridge University Press

parameters and might create problems in signal detection, but it can also dramatically reduce the intensity of Nuclear Overhauser Effects (NOEs) and the efficiency in the transfer of scalar couplings in homonuclear and heteronuclear experiments, thus making spectral assignment and determination of structural restraints not possible through standard approaches. These problems can sometimes be overcome or reduced with suitable, tailored experiments and the effects induced by a paramagnetic center on the NMR parameters can even be turned into precious sources of information on its surroundings, thus compensating for the lack or reduction of the classical structural restraints. Therefore, NMR is particularly suited for structure determination of systems containing metal ions which may undergo redox reactions under irradiation with X-ray, and it can also be efficiently used to characterize oxidation state-dependent structural and dynamical changes.

In the present review we focus on the problems and the approaches developed for determining the solution structure of paramagnetic metalloproteins by NMR. We briefly review the effects produced by a paramagnetic metal ion on the NMR spectra and how these effects, in many cases deleterious for the detection of the NMR signals, can be overcome and turned into advantages. In this way, high resolution structures can be obtained, even in the surrounding of the paramagnetic center.

The power of a suitable paramagnetic ion in providing structural information and the expertise acquired to tackle problems associated to the use of paramagnetic metal ions in NMR are such that paramagnetic centers are nowadays purposely built in the protein frame either by replacing native diamagnetic metal ions with vicariant paramagnetic ions or by attaching paramagnetic probes. A paramagnetic probe with favorable electronic properties can be used to 'enlighten' the protein region of interest. Indeed, paramagnetism-based restraints are very efficient for mapping the binding sites and the interactions with other proteins or small molecules.

The structural information obtained through exploitation of the effects of a paramagnetic center on the NMR resonances are presented and discussed for two classes of proteins: (i) the copper(II)-binding proteins, which constitute an example of paramagnetic proteins containing a metal ion which is not favorable for NMR spectroscopy; (ii) the lanthanide-substituted calcium-binding proteins, which contain very effective paramagnetic probes for NMR spectroscopy. The latter systems summarize many aspects of the most recent advances in the field and suggest novel approaches to the structural characterization of large proteins and protein complexes and of proteins containing diamagnetic and NMR-silent metal ions.

2. General theory

2.1 Nuclear and electron spins

Paramagnetic molecules are characterized by the presence of one or more unpaired electrons, which possess a spin angular momentum $\hbar\mathbf{S}$ where $\mathbf{S}$ is the electron spin angular momentum vector and $\hbar$ is the Planck's constant, and a magnetic moment whose module is given by $\mu_S = -\hbar\gamma_I S = -g_e\mu_B S$, where S is electron spin quantum number, g_e is the free electron g factor, equal to 2·0023, and μ_B is the Bohr magneton. Also magnetic nuclei are characterized by a nuclear spin angular momentum $\hbar\mathbf{I}$, where $\mathbf{I}$ is the nuclear spin angular momentum vector, and by a magnetic moment whose module is given by $\mu_I = \hbar\gamma_I I$, where I is the nuclear spin quantum number (Abragam, 1961). The ratio γ, between the magnetic moment and the angular

https://doi.org/10.1017/S0033583506004161 Published online by Cambridge University Press

momentum is called the magnetogyric ratio. The electron magnetogyric ratio $\gamma_S = g_e\mu_B/\hbar$ is $\sim$658 times larger than that of a proton, which is the stable nucleus with the largest γ_I, and with opposite sign (Koenig *et al.* 1952).

The properties of spins and their interaction with an external magnetic field $\mathbf{B_0}$, as well as with other spins, are conveniently described using the spin Hamiltonian formalism, which operates on spin wave functions only (Stevens, 1976). The electron Zeeman operator, describing the interaction between the electron spin and the magnetic moment is:

$$\widehat{\mathcal{H}} = g_e\mu_B\mathbf{B_0}\cdot\widehat{\mathbf{S}}. \tag{2.1}$$

The effect of the magnetic field is that of splitting the electron spin levels into $2S+1$ energy levels characterized by M_S values ranging from $-S$ to $+S$ (Abragam & Bleaney, 1970). If the spin quantum number S is 1/2, the two levels have energy equal to $-1/2g_e\mu_B$ ($M_S = -1/2$) and $+1/2g_e\mu_B$ ($M_S = 1/2$), then differing in energy by $g_e\mu_B\mathbf{B_0}$. An ensemble of spins in a magnetic field thus possesses a Boltzmann distribution between the two energy levels and, therefore, an induced magnetic moment along $\mathbf{B_0}$, $\langle\mu\rangle$, which is the weighted sum of all the individual magnetic moments of each electron in the ensemble.

At variance with nuclei, electrons are also associated with an orbital function which describes the electron distribution in space. Orbitals are characterized by an *orbital angular momentum* $\mathbf{L}$ and a magnetic moment μ_L. The orbital contribution makes the overall electron magnetic moment anisotropic, i.e. it changes value when changing the orientation of the molecule, containing the unpaired electron, with respect to $\mathbf{B_0}$, at variance with the nuclear magnetic moment which is intrinsically isotropic (Griffith, 1961). As the spin Hamiltonian can operate only on spin wave functions and not on the orbital ones, the orbital contribution to the electron magnetic moment is parameterized by not using the simple g_e constant but a $\mathbf{g}$ tensor to describe the electron spin properties in the various directions of space. Therefore, the Zeeman term in the spin Hamiltonian becomes:

$$\widehat{\mathcal{H}} = \mu_B\mathbf{B_0}\cdot\mathbf{g}\cdot\widehat{\mathbf{S}}. \tag{2.2}$$

The *anisotropy* of the electron spin magnetic moment has profound effects on the behavior of the electrons and on the effects they produce on the nuclei coupled with them. Unpaired electrons generate an additional magnetic field, which acts on nuclear spins and, therefore, changes the effective magnetic field sensed by the nuclei and their resonance frequency; it can also fluctuate and therefore contribute to relaxation of the nuclear spins. Therefore, unpaired electrons dramatically affect the NMR parameters of the nuclei they are coupled with (Bertini *et al.* 2001f).

2.2 Hyperfine coupling

The electron magnetic moment μ_S can interact with the magnetic moment μ_I of a nucleus. This coupling is called hyperfine coupling and occurs through two types of interactions: one is scalar and is also called contact coupling, the other is dipolar and occurs through space (Abragam, 1961). Within the spin Hamiltonian formalism, the hyperfine coupling is described by:

$$\widehat{\mathcal{H}} = \widehat{\mathbf{I}}\cdot\mathbf{A}\cdot\widehat{\mathbf{S}}, \tag{2.3}$$

where $\mathbf{A}$ is the hyperfine coupling tensor.

https://doi.org/10.1017/S0033583506004161 Published online by Cambridge University Press

The contact interaction originates from the fraction of unpaired electron which sits on the resonating nucleus (McConnell & Chesnut, 1958). Unpaired electrons in molecules are not localized in a single point but, in general, are delocalized in space. This determines a fraction of electron spin in every point in space where the molecular orbital (MO) containing the unpaired electron has non-zero value. This fraction is called spin density, ρ, which is proportional to the square of the value of the MO wave function at that point. The contact coupling occurs between the nuclear spin and the electron spin density on the nucleus. Unpaired spin density gets in contact with nuclei only through s-type orbitals, because they are the only ones with a finite electron density at the nucleus (Fermi, 1930). Unpaired electrons can also polarize paired electrons, present in another MO, according to Hund's rule, in such a way that the two paired electrons are no longer evenly distributed in the MO. Each of them preferentially tends to occupy different regions of their MO, as the electron with the spin parallel to the spin of the unpaired electron has a slight preference to occupy regions of its MO close to the unpaired electron, thus determining an unbalanced distribution of the two paired electrons in the MO, and consequently different spin densities in various regions of the space. This process is called spin polarization.

Spin density originating from direct delocalization and from spin polarization sum up to give the total spin density on that nucleus. This can be present either as the unpaired electron is an s-type orbital or its MO has some s-orbital component (direct spin delocalization), or the unpaired electron spin-polarizes the electrons of an s orbital (spin polarization).

Transfer of electron spin density from the paramagnetic center to the resonating nucleus is somehow related to chemical bonds. Therefore, the electron–nucleus contact interaction is analogous to the nucleus–nucleus *J*-coupling (or scalar) interaction (Karplus, 1959), and depends on orbital overlap, and consequently on the dihedral angles formed by chemical bonds.

The spin Hamiltonian term for the contact interaction is:

$$\widehat{\mathcal{H}} = A_c \widehat{\mathbf{I}} \cdot \widehat{\mathbf{S}}. \tag{2.4}$$

The contact coupling constant, A_c, is related to the total unpaired spin density at the nucleus, ρ, through the following equation (Fermi, 1930):

$$A_c = \frac{\mu_0}{3S} \hbar \gamma_{I} g_e \mu_B \rho, \tag{2.5}$$

where μ_0 is the magnetic permeability of the vacuum and the other symbols have been already defined.

Nuclear spins can also interact with unpaired electrons through dipolar coupling. This interaction occurs through space, between the magnetic moment of the nuclear spin and the magnetic moment of the electron spin. In principle, the magnetic nucleus does not see an unpaired electron as localized in a single point, but as spin density distributed throughout the space (Abragam, 1961). This spin density distribution is a relatively small fraction in respect to that residing on the nucleus of the paramagnetic ion and it is difficult to know its distribution with sufficient accuracy. Therefore, as a first approximation, it can be considered as localized on the metal nucleus (metal-centered approximation) or at least distributed within a cage formed by the ligand donor atoms (ligand-centered). As delocalized spin density is small, this latter contribution has only a local effect, i.e. for nuclei at a very short distance from the metal ion. Within the metal-centered approximation the dipolar interaction energy, in an external magnetic

https://doi.org/10.1017/S0033583506004161 Published online by Cambridge University Press

field along z, is:

$$E = \frac{\mu_{I_z}\mu_{S_z}}{r^3}(3\cos^2\theta - 1), \tag{2.6}$$

where r is the metal–nucleus distance, assuming the electron spin can be treated as a point dipole, and θ is the angle between the metal–nucleus vector and the magnetic field direction (Kurland & McGarvey, 1970).

As outlined previously, the electron magnetic moment is not isotropic because of the orbital contribution, and therefore the dipolar interaction does not average to zero upon rotation, but its average value depends on the anisotropic orbital contribution to the electron magnetic moment. Likewise, the intensity of the induced magnetic moment along $\mathbf{B_0}$ depends on the orientation of the molecule and is, therefore, anisotropic. The induced magnetic moment per unit magnetic field (and divided by μ_0), called magnetic susceptibility, χ, is represented by a tensor. The orbital contribution to μ_S causes the induced magnetic moment and magnetic susceptibility to differ from their spin-only values and to be anisotropic (McConnell & Robertson, 1958).

2.3 The effect of the hyperfine coupling on the NMR shift: the hyperfine shift

The presence of unpaired electrons in the surrounding of a nucleus, either as spin density on the nucleus itself or as a dipole close to it, produces an additional magnetic field, thus determining the effective magnetic field sensed by the nuclear spin and its resonating frequency.

The difference in chemical shift for a nucleus in a paramagnetic molecule with respect to that it would have in the corresponding diamagnetic molecule is called the hyperfine shift. It is the sum of two contributions which originate from the two mechanisms of coupling (Abragam, 1961). The contact shift contribution, δ^{con}, is given by (McConnell & Chesnut, 1958; Kurland & McGarvey, 1970):

$$\delta^{\mathrm{con}} = -\frac{A_{\mathrm{c}}}{\hbar\gamma_I \mathbf{B}_0}\langle S_z\rangle = \frac{A_{\mathrm{c}}}{\hbar}\frac{g_e\mu_{\mathrm{B}}S(S+1)}{3\gamma_I kT}, \tag{2.7}$$

where $\langle S_z\rangle$ is the expectation value of the S_z operator of the S multiplet, and is related to the different population of the M_S levels, k is Boltzmann's constant, and T the absolute temperature. This equation is valid for a single electron in an orbital which is well separated from any other excited level. In the absence of strong spin-orbit coupling effects, it holds also in the case of multiple unpaired electrons in different molecular orbitals, A_{c} being the average of the contact coupling constant of each electron.

A general treatment must consider the presence of more than one electron in orbitals close in energy. This electronic level distribution gives rise, through spin-orbit coupling, to zero field splitting of the electron spin levels. Spin-orbit coupling mixes the various orbitals so that electrons reside in orbitals which are linear combinations of all orbitals available. In this case, all thermally populated electronic states must be considered. A complete description of the contact shift is available in the literature (Bertini & Luchinat, 1996; Bertini *et al.* 2001f).

As the contact shift is due to the scalar interaction between the electron and the nuclear spin, it has been traditionally treated as an isotropic interaction. Actually, due to electron orbital

https://doi.org/10.1017/S0033583506004161 Published online by Cambridge University Press

contributions, the contact shift depends on the orientation of the molecule in the magnetic field, if $\mathbf{g}$ is anisotropic (Kurland & McGarvey, 1970). However, in solution, it averages to a mean value upon rotation.

The value of δ^{con}, in most of the cases, decreases as the number of chemical bonds connecting the metal ion and the nucleus increases, not counting π bonds which allow electron delocalization. The presence of π bonds contributes to spin polarization. In general, electron spin delocalization patterns are not easily predicted. Information can be obtained from other techniques, e.g. Electron Paramagnetic Resonance (EPR) and X-ray Absorption Spectroscopy (XAS). When direct overlap effects are operative between orbitals containing unpaired spin density and other MOs, A_c can be a function of some dihedral angles involving the paramagnetic metal ion to its nuclear environment (Karplus, 1959). This concept has been translated into structural restraints that help in defining the coordination environment of the metal in paramagnetic metalloproteins and will be discussed in Section 3.

The contribution to the shift due to dipolar coupling is called pseudocontact shift, δ^{pc} which depends on the anisotropy of the magnetic susceptibility tensor, i.e. on what does not average upon rapid rotation (McConnell & Robertson, 1958; Kurland & McGarvey, 1970):

$$\begin{aligned}\delta^{pc} &= \frac{1}{24\pi}\frac{1}{r^3}\{[2\chi_{zz}-(\chi_{xx}+\chi_{yy})](3\cos^2\theta-1)+3(\chi_{xx}-\chi_{yy})\sin^2\theta\cos 2\Omega\} \\ &= \frac{1}{24\pi}\frac{1}{r^3}\{2\Delta\chi_{ax}(3\cos^2\theta-1)+3\Delta\chi_{rh}\sin^2\theta\cos 2\Omega\},\end{aligned} \tag{2.8}$$

where θ and Ω are the polar coordinates of the nucleus in the reference frame of the magnetic susceptibility tensor χ, centered on the metal. δ^{pc} does not depend on the total susceptibility value (i.e. on the trace of the tensor), but on its axial ($\Delta\chi_{ax}$) and rhombic ($\Delta\chi_{rh}$) anisotropies only. When the structure of the molecule is available, five parameters must be known ($\Delta\chi_{ax}$, $\Delta\chi_{rh}$, and the three Euler angles defining the magnetic susceptibility tensor axes) to obtain the values of δ^{pc}. Conversely, δ^{pc}, when the above parameters are known, provides information on the position of the nuclei within the molecular frame (see later).

It should be noted that both δ^{con} and δ^{pc} values do not depend on the nature of the nuclear spin, as Eq. (2.8) does not contain γ_I, while in Eq. (2.7), γ_I is cancelled by γ_I contained in Eq. (2.5).

2.4 The effect of the hyperfine coupling on nuclear relaxation

Relaxation is the process through which spins re-establish the equilibrium distribution after any perturbation of such distribution. This occurs through spontaneous transitions between spin states, induced by frequencies generated by the randomly fluctuating magnetic fields within the environment of the nucleus, called a lattice. These fluctuating fields can be caused by reorientations of magnetic moments or by changes in their state. These time-dependent phenomena produce a broad range of frequencies (spectral density). When frequencies corresponding to nuclear spin transitions are present, fluctuating magnetic fields induce spin transitions and, therefore, contribute to its relaxation. As the frequencies of the nuclear spin transitions depend on the strength of the external magnetic field, nuclear relaxation rates are field dependent. Nuclear relaxation depends also on the square of the interaction energy between the

https://doi.org/10.1017/S0033583506004161 Published online by Cambridge University Press

nuclear spin and the lattice which generates the effective fluctuating magnetic fields, according to the general relation:

$$R_{1,2} \propto E_{\text{int}}^2 \cdot f(\omega, \tau_c). \tag{2.9}$$

Unpaired electrons contribute to relaxation of nuclear spins at two levels: affecting the interaction energy and the correlation time (Banci *et al.* 1991). Paramagnetic relaxation enhancement is, therefore, proportional to the square of the hyperfine interaction energy. The paramagnetic center can also determine the correlation time τ_c of the mechanism which causes relaxation. Electrons have very efficient mechanisms for relaxation which give rise to very fast electron relaxation rates, much faster than for nuclei, and much faster than what would be expected only on the basis of the larger electron γ (Banci *et al.* 1991). As a general rule, the presence of low-lying excited electronic states induces efficient electron relaxation and therefore short electron correlation times τ_s. Electron relaxation rates (Table 1) can be strongly field dependent, which makes them decrease as the magnetic field increases.

The contact contribution to nuclear relaxation is due to the modulation of the contact coupling, through fluctuations of the electron magnetic field at the nucleus, as a consequence of electron spin relaxation, or, if present, of chemical exchange. Therefore, this contribution is essentially modulated by τ_s and is given by the Bloembergen equations (Bloembergen, 1957):

$$R_1^{\text{con}} = \tfrac{2}{3} S(S+1) \left(\frac{A_c}{\hbar}\right)^2 \frac{\tau_s}{1+\omega_S^2 \tau_s^2}, \tag{2.10}$$

$$R_2^{\text{con}} = \tfrac{1}{3} S(S+1) \left(\frac{A_c}{\hbar}\right)^2 \left(\frac{\tau_s}{1+\omega_S^2 \tau_s^2} + \tau_s\right), \tag{2.11}$$

where ω_S is the electron Larmor frequency. This contribution rarely affects protons, while it has some relevance for nuclei with low γ, for which the dipolar contribution is small, and of residues directly coordinated to the metal ion, for which the A_c value is large.

The paramagnetic dipolar contribution to relaxation is caused by the modulation of the dipole–dipole (DD) coupling between the nuclear and the electron magnetic moments. It is given by the Solomon equations (Solomon, 1955):

$$R_1^{\text{dip}} = \frac{2}{15} \left(\frac{\mu_0}{4\pi}\right)^2 \frac{\gamma_I^2 g_e^2 \mu_B^2 S(S+1)}{r^6} \left[\frac{7\tau_c}{1+\omega_S^2 \tau_c^2} + \frac{3\tau_c}{1+\omega_I^2 \tau_c^2}\right], \tag{2.12}$$

$$R_2^{\text{dip}} = \frac{1}{15} \left(\frac{\mu_0}{4\pi}\right)^2 \frac{\gamma_I^2 g_e^2 \mu_B^2 S(S+1)}{r^6} \left[4\tau_c + \frac{13\tau_c}{1+\omega_S^2 \tau_c^2} + \frac{3\tau_c}{1+\omega_I^2 \tau_c^2}\right]. \tag{2.13}$$

It can be seen that dipolar relaxation, as it depends on the square of the interaction energy, depends on the inverse sixth power of the distance between the electron and the nucleus and is proportional to the square of the electron magnetic moment, which is large. At variance with contact relaxation, molecular tumbling is also a mechanism able to modulate the dipolar interaction as the electron and nuclear spins do not coincide in space. Therefore, τ_c is determined by the fastest process among the three modes of modulation of the hyperfine interaction:

$$\tau_c^{-1}(\text{dip}) = \tau_s^{-1} + \tau_m^{-1} + \tau_r^{-1}, \tag{2.14}$$

https://doi.org/10.1017/S0033583506004161 Published online by Cambridge University Press

https://doi.org/10.1017/S0033583506004161 Published online by Cambridge University Press

Table 1. *Electron relaxation times (τ_s) at room temperature (298 K) for some common paramagnetic metal ions (Bertini & Luchinat, 1996). Dipolar and Curie contributions to R_2 (s^{-1}) for a proton at 5 Å and at 10 Å from the metal, calculated at two different magnetic fields, at 298 K and assuming $\tau_r = 10^{-8}$ s. The corresponding contributions to proton linewidth, $\Delta\nu$, are equal to R_2/π*

			11·7 T (500 MHz)[a]				21·1 T (900 MHz)[a]			
			$r = 5$ Å		$r = 10$ Å		$r = 5$ Å		$r = 10$ Å	
Paramagnetic system	S	τ_s (s)	R_2^{dip}	R_2^{Curie}	R_2^{dip}	R_2^{Curie}	R_2^{dip}	R_2^{Curie}	R_2^{dip}	R_2^{Curie}
Ti^{3+}	1/2	10^{-10}–10^{-11}	60–530	20	0–10	0	60–490	70	0–10	0
VO^{2+}	1/2	10^{-8b}	15840	20	250	0	15810	70	250	0
V^{3+}	1	10^{-11}	150	160	0	0	150	510	0	10
V^{2+}	3/2	10^{-9}	15530	560	240	10	14750	1800	230	30
Cr^{3+}	3/2	5×10^{-9}–5×10^{-10}	9260–53000	560	140–830	10	8200–52750	1800	130–820	30
Cr^{2+}	2	10^{-11}–10^{-12}	60–440	1420	0–10	20	50–440	4600	0–10	70
Mn^{3+}	2	10^{-10}–10^{-11}	440–4210	1420	10–70	20	440–3930	4600	10–60	70
Mn^{2+}	5/2	10^{-8b}	184810	3020	2890	50	184420	9790	2880	150
Fe^{3+} (HS)	5/2	10^{-9}–10^{-11b}	650–36240	3020	10–570	50	640–34420	9790	10–540	150
Fe^{3+} (LS)	1/2	10^{-11}–10^{-13}	60	20	0	0	0–60	70	0	0
Fe^{2+} (HS)	2	10^{-12}–10^{-13}	10–60	1420	0	20	10–50	4600	0	70
Co^{2+} (HS, 5–6 coord)	3/2	5×10^{-12}–10^{-13}	10–140	560	0	10	10–140	1800	0	30
Co^{2+} (HS, 4 coord)	3/2	10^{-11}	280	560	0	10	280	1800	0	30
Co^{2+} (LS)	1/2	10^{-9}–10^{-10}	1850–3110	20	30–50	0	1640–2950	70	30–50	0
Ni^{2+} (5–6 coord)	1	10^{-10b}	1400	160	20	0	1310	510	20	10
Ni^{2+} (4 coord)	1	10^{-12}	20	160	0	0	20	510	0	10
Cu^{2+}	1/2	$(1–5) \times 10^{-9}$	3110–10600	20	50–170	0	2950–10550	70	50–160	0
Ru^{3+}	1/2	10^{-11}–10^{-12}	10–60	20	0	0	10–60	70	0	0
Re^{3+}	2	10^{-12}–10^{-13}	10–60	1420	0	20	10–50	4600	0	70
Gd^{3+}	7/2	10^{-8}–10^{-9b}	65240–332650	9790	1020–5200	150	61950–331960	31700	970–5190	500
Ln^{3+}		10^{-12}–10^{-13}	10–40	560	0	10	10–30	1800	0	30

[a] Magnetic field strength and proton Larmor frequency (in parentheses).
[b] τ_s is field dependent, this value is measured at 500 MHz.

where τ_r is the reorientational correlation time and τ_m is the time constant for chemical exchange. In paramagnetic metalloproteins the correlation time for nuclear relaxation is often determined by τ_s since rotation is slow and exchange, if present, is usually slower than τ_s. The latter strongly depends on the nature of the metal ion (see Table 1 and Section 2.5). When $S>1$, τ_s can be field dependent which could make the value of τ_s at high magnetic fields even longer than τ_r. In these conditions, the reorientation mechanism dominates the correlation time and, as τ_r is long and the interaction energy with the unpaired electrons is quite large, nuclear relaxation rates are high and the NMR lines broad (Banci *et al.* 1991; Bertini & Luchinat, 1996).

As described in Section 2.1, unpaired electrons are also characterized by a time-averaged induced electron magnetic moment $\langle\mu\rangle$, which is proportional to the small difference in population between the electronic spin levels, according to the Boltzmann distribution. Modulation of the DD coupling of the nuclear spin with this averaged moment provides a further relaxation contribution, called Curie spin (CS) relaxation. As the average magnetic moment depends on $\mathbf{B_0}$, this contribution depends on the square of $\mathbf{B_0}$ and is given by Gueron (1975):

$$R_1^{\text{Curie}} = \frac{2}{5}\left(\frac{\mu_0}{4\pi}\right)^2 \frac{\omega_I^2 g^4 \mu_B^4 S^2(S+1)^2}{(3kT)^2 r^6}\left[\frac{3\tau_c}{1+\omega_I^2\tau_c^2}\right], \tag{2.15}$$

$$R_2^{\text{Curie}} = \frac{1}{5}\left(\frac{\mu_0}{4\pi}\right)^2 \frac{\omega_I^2 g^4 \mu_B^4 S^2(S+1)^2}{(3kT)^2 r^6}\left[4\tau_c + \frac{3\tau_c}{1+\omega_I^2\tau_c^2}\right]. \tag{2.16}$$

This coupling cannot be modulated by electron relaxation, as the nuclear spins are coupled with the time average of the electron spin moments and only the reorientational correlation time, τ_r or τ_m modulate this contribution. As it can be derived from these equations, at the high magnetic fields used for high resolution structural studies, it can have a significant contribution only to R_2.

The CS contribution to relaxation has similarities with chemical shift anisotropy (CSA), in particular for its dependence with $\mathbf{B_0}^2$. It may represent a serious limitation to high magnetic field investigations of paramagnetic metalloproteins. Indeed, for large molecules, i.e. with long rotational correlation times, and containing metal ions with large S values, the Curie contribution to R_2 at high magnetic fields could be quite severe (Table 1).

Another similarity between CS relaxation and CSA is that CS relaxation can also cross correlate with other contributions to relaxation which are modulated by the same rotational correlation time, τ_r (Wimperis & Bodenhausen, 1987; Werbelow, 1996; Kumar *et al.* 2000). Among them, the most widely studied, and the most useful for structure calculations, is the cross correlation between CS relaxation and DD relaxation (Bertini *et al.* 1993, 1994b). Cross correlation contributes to both shift and relaxation properties of the NMR signals; while the contribution to the former is generally small (Ghose & Prestegard, 1997) and, even if determined, it cannot be straightforwardly converted into structural information (Desvaux *et al.* 2004), the latter can be sizable and contains structural information which can be easily extracted. As CS relaxation essentially affects R_2 [Eq. (2.16)], the cross-correlation term η to relaxation is also measured only on R_2. For a given nucleus X, experiencing a CS relaxation and DD coupled with the nucleus Y, η is (Bertini *et al.* 1993, 1994b; Ghose & Prestegard, 1997):

$$\eta_{X,XY}^{CS-DD} = \frac{1}{5}\left(\frac{\mu_0}{4\pi}\right)^2 \frac{\hbar\gamma_X^2\gamma_Y \mathbf{B}_0 g^2 \mu_B^2 S(S+1)}{(3kT) r_{MX}^3 r_{XY}^3}\,\frac{(3\cos^2\theta - 1)}{2}\left[4\tau_c + \frac{3\tau_c}{1+\omega_X^2\tau_c^2}\right], \tag{2.17}$$

https://doi.org/10.1017/S0033583506004161 Published online by Cambridge University Press

where θ is the angle between the MX vector (X being the nucleus for which CS relaxation is operative), and the XY vector. When X and Y are also scalarly coupled, like the case of an H–N coupling, the linewidths of the two individual components of the doublet arising from the X–Y coupling are differently affected by cross correlation, according to

$$R_{2X}^{\alpha,\beta} = R_{2X}^{all} \pm \eta_{X,XY}^{CS-DD}, \tag{2.18}$$

where R_{2X}^{all} is the sum of all other contributions to R_{2X}. Therefore a cross-correlation rate, indicated as $\Gamma_{X,XY}^{CS-DD}$, can be measured as the differential transverse relaxation rates of the two individual doublet components, according to

$$R_{2X}^{\alpha} - R_{2X}^{\beta} = 2\eta_{X,XY}^{CS-DD} = \Gamma_{X,XY}^{CS-DD}. \tag{2.19}$$

2.5 Interplay between electron spin properties and features of the NMR spectra

For high-resolution NMR studies, the presence of unpaired electrons is a limitation which may be more or less severe, depending on the paramagnetic center which originates the effect. At the same time, precious information can be obtained from the effects induced by the hyperfine coupling. Ideally, a paramagnetic center should give rise to large hyperfine shifts and to small line broadening. The general approach is that of minimizing the effects on nuclear R_1 and R_2, which reduce the detectability of NMR signals, although at different extent for the various nuclei. As a consequence, cross peaks originating from dipolar and scalar nucleus-nucleus interactions are not detected (Bertini & Luchinat, 1996). In favorable cases the loss of cross peaks is limited and is compensated and even overcome by the gain of information obtained from the paramagnetism-based restraints. In unfavorable cases the lines are so broadened that cross peaks and even signals in one-dimensional spectra escape detection.

The dipolar and Curie contributions to R_2, calculated for a proton at distances of 5 and 10 Å from the metal and at two different magnetic fields (11·7 and 21·1 T, corresponding to 500 and 900 MHz ^{1}H Larmor frequencies, respectively) are reported in Table 1. As discussed in Section 2.4, the effect of a paramagnetic center on the relaxation rates also depends on the S number, i.e. on the number of unpaired electrons. When only the dipolar contribution is considered, high-resolution NMR spectra can be obtained, as a gross borderline, in the presence of metal ions with τ_s shorter than 10^{-11} s and with up to three unpaired electrons (Fig. 1). When τ_s is longer, high resolution NMR spectra for the detection of nuclei coupled with the paramagnetic center can only be obtained with tailored approaches. For large S values, τ_s shorter than 10^{-11} s are necessary to obtain high-resolution spectra (Fig. 1) (Bertini & Luchinat, 1996; Bertini *et al.* 2001f). The dependence of relaxation with S is even more effective on the Curie contribution to R_2 (Table 1).

Generally, metal ions with short τ_s have low-lying excited levels and strong spin orbit coupling effects, which cause magnetic susceptibility anisotropy, and then pseudocontact shifts. This happens, for example, for lanthanides, cobalt(II) (with coordination number higher than 4) or low-spin iron(III) ions. Hyperfine-shifted signals often fall outside the range of diamagnetic signals, and this makes the signals and cross-peak detection and assignment more readily accessible. Moreover, when τ_s is short, nuclear longitudinal relaxation is moderately affected, and ^{1}H–^{1}H NOEs, which depend on R_1 of the connected nuclei, can be easily measured. The same holds for the detection of scalar coupling coherence transfer, which depends on R_2.

https://doi.org/10.1017/S0033583506004161 Published online by Cambridge University Press

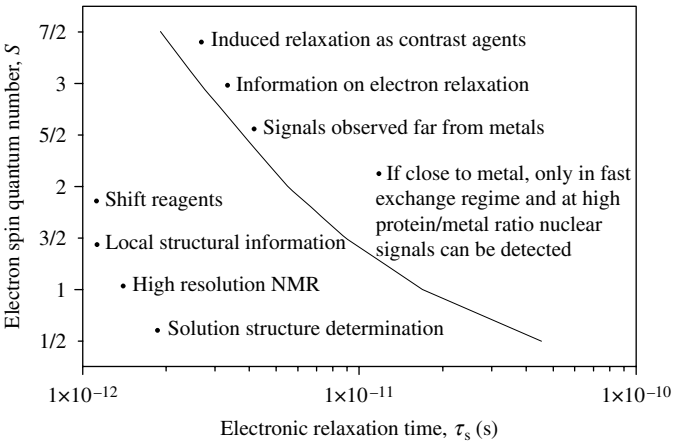


Fig. 1. Nature of the information which can be obtained from NMR experiments applied to paramagnetic systems, when weak (lower left) and strong (upper right) contributions to nuclear relaxation are operative. The effect on nuclear relaxation increases with increasing electron spin quantum number and electronic relaxation time τ_s. Only the dipolar contribution is taken into account. A line broadening of 300 Hz is taken as limit of detectability.

In the case of metal ions with long τ_s and large S values, e.g. Mn^{2+} and Gd^{3+}, the broadening is as large as thousands of Hz and signals are broadened beyond detection, also at relatively long distances from the metal. Furthermore, these metal ions provide limited effects on the shifts, thus leaving the broad signals beneath the sharp diamagnetic signal envelope. Between the above limit cases, there are other cases for which the hyperfine-shifted signals fall outside the diamagnetic envelope but may suffer of sizable line broadening, e.g. in the case of type-I copper(II) complexes. As it will be shown in Section 6, precious structural information can be still derived also for these systems, provided that optimized experiments are acquired.

As the dipolar contribution to relaxation depends on r^{-6} and on τ_s, the longer τ_s the larger is the contribution to linewidth and therefore farther away from the metal ion is the signal broadening appreciated. In Mn^{2+}, broadening can be observed up to 25 Å away, at 500 MHz. On the other limit, when τ_s is short, no hyperfine broadening is observed farther than 10 Å away or even less. As many as 11 lanthanides (excluding the diamagnetic ones, Gd^{3+}, and the radioactive Pm^{3+}) can be easily used as paramagnetic probes with favorable NMR properties (Allegrozzi *et al.* 2000). The rationale behind the success of lanthanides lies in their short electron relaxation times, coupled with sizable magnetic anisotropy (Bleaney *et al.* 1972). This feature minimizes the broadening effects on NMR lines, while at the same time they retain a variety of other paramagnetic effects which contain useful structural and dynamic information and in particular pseudocontact shifts which spread the signals outside the diamagnetic envelope (see Section 5). In lanthanides, spin (**S**) and orbital (**L**) angular momenta are strongly coupled giving rise to a *total angular momentum*, **J**, which takes values from |L+S| to |L − S|. As the spin orbit coupling is strong, the free-ion terms are described by the spin-orbit quantum number J which replaces the purely electron spin quantum number S in all equations of Section 2 (Bleaney, 1972). For lanthanides with large J values, the lines of nuclei of the directly coordinated residues are broadened beyond detection, due to Curie relaxation, which is proportional to the square of $J(J+1)$ (Bertini *et al.* 2001f).

https://doi.org/10.1017/S0033583506004161 Published online by Cambridge University Press

When the system contains two or more metal ions, they can be *magnetically coupled*. If the magnetic coupling energy, divided by $\hbar$, is larger than τ_s of each individual metal ion, only one τ_s describes electron relaxation. In these conditions, τ_s becomes smaller than that of the individual metal ions as the magnetic coupling provides low-lying electron spin states, making electron relaxation more efficient. In these systems the shifts might have a complex pattern as well as strong temperature dependence as the electron spin levels, having low energy separation, can change their population significantly with temperature. Approaches to interpret the shifts and relaxation properties in magnetically coupled systems are available in the literature (Banci *et al.* 1990; Bertini & Luchinat, 1996).

The effect of paramagnetic enhancements on R_1 and R_2 as a function of the distance from the metal ion are different on ^{1}H, ^{13}C and ^{15}N relaxation rates and, consequently, on signal and cross-peak detectability. Due to the smaller magnetogyric ratio of heteronuclei, heteronuclear detection is less affected by the paramagnetic center. Therefore, in the most recent years, new purely heteronuclear experiments are being developed which completely avoid ^{1}H detection (see Section 4). These experiments allowed, for example, structure determination of proteins containing type-II copper(II) as paramagnetic center, which severely affects linewidths (Arnesano *et al.* 2003a; Bermel *et al.* 2003).

3. Paramagnetism-based structural restraints

The first solution structure of a paramagnetic protein has been obtained in 1994 (Banci *et al.* 1994a), for the reduced form of the high potential iron sulfur protein (HIPIP) from *E. halophila*. This protein contains a Fe_4S_4 cluster, in which the metal ions have two formal oxidation states (two Fe^{2+} and two Fe^{3+}) and are magnetically coupled. Actually, the unpaired electrons are delocalized over the four iron ions which are therefore equivalent, with oxidation state $Fe^{2.5+}$ (Mullinger *et al.* 1975). This produces a ground state with electron spin $S=0$ and paramagnetism arising from low-lying excited spin states (Poe *et al.* 1970). However, the paramagnetic effects are quite severe, particularly on relaxation properties. The βCH_2 of the Cys ligands to the iron ions are characterized by R_1 of 3–5 ms and linewidths of 200–400 Hz (Bertini *et al.* 1992). To achieve the goal of determining the solution structure, all experiments were 'tailored' to minimize the loss of information due to quench of NOEs and line broadening induced by the paramagnetic cluster. A combination of tailored 2D experiments and 1D NOE difference spectra provided enough constraints even in the immediate proximity of the Fe_4S_4 cluster to obtain a structure with a resolution comparable to that obtained in structures of diamagnetic proteins (Banci *et al.* 1994a; Bertini *et al.* 1995b, 1996).

Since then, efforts have been focused on exploiting the structural information contained in the hyperfine interaction. The frontier in NMR solution structure of paramagnetic molecules rapidly moved ahead from the optimization of existing pulse sequences (Banci *et al.* 1994b) and from the minimization of losses in signal intensity due to fast relaxation (Banci *et al.* 1992) to constructively use the hyperfine interaction to obtain information which is not available in diamagnetic systems (Bertini *et al.* 2001b, g).

Paramagnetism-based structural restraints are highly complementary to classical restraints. Solution structures of paramagnetic proteins determined only with classical restraints have a lower resolution in the proximity of a paramagnetic center than in any other part of the protein. However, paramagnetism-based restraints compensate for lack of NOEs and dihedral angles, or

https://doi.org/10.1017/S0033583506004161 Published online by Cambridge University Press

better still, provide, even in the surrounding of the metal ion, high resolution in the structure conformation. Paramagnetism-based restraints can be collected also in protein regions far from the metal center, where they add to NOEs and dihedral angles. Therefore, even for those protein regions which are accurately defined by classical restraints, the availability of paramagnetism-based restraints contributes to an overall improvement of the structure and, as they are based on different and independent interactions, they can point out possible structural inconsistencies originating from misassignments. Even more important is the fact that paramagnetism-based restraints are the only source of information to locate the metal ion in the protein frame, with the only exception of few metal ion, e.g. ^{113}Cd, ^{109}Ag, ^{199}Hg, which have an NMR active nucleus and on which direct spectra can be obtained in the diamagnetic form.

For these reasons the use of paramagnetism-based restraints is also becoming popular in diamagnetic proteins, where a paramagnetic probe can be attached to the protein, either through metal substitution (Bertini *et al.* 1985; Banci & Piccioli, 1996; Allegrozzi *et al.* 2000; Gochin, 2000) or with a metal-binding tag (Feeney *et al.* 2001; Wöhnert *et al.* 2003; Ikegami *et al.* 2004) or a spin label tag (Dunham & Lippard, 1995; Ramos & Varani, 1998; Battiste & Wagner, 2000; Gaponenko *et al.* 2000b, 2004; Lewin *et al.* 2002) attached to the protein.

When the native metal ion can be substituted with various paramagnetic metal ions, independent structural information for each metal-substituted derivative can be obtained, as the different metal ions induce different paramagnetic effects (Bertini *et al.* 1985; Moura *et al.* 1991; Holz *et al.* 1992; Krizek & Berg, 1992; Banci & Piccioli, 1996; Donaire *et al.* 1998). Examples will be given in which the simultaneous use of paramagnetism-based restraints obtained from different metal-substituted derivatives in structure calculation, leads to solution structures with resolution significantly improved with respect to the corresponding diamagnetic protein (Bertini *et al.* 2001b, c).

Historically, the first step was the use of relaxation rates as structural restraints (Bertini *et al.* 1995a), soon after followed by the pseudocontact shifts (Banci *et al.* 1996). Since then, continuous efforts were focused to the exploitation of phenomena involving hyperfine interactions as sources of structural restraints. We are now going to briefly evaluate them as well as the effects due to self-orientation induced by the presence of a paramagnetic center. We will first consider those restraints which provide information in a shell close to the metal ion and then those which can provide information much farther, possibly over the entire protein.

3.1 Contact shifts and relaxation rates as restraints

Contact shifts, δ^{con}, depend on the unpaired electron spin density on the resonating nucleus (McConnell, 1956), as discussed in Section 2 and quantified by Eq. (2.8). They can provide structural information essentially only for a few nuclei connected to the metal through a few bonds, i.e. nuclei in the first coordination sphere (Bertini *et al.* 2001f) and, even for them, only in a few types of systems this information can be translated in structural restraints. Contact shifts can be experimentally determined from the total shift, provided that pseudocontact shifts (see later) can be either subtracted or neglected. Also the diamagnetic contribution needs to be known and subtracted.

For ^{1}H nuclei being three bonds away from the paramagnetic center, the δ^{con} depends on the dihedral angle M–D–C–H (Fig. 2), through a Karplus-type (Karplus, 1959) equation of the form

$$\delta^{con} = a \cos^2 \theta + b \cos \theta + c, \tag{3.1}$$

https://doi.org/10.1017/S0033583506004161 Published online by Cambridge University Press

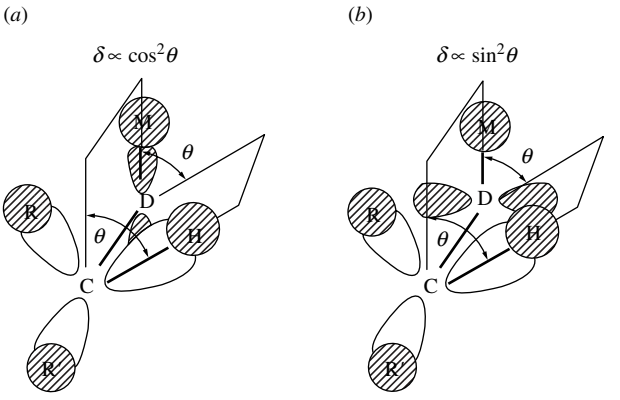


Fig. 2. The dihedral angle θ between M–D–C and D–C–H planes, determining the metal-proton contact coupling. The different angular dependency of the overlap between the 1 s orbital of ^{1}H and the orbitals of the donor atom D, is shown. (*a*) The case of spin density being along the M–D bond. (*b*) The case of the spin density being in a p orbital of the D atom orthogonal to the M–D bond.

where θ is the M–D–C–H dihedral angle, M is the metal ion, D is the donor atom (typically N or S) and *a*, *b* and *c* are numerical coefficients which depend on the nature of the bonds and atoms involved and which have been heuristically determined (Fitzgerald & Drago, 1967). The 1s orbital of the proton overlaps with the electron spin density localized on the metal-donor bond, so that the relative orientation of the M–D and C–H vectors modulates the overlap and gives rise to Eq. (3.1) (Fig. 2*a*). This is similar to what occurs for any ^3J coupling constant between two nuclei separated by three bonds (Karplus & Fraenkel, 1961). The situation may be different when the donor atom is a sulfur atom, which has two lone pairs and only one is used in the M–S bond. Depending on the metal ion and on the coordination geometry, the electron spin density may be localized on the lone pair along the M–S bond (Fig. 2*a*), or in the other lone pair which is in a p orbital of the sulfur atom, orthogonal to the M–S bond (Fig. 2*b*) (Heller & McConnell, 1960; Stone & Maki, 1962). In the latter case the geometrical dependence of the contact shift has the form

$$\delta^{\text{con}} = a \sin^2\theta, \tag{3.2}$$

An independent parametrization, therefore, needs to be performed for each type of coordination site, because the geometrical dependence of contact shifts depends on donor atoms, metal ions and coordination geometry. For example, in the case of cysteine residues bound to iron ions in iron–sulfur proteins, both electron delocalization mechanisms depicted in Fig. 2 contribute to the contact shift of βCH_2 of the coordinated Cys residues. The unpaired electron is predominantly located in the lone pair orthogonal to the M–S bond (Fig. 2*b*) and the overall geometrical dependence is a combination of Eqs (3.1) and (3.2):

$$\delta^{\text{con}} = a \sin^2\theta + b \cos\theta + c, \tag{3.3}$$

with $a = 10{\cdot}3$, $b = -2{\cdot}2$ and $c = 3{\cdot}9$. The much larger value of *a* is such that the $\sin^2\theta$ term dominates (Bertini *et al.* 1994a). This heuristically determined equation was exploited to use the dihedral angle Fe–S–C–H as a dihedral angle restraint in structure calculations for iron–sulfur proteins containing a $[Fe_4S_4]^{2+}$ cluster (Bertini *et al.* 1994a). Also for Cys ligands bound to Cu^{2+}

https://doi.org/10.1017/S0033583506004161 Published online by Cambridge University Press

ions in blue copper proteins a $\sin^2 \theta$ dependency, with different coefficients, was found (Bertini *et al.* 1999a, 2000a; Donaire *et al.* 2002).

The contact shift of heme substitutents are found to be dependent on the dihedral angle between the plane orthogonal to the heme and containing the methyl group-iron vector and the plane defining the orientation of the axial ligand (Walker, 1999). The angular dependence is different for the low spin ferric and the high spin ferrous case, but in both cases is related to this angle by Karplus-type relationships which have been parameterized (Bertini *et al.* 1998a, 1999b).

So far, Karplus-type equations were successfully parameterized for ^{1}H shifts, but Eq. (3.3) was found to account also for the ^{13}C contact shift experienced by $^{13}C^{\alpha}$ of Cys residues in iron–sulfur proteins (Bertini *et al.* 1994a). However, this behavior can not be generalized. Several terms may contribute to the contact shift of ^{13}C nuclei which are three bonds away from a metal center, so that the information on conformational arrangement contained in contact shifts is generally hidden in the case of heteronuclei (Bertini *et al.* 2001f).

Even if the conversion of contact shifts into dihedral angle restraints could suffer of a lack in general applicability, these restraints are important because they provide the spectroscopic evidence of the nature of the donor atoms to the metal ion and allow one, within structure calculations, to impose a link between the donor atom of the coordinating residues and the paramagnetic center.

Longitudinal relaxation rates arising from a paramagnetic center, R_{1p}, were the first paramagnetism based restraints successfully used in structure calculations. They depend on the r^{-6} of the metal-to-nucleus distance [Eqs (2.10), (2.12) and (2.15)] and, therefore, they have spherical symmetry, behave like metal-nucleus NOEs (Bertini *et al.* 1997) and can straightforwardly be converted into distance restraints (Bertini *et al.* 1996). Initially limited to ^{1}H detection, R_{1p} can nowadays also be obtained from ^{13}C and ^{15}N nuclei (Wilkens *et al.* 1998a, b; Ma *et al.* 2000; Arnesano *et al.* 2003a; Baig *et al.* 2004). The use of R_{1p} of ^{13}C and ^{15}N signals in structure calculations can be important because direct detection of heteronuclei allows nowadays to extend the assignment also in regions close to the metal ion where no information can be extracted from ^{1}H NMR (see Section 4). However, caution should be taken when they are translated in distances as a nonlinear dependence with r^{-6} at long distance has been observed. This behavior is still not fully understood, even if it has been suggested to originate from extensive spin delocalization (Ma *et al.* 2000).

Experimentally observed R_1 values are the sum of the paramagnetic contribution, R_{1p}, and of all the diamagnetic contributions, R_{1d}. Therefore R_{1d} must be known in order to convert observed relaxation rates into structural restraints. This can be obtained by measuring R_{1d} on a diamagnetic analog of the investigated system or, when this is not possible, the diamagnetic contribution can be estimated from the average of R_1 values observed on the same paramagnetic protein but far away from the metal center, where the paramagnetic contributions to relaxation can be safely ruled out (Bertini *et al.* 1995a; Goasdoue *et al.* 2000).

Once the diamagnetic contribution is factorized out, R_{1p} values can contain both the contact and the dipolar contributions. The former, as discussed in Section 2.4, has some relevance only for nuclei of the metal ligand residues and for nuclei with low γ. For most of the resonances, R_{1p} is determined only by the dipolar contribution and they can be converted into distance restraints in analogy to NOE intensities. The main difference between them is that, while NOEs relate pairs of nuclei, R_{1p} are metal centered, i.e. provide restraints between various nuclei and the metal ion. This is illustrated in Fig. 3(*a*, *b*). Therefore R_{1p} restraints accurately

https://doi.org/10.1017/S0033583506004161 Published online by Cambridge University Press

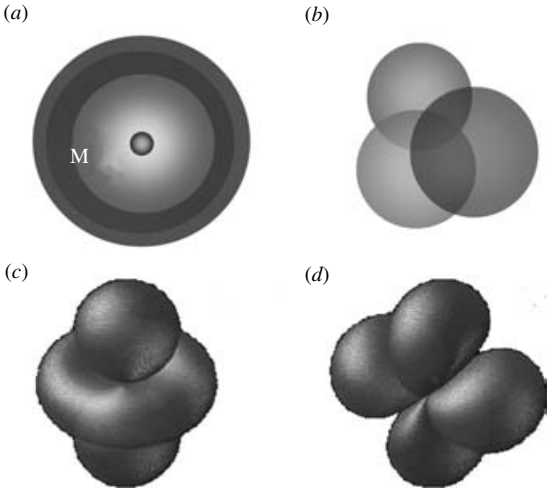


Fig. 3. Spatial dependence distributions of various types of NMR restraints. (*a*) R_{1p} restraints have a spherical symmetry centered on the metal nucleus. (*b*) NOEs have also a spherical symmetry but they are effective between different pairs of nuclei, therefore they are centered on each active nuclear spin. δ^{pc} have an axial (*c*) and rhombic (*d*) contribution centered on the metal ion.

locate the metal within the protein frame and can contribute to define the conformation of metal-binding residues. The use of a few R_{1p} restraints together with the standard set of NOEs, even in the absence of other paramagnetic restraints, decreases the local r.m.s.d. around the metal ion (Bertini *et al.* 1995a). Even if the effect on the global r.m.s.d. could be negligible, the local contributions are important because they correctly locate the metal ion within the protein frame.

3.2 Locating the metal ion within the protein frame: pseudocontact shifts

Pseudocontact shifts (δ^{pc}) are precious sources of structural information as, according to Eq. (2.8), they have a non-spherical symmetry, as shown in Fig. 3(*c*, *d*), and depend on r^{-3} rather than on r^{-6}, i.e. they are long-distance restraints. To properly analyze δ^{pc} we should first factorize the various contributions to the observed shift, which is mandatory to obtain δ^{pc}.

Neglecting contributions to the chemical shift arising from self-orientation (residual dipolar shifts; Bertini *et al.* 1998b) and from cross correlations (dynamic frequency shifts; Ghose *et al.* 1998; Desvaux *et al.* 2004), the observed shift is given by

$$\delta^{obs} = \delta^{dia} + \delta^{con} + \delta^{pc}, \tag{3.4}$$

where δ^{dia} is the diamagnetic contribution to the observed shift, δ^{pc} and δ^{con} are the pseudocontact and contact hyperfine shifts. Factorizing out the contact shift is relatively simple, because the contact shift vanishes a few bonds away from the metal center and is experienced only by the coordinated residues and in very specific cases by the neighboring ones (Bren *et al.* 1995; Xia *et al.* 1995; Caillet *et al.* 2006). Therefore, in the following analysis, the shifts of the nuclei of the metal-coordinating residues are excluded. On the contrary, the factorization of pseudocontact and diamagnetic contributions to the chemical shift is a critical issue. For this purpose the availability of a diamagnetic analog is useful; this can be obtained either

https://doi.org/10.1017/S0033583506004161 Published online by Cambridge University Press

by replacing the paramagnetic metal ion with a diamagnetic metal ion, possibly with the same charge, or by changing the oxidation state of the paramagnetic center in order to make it diamagnetic. It should, however, be considered that metal replacement may induce structural changes and consequently chemical shift variations. Also, redox state and charge-dependent chemical shift changes can occur (Vathyam *et al.* 2000; Lehmann *et al.* 2002); they may affect the diamagnetic term of the observed shift and constitute a bias for the determination of δ^{pc}. Indeed, it has been shown that, in Ca^{2+}-binding proteins, upon replacement with the diamagnetic La^{3+} ion, the resonances of the residues belonging to the metal coordination sphere experience some shift (Allegrozzi *et al.* 2002). This has not been attributed to structural differences that should be negligible in this case, but it is rather due to the higher charge of the trivalent La^{3+} with respect to the divalent Ca^{2+} cation. In the absence of a suitable experimental diamagnetic reference, the diamagnetic contribution can be estimated from calculations (Wishart & Case, 2001) or from the temperature dependence of the observed shifts (Bentrop *et al.* 1997).

In general, for ^{1}H resonances reliable diamagnetic shifts can be determined. In the case of ^{13}C resonances, reliable estimates of δ^{pc} can be obtained for $^{13}C'$ while $^{13}C^{\alpha}$ and $^{13}C^{\beta}$ resonances are more sensitive than their corresponding ^{1}H resononaces to subtle structural variations, and therefore their use as δ^{pc} might be difficult (Yao *et al.* 1997). More complex is the case for ^{15}N resonances. For heme proteins, it has been pointed out that the diamagnetic ^{15}N chemical shifts in oxidized cytochrome *c* and cytochrome b_5, determined by subtracting from δ^{obs}, the calculated δ^{pc} (δ^{con} being zero), being the structures and the $\Delta\chi^{para}$ values known, are different from those observed in the reduced diamagnetic analogues (Boyd *et al.* 1999; Bertini *et al.* 2000b). Even for some Fe_4S_4-containing proteins, the ^{15}N diamagnetic chemical shifts were found to be oxidation state-dependent (Bertini *et al.* 1995b). Polarizabilities of the shielding tensor and electric field gradients might be responsible for electronic effects non arising from the hyperfine interactions (Biekofsky *et al.* 1998; Boyd *et al.* 2003). Therefore, caution should be taken when using ^{15}N δ^{pc} for structural determinations.

In principle, pseudocontact contributions arise also form ligand-centered contributions. However, when residues of the first coordination sphere are not taken into account, the ligand-centered contribution is not relevant for the use of shifts in structural calculations, because nuclei far from the paramagnetice center still 'see' the unpaired electron as completely localized on the metal ion.

Depending on the way the δ^{dia} values are determined, the tolerance on δ^{pc} used in structural calculations should be different. When the diamagnetic contribution is estimated by considering the same system in a diamagnetic state, a reasonable choice for the tolerance is 0·3 ppm for H_N protons and 0·1 ppm for non-exchangeable protons. Values of 0·1 and 0·5 ppm can be used for ^{13}C and ^{15}N nuclei (Bertini *et al.* 2001b). The different tolerance for H_N with respect to the other protons derives from the larger variability of the chemical shifts of amide protons (Bentrop *et al.* 1997). When diamagnetic shifts are calculated, larger tolerances, i.e. of $\sim$1 ppm for H_N and 0·5 ppm for all other non-exchangeable protons, should be used (Ösapay & Case, 1991; Banci *et al.* 1998a). It has been also suggested not to use a fixed tolerance for all δ^{pc} values, particularly for the large ones. As δ^{pc} depends on r^{-3} of the distance between the nucleus and the paramagnetic center, when using the same tolerance value, nuclei near the paramagnetic center are allowed to experience smaller movements than nuclei far from the metal ion. To circumvent this bias, a tolerance proportional to the absolute value of δ^{pc} was suggested, thus avoiding possible over-refinement of nuclei close to the paramagnetic center which in

https://doi.org/10.1017/S0033583506004161 Published online by Cambridge University Press

general experience larger δ^{pc} than nuclei far from the metal center (Bentrop *et al.* 1997; Banci *et al.* 1998a).

Once pseudocontact shifts have been estimated, they need to be converted into structural restraints. The atomic coordinates are related to δ^{pc} by Eq. (2.8), which is fully defined by five parameters: two magnetic susceptibility anisotropies and three angles that define the orientation of the χ tensor axes with respect to a metal-centered axis system (Emerson & La Mar, 1990; Banci *et al.* 1996, 1997a). It is also possible to leave the position of the metal free to be determined by the fitting of the δ^{pc} in the calculations. In such case, three more parameters, which are the coordinates of the metal ion in the protein frame, need to be fitted (Bertini *et al.* 2001c). An estimate of the five parameters describing the magnetic anisotropy tensor should be available for the calculations. If the protein structure is known, for example from early structural calculations without the inclusion of δ^{pc}, then δ^{pc} can be fitted to Eq. (2.8) to calculate an estimate of the values and orientation of magnetic anisotropy tensor. Among the programs that have been developed for this procedure, FANTASIAN (Banci *et al.* 1997b) is widely used. Then the structure can be calculated again from random conformations using NOEs and pseudocontact shifts simultaneously as restraints. The magnetic susceptibility tensor parameters as well as the coordinates of the metal ion can be then iteratively fitted within structural calculations until convergence (Banci *et al.* 1997a).

Due to their complex angular dependence, the use of δ^{pc} as structural restraints requires specific routines in the structure calculation programs. DIANA (Güntert *et al.* 1991), initially, and then DYANA (Güntert *et al.* 1997) and CYANA (Herrmann *et al.* 2002a), as well as XPLOR-NIH (Clore *et al.* 1985; Brunger *et al.* 1998; Schwieters *et al.* 2003) have been implemented with a module that uses δ^{pc} as restraints, together with all the other restraints since the early steps of structure calculations (Turner *et al.* 1998; Banci *et al.* 1998a, 2002; Barbieri *et al.* 2002a; Bertini *et al.* 2002a, 2003; Banci *et al.* 2004; Gaponenko *et al.* 2004).

As δ^{pc} have a non-spherical symmetry, they contribute not only to restraint the metal–nucleus distance, but also to rearrange vector orientations within the protein frame. The distance from the metal up to which measurable δ^{pc} can be determined depends on the anisotropy of the magnetic susceptibility, which is essentially determined by the nature of the metal ion and by its coordination sphere. Table 2 provides predicted δ^{pc} on the basis of available magnetic anisotropies for various metal ion coordination spheres. It should also be pointed out that δ^{pc} depends on the orientation of the metal–nucleus vector with respect to the principal axes of the magnetic susceptibility tensor. As it results from Eq. (2.8), at a given distance, $|\delta^{pc}|$ along the z direction ($\cos^2\theta = 1$) is double, in the absence of rhombicity, than that in the *x,y* plane ($\cos^2\theta = 0$). However, paramagnetic relaxation might also broaden beyond detection signals around the paramagnetic center. The portion of space in which δ^{pc} can be exploited is, therefore, not simply a region centered on the metal ion but rather a region, as depicted in Fig. 4, with an upper limit given by the smallest observable shift and a lower limit given by the largest broadening which still makes signals detectable (Bertini *et al.* 2005b). The interplay between relaxation effects and shift effects (Fig. 4) tunes the efficiency of a given paramagnetic center as a source of δ^{pc} restraints.

3.3 Cross-correlation rates

Cross-correlation rates between CS relaxation and DD relaxation, $\Gamma^{CS-DD}_{X,XY}$, defined by Eqs (2.17)–(2.19) are, in principle, a precious source of structural restraints because they are related

https://doi.org/10.1017/S0033583506004161 Published online by Cambridge University Press

Table 2. *Predicted pseudocontact shift values for different metal ion coordination spheres. Reported values are calculated for metal–nucleus distances of 7 and 10 Å, assuming a* $\Delta\chi_{rh} = 0$ *and a nucleus in an axial position with respect to the* χ *tensor* ($\theta = 0$, $3\cos^2\theta - 1 = 2$)

Paramagnetic system	S or J	$\Delta\chi_{ax}$ (10^{-32} m^3)[a]	δ^{pc} (ppm) $r = 7$ Å	$r = 10$ Å
Fe^{3+} (HS)	5/2	3·0	4·6	1·6
Fe^{3+} (LS)	1/2	2·4	3·7	1·3
Fe^{2+} (HS)	2	2·1	3·2	1·1
Co^{2+} (HS, 6 coord)	3/2	7	10·8	3·7
Co^{2+} (HS, 4 coord)	3/2	3	4·6	1·6
Cu^{2+}	1/2	0·6	0·9	0·3
Gd^{3+}	7/2	0·2	0·3	0·1
Ce^{3+}	5/2	2	3·1	1·1
Dy^{3+}	15/2	35	54·1	18·6
Tb^{3+}	6	35	54·1	18·6
Yb^{3+}	7/2	7	10·8	3·7
Tm^{3+}	6	20	30·9	10·6

[a] $\Delta\chi_{ax}$ values at 298 K are taken from Bertini *et al.* (2005b).

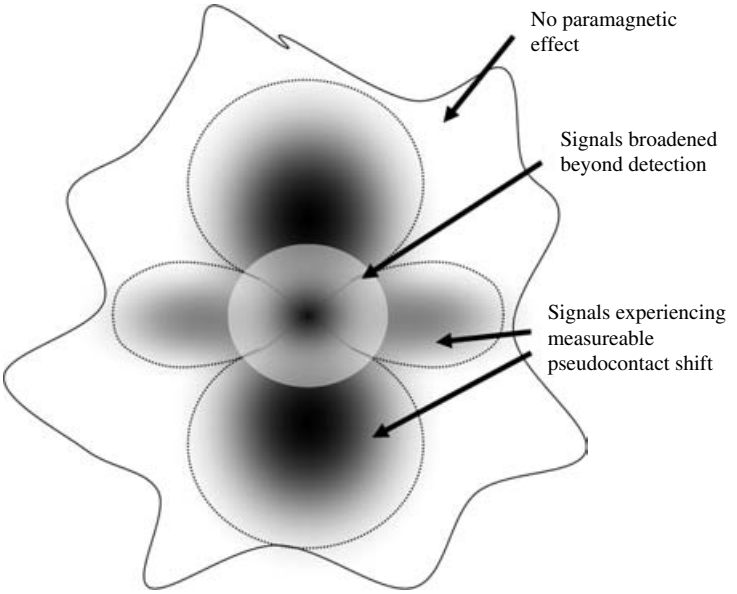


Fig. 4. Interplay between measurable pseudocontact shifts and line broadening. The lobe-shaped region of measurable δ^{pc} is compared to the region affected by the paramagnetism-induced line broadening (light gray sphere). The extent of the protein region in which δ^{pc} can be exploited varies depending on the metal ion. In favorable cases, the inner sphere, in which signals are lost due to line broadening can be very small, so that only few resonances are lost. In unfavorable cases signal losses, due line broadening, propagate farther in space with respect to the region were δ^{pc} can be measured and the latter cannot, therefore, be exploited.

to two structural parameters, the metal–nucleus distance and the relative orientation of the MX and XY vectors (Hus *et al.* 2000; Mandal *et al.* 2001; Bertini *et al.* 2002a). However, this contribution cannot be separated from the cross-correlation term originating from chemical shift

https://doi.org/10.1017/S0033583506004161 Published online by Cambridge University Press

anisotropy of the X nucleus and the XY–DD coupling, Γ^{CSA-DD}, which is independent of paramagnetism (Wimperis & Bodenhausen, 1987, 1989; Kay *et al.* 1992; Palmer *et al.* 1992; Tessari *et al.* 1997; Fushman & Cowburn, 2001). For the X doublet, originating from the coupling with Y, the observed difference in R_2 relaxation between the two doublet components [Eq. (2.19)] is given by $\Gamma^{obs}_{X,XY} = \Gamma^{CSA-DD}_{X,XY} + \Gamma^{CS-DD}_{X,XY}$. Therefore a diamagnetic reference should be available in order to factorize out the paramagnetic contribution.

Although cross-correlation effects involving CS relaxation have been described 10 years ago for small homonuclear H–H couplings (Bertini *et al.* 1993), their power in providing structural information has been exploited more recently for ^1H_N CS and H–N DD coupling (Boisbouvier *et al.* 1999). Assuming a protein in solution with an isotropic and rigid tumbling in the slow-motion regime (Bertini *et al.* 2001d), the difference in transverse relaxation rates of the two components of a H_N doublet depends on the relative orientation of the two MH and NH vectors and are mediated by the r^{-3} dependence of the metal–proton distance [Eq. (2.17)]. Cross-correlation rates have been also measured between H^α CS relaxation and H^α–C^α dipole coupling (Kateb & Piccioli, 2003), and between H CS and H–H dipole couplings among methyl protons (Mandal *et al.* 2000; Madhu *et al.* 2002). As $\Gamma^{CS-DD}_{X,XY}$ [Eqs. (2.17)–(2.19)] is scaled by $\gamma_X^2\gamma_Y$, where X is the nucleus undergoing CS relaxation and Y is the nucleus giving rise to DD coupling with X, the effect is smaller respectively by a factor of 4 and by a factor of 10 when, considering the same dipolar coupling, ^{13}C and ^{15}N are observed rather than ^1H. Up to now, $\Gamma^{CS-DD}_{X,XY}$could be successfully converted into structural restraints only when X is ^1H; however, experiments to measure cross-correlation rates involving low γ nuclei have been successfully developed so that the measure of $\Gamma^{CS-DD}_{X,XY}$ is, in principle, feasible also when the X nucleus is ^{13}C or ^{15}N (Tjandra *et al.* 1996; Yang *et al.* 1999; Boisbouvier *et al.* 2000).

Cross-correlation rates can be experimentally measured via several approaches. TROSY-based experiments were suggested (Boisbouvier *et al.* 1999) but, for paramagnetic systems, measurement of the build up of relaxation-allowed coherence transfer due to cross correlation was shown to be the most suitable approach (Bertini *et al.* 2002a; Kateb & Piccioli, 2003). Also, the linewitdh difference of doublet components directly provides Γ values (Pintacuda *et al.* 2004). Cross-correlation rates can be used as structural restraints through an additional module in the existing programs for structure calculations (Bertini *et al.* 2002a). Despite the number of Γ^{CS-DD} restraints is always very small compared to NOEs (Bertini *et al.* 2002a; Turano *et al.* 2003; Pintacuda *et al.* 2003), they have a non-negligible contribution to structure resolution, providing a decrease in r.m.s.d., accomplished by an improvement of the Ramachandram plot (Bertini *et al.* 2002a). In the immediate proximity of the metal center, where NOEs can be scarce and the structure relatively disordered, Γ^{CS-DD} can be extremely helpful for the definition of backbone dihedral angles, because they fix the vector orientations within the protein frame, thus contributing to the precision of the structure around the metal center (Boisbouvier *et al.* 1999; Bertini *et al.* 2002a).

3.4 Residual dipolar couplings

Paramagnetic systems possessing an anisotropic magnetic susceptibility partially orient in a magnetic field (Bothner-By *et al.* 1981). In this condition, dipolar couplings are not completely averaged to zero upon rapid rotation and the residual term observed in solution (residual dipolar

https://doi.org/10.1017/S0033583506004161 Published online by Cambridge University Press

coupling, rdc hereafter) increases with the square of the magnetic field and adds to field-independent scalar couplings.

Described in literature for decades (Bothner-By *et al.* 1981; Gayathri *et al.* 1982), rdc became popular once their practical exploitation to obtain structural information was shown by Prestegard and co-workers in a seminal article on myoglobin (Tolman *et al.* 1995). Molecules capable of orienting properties at high magnetic fields have been used to induce orientation in diamagnetic proteins in order to use rdc as structural restraints and for the characterization of the dynamics of diamagnetic biological macromolecules (Bax & Tjandra, 1997; Tjandra & Bax, 1997; Clore & Gronenborn, 1998; Cavagnero *et al.* 1999; Brunner, 2001; Meiler *et al.* 2001; Zweckstetter & Bax, 2001; Prestegard *et al.* 2004, 2005). The molecular alignment resulting from the anisotropy of the paramagnetic center can be as strong as that imposed by orienting media (Barbieri *et al.* 2002a), with the fundamental advantage that the former is an intrinsic molecular property, i.e. it does not perturb the solute.

Self-orientation induced by the magnetic anisotropy means the paramagnetic center does not depend on the hyperfine interaction, which is at the origin of all other contributions, but only depends on the magnetic anisotropy generated by the metal ion. On a practical ground, the major consequence is that rdc's do not depend on the metal–nucleus distance. Assuming a rigid isotropic molecule, and neglecting sensitivity limitations due to paramagnetism-induced line broadening, rdc induced by a metal ion can be measured with the same precision independently of the distance from the metal ion.

Rdc's can be measured either as the difference in couplings at two magnetic fields or, at the same magnetic field, measuring the difference in the observed couplings between a paramagnetic and a corresponding diamagnetic derivative. In the former case experimental rdc values are given by (Tolman *et al.* 1995):

$$\mathrm{rdc}(H\hat{z}) = -\frac{1}{4\pi}\frac{\Delta\mathbf{B_0}^2}{30kT}\frac{\gamma_X\gamma_Y h}{4\pi^2 r_{XY}^3}\left[2\Delta\chi_{ax}^{mol}(3\cos^2\theta - 1) + 3\Delta\chi_{rh}^{mol}\sin^2\theta\cos 2\phi\right], \tag{3.5}$$

where $\Delta\chi_{ax}^{mol}$ and $\Delta\chi_{rh}^{mol}$ are the axial and the rhombic anisotropies of the molecular magnetic susceptibility tensor, θ and ϕ are the polar coordinates describing the orientation of the XY vector in the axis system of the molecular magnetic susceptibility tensor, r_{XY} is the XY distance.

The molecular magnetic anisotropy tensor ($\Delta\chi^{mol}$) of Eq. (3.5) is, in paramagnetic metalloproteins, given by the tensorial sum of two contributions, i.e. that due to the anisotropy of the metal ion, which also gives rise to δ^{pc}, and the magnetic anisotropy of the diamagnetic protein frame, $\Delta\chi^{dia}$ (Banci *et al.* 1998b). When a diamagnetic analog is available, the two individual tensors can be experimentally determined by fitting experimental rdc measured on the paramagnetic and the diamagnetic molecules, independently (Banci *et al.* 1998b).

When rdc are measured at the same magnetic field, as difference between couplings observed in the paramagnetic system and in the corresponding diamagnetic derivative, they are dependent on $\Delta\chi^{para}$ only, and therefore they are different from those given by Eq. (3.5) which depend on $\Delta\chi^{mol}$. Rdc's arising from $\Delta\chi^{para}$ are determined by the same tensor which determines δ^{pc} and therefore, in structural calculations, they can be used together with δ^{pc}. Compared to the structure obtained by using δ^{pc} only, rdc can contribute to the improvement in structure quality (Baig *et al.* 2004). As extensively shown for diamagnetic proteins in orienting media, rdc's are very much influenced by even small, local changes of the θ and ϕ angles of NH vectors (Tjandra *et al.* 1997), and therefore they contribute more to the quality of the structure than to

https://doi.org/10.1017/S0033583506004161 Published online by Cambridge University Press

the precision. Furthermore, partial quench of rdc is commonly used as an indication of local motions.

Because of the advantages of the use of self-orienting systems with respect to orienting media for the determination of residual dipolar coupling, several cases are reported in which proteins, not containing metal-binding sites, have been modified to attach paramagnetic probes (Dunham & Lippard, 1995; Ramos & Varani, 1998; Battiste & Wagner, 2000; Gochin, 2000; Gaponenko *et al.* 2000b; Feeney *et al.* 2001; Lewin *et al.* 2002; Wöhnert *et al.* 2003; Ikegami *et al.* 2004; Gaponenko *et al.* 2004; Prudencio *et al.* 2004). The latter can be attached either at one of the termini of the protein (Feeney *et al.* 2001) or via chemical modification of cysteine residues (Gaponenko *et al.* 2002). Suitable tags should have very high affinity for a given metal ion and should not interfere with the protein nor induce structural changes. Different classes of compounds, from polypeptides (Wöhnert *et al.* 2003) to caged complexes (Ikegami *et al.* 2004; Prudencio *et al.* 2004) were used to bind lanthanides which, due to their electronic properties, are the best paramagnetic probes to induce magnetic anisotropy (see Section 5). Also, small EF-hand proteins (Ma & Opella, 2000; Feeney *et al.* 2001) or Co^{2+}-substituted zinc fingers (Gaponenko *et al.* 2000a) can be fused at one term of the protein to be investigated.

3.5 Interplay between different restraints

The relative weight of the various restraints in structure determination depends first of all on the number of experimental values that can be achieved for each class. Because ^{1}H and, in most cases, ^{13}C give reliable δ^{pc} values, up to some hundreds of δ^{pc} can be obtained for a small protein ($\sim$100 amino acids). In principle, rdc and Γ^{CS-DD} may also provide $>$100 restraints, because there are several large ^{1}J couplings (H_N–N, $H^{\alpha}-C^{\alpha}$, C^{α}–C', C^{α}–C^{β}) which may provide reliable rdc values (Hus *et al.* 2000; Bax *et al.* 2001) and Γ^{CS-DD} values involving ^{1}H or ^{13}C nuclei. The short-range restraints, i.e. restraints from R_{1p} and from dihedral angles of M–D coordination bonds, are much lower in number. Therefore, the effect to the overall structure quality, as measured on r.m.s.d. and Ramachandram plot, provided by δ^{pc}, is usually dominant. However, in the first coordination sphere, δ^{pc} values in practice can not be measured, due to the occurrence of contact shifts, and other restraints, like R_{1p}, Γ and contact shifts, wherever they are available and with some caution, can be used to refine the first coordination sphere. In terms of local effect of each individual restraint, R_{1p} and Γ have larger effects as they are much more localized than δ^{pc}.

The effect of Γ^{CS-DD} on the structure quality is similar to that of R_{1p} because they substantially contribute to the precision in protein regions in which usually no NOEs are available. They have the same r^{-3} dependency as δ^{pc}, but they depend on different molecular properties (Desvaux & Gochin, 1999; Bertini *et al.* 2001d; Pintacuda *et al.* 2003) and there is no redundancy between them.

The interplay between δ^{pc} and rdc deserves a comment. The magnetic anisotropy tensor can be partially averaged in the presence of internal motions and, therefore, the measured rdc and δ^{pc} are affected by these motions. If δ^{pc} can be measured in protein regions that are rigid with respect to the paramagnetic center, then $\Delta\chi^{para}$ can be obtained and used to predict δ^{pc} and rdc throughout the protein. Comparison of predicted and expected values provides an indication of the possible presence of internal mobility for specific regions of the protein. These properties of δ^{pc} and rdc have been exploited to map internal motions and domain reorientations, as it has been done in Calmodulin (Bertini *et al.* 2004a).

https://doi.org/10.1017/S0033583506004161 Published online by Cambridge University Press

4. NMR without ^{1}H detection

Sensitivity in NMR experiments depends on $\gamma^{3/2}$ of the observed nucleus and on γ of the excited one (Ernst *et al.* 1987), therefore, polarization transfer from ^{1}H to the heteronucleus and detection of ^{1}H is the obvious choice for any standard application (Bodenhausen & Freeman, 1977). However, one of the main limitations in the NMR experiments is the extent of transverse relaxation rates, which might broaden signals beyond detection and affect coherence transfer, thus making the corresponding cross-peaks disappear. The loss of signal intensity for a given heteronucleus X during coherence transfer, chemical shift evolution and magnetization transfer delays is $(\gamma_H/\gamma_X)^2$ smaller than for a ^{1}H nucleus. Therefore, passing from ^{1}H to ^{13}C detection, the loss in sensitivity due to the detection of a low γ nucleus can be more than compensated for by the smaller losses in signal intensity due to relaxation.

In paramagnetic systems, where relaxation rates essentially depends on the metal–nucleus distance, this may allow the identification of signals and cross peaks that were unobservable in ^{1}H-detected experiments (Kolczak *et al.* 1999; Bertini *et al.* 2001e; Machonkin *et al.* 2002; Arnesano *et al.* 2003a). While in ^{1}H-detected experiments the magnetization may be completely lost during the coherence transfer from ^{1}H to ^{13}C and back, because of ^{1}H relaxation, the excitation and detection of the low γ ^{13}C and the development of experiments which rely only on ^{13}C–^{13}C couplings is such that only ^{13}C relaxation is operative during coherence transfer and evolution times. The same consideration would hold, even at a larger extent, for ^{15}N nuclei, in which paramagnetism-induced relaxation is scaled down by a factor of $\sim$100 with respect to ^{1}H nuclei. The sensitivity of ^{15}N direct-detected experiments presently achieved is, however, quite low and constitutes a limitation. Nevertehless, cases have been described in which ^{15}N-detected experiments have been successfully used in paramagnetic proteins (Oh & Markley, 1990; Xia *et al.* 1995; Wilkens *et al.* 1998b; Caillet *et al.* 2006).

In Fig. 5, the line broadening effects due to coupling with a paramagnetic center are reported for the three most common nuclei. For a system containing Ce^{3+}, with $J=5/2$ and $\tau_s = 2\times10^{-13}$ s (Allegrozzi *et al.* 2000), electron–nucleus dipolar relaxation contributions can be operative up to 13 Å on ^{1}H detection, while lower limits are observed for ^{13}C and ^{15}N (8 and 6 Å respectively). At distances from the metal larger than the above values, paramagnetism-induced relaxation vanishes and the system can be treated as diamagnetic. For distances shorter than the above limits, signal linewidths are affected and signals can be broadened beyond detection. The linewidth limit for detectability depends from the type of experiment that is performed. One-dimensional experiments allow the observation of signals with several kHz linewidth, while in standard triple resonance experiments signals with $<$100 Hz linewidth are already beyond detection. Considering a detectability threshold of $\sim$1000 Hz, for the case depicted in Fig. 6, ^{1}H signals from resonances at $<$5 Å from the metal are lost, while ^{15}N signals can be observed up to 3·5 Å away from the metal center, i.e. no ^{15}N signals are lost because of paramagnetism-induced broadening. These values vary depending on the metal ion, on the magnetic field and on the molecular mass of the protein investigated. However, the ratios between limit values for ^{1}H, ^{13}C and ^{15}N are maintained. Table 3 reports the metal–nucleus distances which can roughly be associated to the useful ranges for the three different nuclei as a function of the various metal ions.

The advantages of low γ nuclei are not limited to line narrowing during acquisition but can be extended to all building blocks of a pulse sequence, provided that the exploited coherence

https://doi.org/10.1017/S0033583506004161 Published online by Cambridge University Press

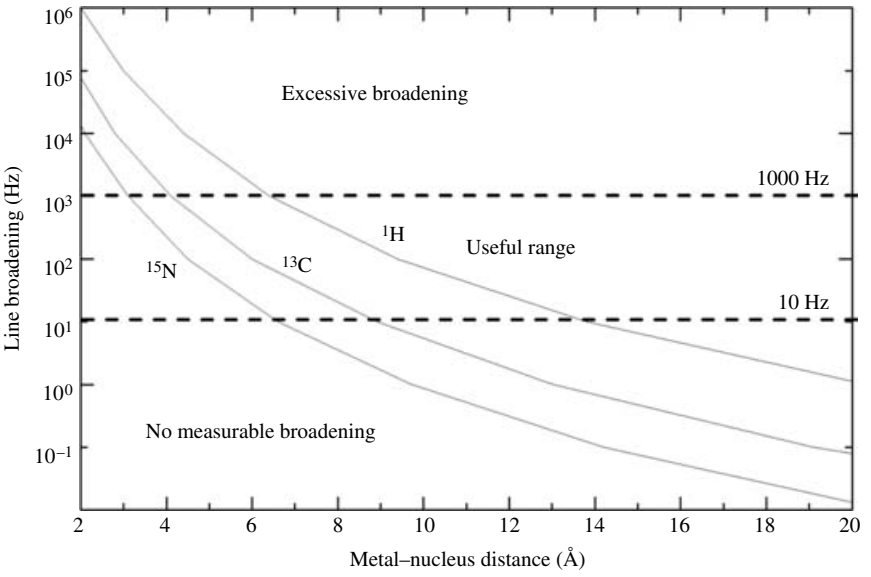


Fig. 5. Line broadening effects produced by a paramagnetic center on different nuclei. The useful linewidth range for obtaining structural information is within the dashed lines. The curves are calculated for dipolar and Curie relaxation induced at 11·7 T by an $S=5/2$ ion with $\tau_s=10^{-10}$ s in a molecule with $\tau_r=10^{-8}$ s.

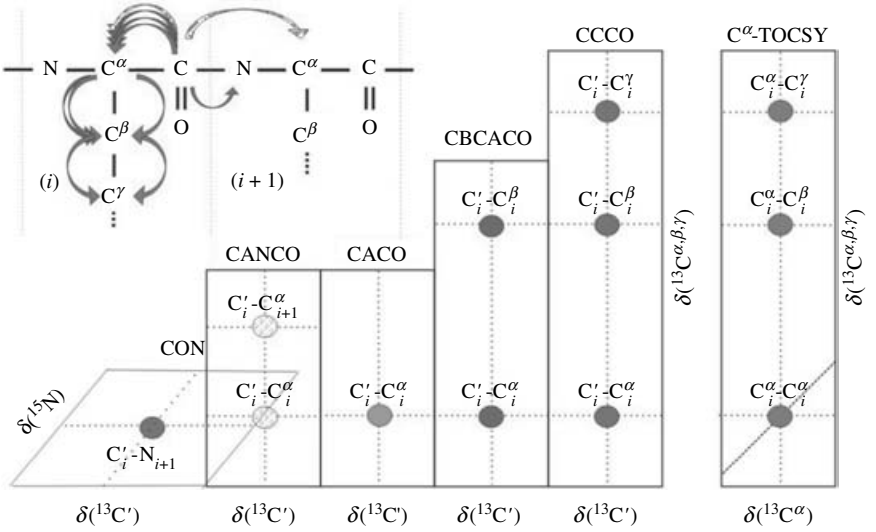


Fig. 6. Experiments used for sequence-specific assignment through purely heteronuclear NMR spectroscopy. In each panel, the cross peaks detected in that specific experiment, indicated on the top of the panel, are shown. Also the pattern of coherence transfer involved in each experiment is reported in the inset at the top. The experiments based on C′ acquisition are reported on the left side. For the sake of clarity, the 2D versions of CANCO, CACO, CBCACO and CCCO are shown. The CBCACO and the CCCO can also be acquired in the 3D mode, by evolving C^α in the third dimension, which removes ambiguities deriving from C′ degeneracy. The CON experiment is shown in a perspective view and it can be combined with CACO, CBCACO and CCCO experiments, by including N evolution, thus obtaining the corresponding 3D experiment (CACON, CBCACON and CCCON). The TOCSY experiment with C^α acquisition is reported on the right.

https://doi.org/10.1017/S0033583506004161 Published online by Cambridge University Press

https://doi.org/10.1017/S0033583506004161 Published online by Cambridge University Press

Table 3. *Metal–nucleus distances, R_{MX} (Å) corresponding to paramagnetic R_2 enhancements of 1000 and 10 s^{-1}, calculated, at 11·7 and at 21·1 T, for ^1H, ^{13}C and ^{15}N nuclei and some common paramagnetic metal ions at 298 K, taking into account dipolar and Curie contributions to transverse relaxation rates and assuming $\tau_r = 10^{-8}$ s. The upper values of τ_s reported in Table 1 were used in the calculations*

		11·7 T (500 MHz)[a] R_{MX} (Å)						21·1 T (900 MHz)[a] R_{MX} (Å)					
		$R_2^{dip}+R_2^{Curie}=1000\ s^{-1}$			$R_2^{dip}+R_2^{Curie}=10\ s^{-1}$			$R_2^{dip}+R_2^{Curie}=1000\ s^{-1}$			$R_2^{dip}+R_2^{Curie}=10\ s^{-1}$		
Paramagnetic system	S	^1H	^{13}C	^{15}N	^1H	^{13}C	^{15}N	^1H	^{13}C	^{15}N	^1H	^{13}C	^{15}N
Ti^{3+}	1/2	4·5	2·9	2·1	9·7	6·2	4·6	4·5	2·9	2·2	9·8	6·3	4·6
VO^{2+}[a]	1/2	7·9	5·0	3·8	17·1	10·9	8·2	7·9	5·0	3·7	17·1	10·8	8·1
V^{3+}	1	4·1	2·6	1·9	8·8	5·6	4·1	4·7	2·9	2·2	10·0	6·3	4·7
V^{2+}	3/2	7·9	5·3	4·0	17·1	11·4	8·6	8·0	5·2	4·0	17·2	11·2	8·6
Cr^{3+}	3/2	9·7	6·2	4·8	20·9	13·4	10·2	9·7	6·2	4·7	21·0	13·3	10·0
Cr^{2+}	2	5·5	3·5	2·6	11·9	7·6	5·6	6·6	4·1	3·1	14·1	8·9	6·6
Mn^{3+}	2	6·7	4·2	3·1	14·4	9·1	6·8	7·2	4·5	3·4	15·4	9·8	7·3
Mn^{2+}[a]	5/2	12·0	7·6	5·8	25·8	16·4	12·4	12·0	7·6	5·7	25·9	16·4	12·2
Fe^{3+} (HS)[a]	5/2	9·2	6·1	4·6	19·9	13·2	9·9	9·4	6·1	4·7	20·3	13·2	10·0
Fe^{3+} (LS)	1/2	3·3	2·1	1·5	7·0	4·4	3·3	3·6	2·2	1·7	7·6	4·8	3·6
Fe^{2+} (HS)	2	5·3	3·4	2·5	11·5	7·3	5·4	6·5	4·1	3·0	13·9	8·8	6·5
Co^{2+} (HS, 5–6 coord)	3/2	4·7	3·0	2·2	10·1	6·4	4·8	5·6	3·5	2·6	12·0	7·6	5·6
Co^{2+} (HS, 4 coord)	3/2	4·8	3·1	2·3	10·4	6·6	4·9	5·6	3·6	2·6	12·2	7·7	5·7
Co^{2+} (LS)	1/2	6·0	4·0	3·0	13·0	8·7	6·5	6·0	3·9	3·0	13·0	8·5	6·5
Ni^{2+} (5–6 coord)[a]	1	5·4	3·4	2·5	11·6	7·4	5·4	5·5	3·5	2·6	11·9	7·6	5·6
Ni^{2+} (4 coord)	1	3·7	2·4	1·8	8·1	5·1	3·8	4·5	2·8	2·1	9·7	6·1	4·5
Cu^{2+}	1/2	6·0	4·0	3·0	13·0	8·7	6·5	6·0	3·9	3·0	13·0	8·5	6·5
Ru^{3+}	1/2	3·3	2·1	1·5	7·0	4·4	3·3	3·6	2·2	1·7	7·6	4·8	3·6
Re^{3+}	2	5·3	3·4	2·5	11·5	7·3	5·4	6·5	4·1	3·0	13·9	8·8	6·5
Gd^{3+}[a]	7/2	13·2	8·4	6·4	28·5	18·1	13·7	13·4	8·4	6·3	28·8	18·2	13·6
Ln^{3+}	5/2	6·0	3·8	2·8	13·0	8·2	6·1	7·3	4·6	3·4	15·8	10·0	7·4

[a] τ_s is field dependent.

transfers never go through ^{1}H spins. We, therefore, refer to this approach as 'protonless NMR' (Bermel *et al.* in press). Throughout all the sequences that are discussed below, a broadband decoupling is applied on ^{1}H spins (or on ^{2}H spins in case of deuterated proteins) in order to avoid all coherence transfers and all couplings involving ^{1}H (or ^{2}H) spins.

Protonless heteronuclear NMR spectroscopy is not limited to paramagnetic proteins, but it has been also developed for diamagnetic proteins and turned out to be extremely useful in all cases in which ^{1}H transverse relaxation is the limiting factor, such as systems affected by chemical exchange or large molecular mass. For the latter cases, ^{13}C direct detection can be combined with uniform sample deuteration, which is a well established avenue to increase the range of systems that can be successfully investigated via NMR (LeMaster, 1990, 1994).

Also for partially unfolded systems ^{13}C-detected experiments are quite powerful as they can exploit the largest ^{13}C chemical shift dispersion even in unfolded systems at variance with the very limited ^{1}H chemical shift dispersion in these systems.

4.1 The protocol for ^{13}C-detected protonless assignment of backbone and side-chains

In order to make ^{13}C-detected methods effective, two different problems should be addressed: the low sensitivity and the ^{13}C–^{13}C couplings. The former has been overcome by hardware developments that, in less than 10 years, almost revolutionized the sensitivity of NMR spectroscopy. The use of cryogenically cooled probes (Kovacs *et al.* 2005) and the development of probes designed for optimized ^{13}C sensitivity dramatically increased the S/N ratio for ^{13}C observation. As far as homonuclear ^{13}C couplings are concerned, they are, of course, necessary for coherence transfer but are detrimental to resolution in the acquisition dimension, because carbonyl resonances are split by the strong $^{1}J_{C^{\alpha}C'}$ couplings, while C^{α} resonances experience both C^{α}–C' and C^{α}–C^{β} couplings. Several methods have been proposed for collapsing the *J*-coupling splitting, based either on homodecoupling approaches, or on spin-state selective schemes, such as In Phase-Anti Phase (IPAP) (Bertini *et al.* 2004b, c) and S^{3}E (Bermel *et al.* 2005a), both widely used in ^{1}H NMR spectroscopy (Ottiger *et al.* 1998; Andersson *et al.* 1998; Sørensen *et al.* 1997; Duma *et al.* 2003).

The ^{13}C nuclear spins with the most suitable transverse relaxation properties at high magnetic fields and in systems of high molecular mass are, in principle, the aliphatic carbon nuclei, such as $^{13}C^{\alpha}$. This is even more the case in deuterated samples. $^{13}C^{\alpha}$ signals are, however, split in quadruplets as a result of the two strong C^{α}–C' and C^{α}–C^{β} homonuclear couplings, which are $\sim$55 and $\sim$35 Hz respectively. Carbonyl nuclei present a simpler coupling pattern, with just a strong carbon–carbon one-bond scalar coupling. On the other hand, they are characterized by large CSA, that increases with the square of the magnetic field. This term constitutes the dominant effect on transverse relaxation (Zeng *et al.* 1996; Dayie & Wagner, 1997; Pellecchia. *et al.* 1999), except for those C' nuclei in the immediate proximity of the paramagnetic center, where hyperfine contributions, given by Eqs (2.11), (2.13) and (2.16), can become larger than all the diamagnetic contributions.

Within this scheme, acquisition of $^{13}C'$ is the most suitable choice for non-deuterated proteins of medium size, because of the simpler coupling pattern, while at increasing molecular weights and in the case of fully deuterated systems, direct acquisition of aliphatic ^{13}C is the most appropriate choice. The set of experiments to perform complete resonance assignment without using ^{1}H that we describe here has been built mainly by relying on the detection of $^{13}C'$ (Bertini *et al.* 2004b; Bermel *et al.* 2005a, b, in press). They are based on the most efficient

https://doi.org/10.1017/S0033583506004161 Published online by Cambridge University Press

building blocks of the conventional triple-resonance experiments (Kay *et al.* 1990; Grzesiek & Bax, 1992a, b; Sattler *et al.* 1999) which have been modified to avoid excitation and observation of ^{1}H spins. The observed pattern of peaks is shown in Fig. 6, where the couplings involved are also indicated. An analogous set of experiments can be designed to operate with direct acquisition of aliphatic ^{13}C resonances.

The exclusively heteronuclear assignment strategy starts with the most sensitive experiments, based on C′ acquisition and exploiting the large one-bond coupling constants $^{1}J_{C'C^{\alpha}}$, $^{1}J_{C^{\alpha}C^{\beta}}$, and $^{1}J_{NC'}$, as depicted in Fig. 6. The most sensitive and simplest experiment is the CACO experiment (Bermel *et al.* 2003), which yields the intra-residue C'_i–C_i^{α} correlation (n correlations for a n amino-acid protein) together with the correlations involving carbonyl/carboxylate of side-chains, i.e. C_i^{β}–C_i^{γ} for Asp and Asn and C_i^{γ}–C_i^{β} for Glu and Gln. Several variants of the CACO experiment are available (Bertini *et al.* 2005a), which were optimized according to the resolution needed to investigate the system and to its relaxation properties. Then, the CBCACO experiment exploits the $^{1}J_{C^{\alpha}C^{\beta}}$ in a COSY-type approach and provides, in addition to the C'_i–C_i^{α} correlations, also the C'_i–C_i^{β} correlations, which are useful to reduce the overlap in the CACO experiment and to identify amino acids on the basis of C^{α} and C^{β} chemical shifts (Bermel *et al.* 2005a). The remaining side-chain carbons can be identified via C–C TOCSY-based experiments, which have been developed either with carbonyl detection (Bermel *et al.* 2006) (CCCO) or with detection of aliphatic carbon nuclei (HCC-TOCSY) (Hu *et al.* 2005). When overlap is severe, CBCACO and CCCO experiments can be resolved in a third dimension, by evolving the C^{α} chemical shift to resolve ambiguities due to C′ overlap. Once the identification of intra-residue ^{13}C resonances is accomplished, connection to ^{15}N spin is performed using the CON experiment which exploits the $^{1}J_{C'N}$ coupling (Kostic *et al.* 2002). The experiment yields the sequential C'_i–N_{i+1} correlation ($n-1$ correlations for a protein of n amino acids), the C_i^{β}–N_i^{γ} correlations of Asn and the C_i^{γ}–N_i^{δ} of Gln residues. It is the most sensitive experiment involving ^{15}N nuclei and detect resonances, i.e. ^{15}N and ^{13}C′, generally characterized by a very good chemical shift dispersion. This makes CON suitable for being combined with other building blocks (CACO, CBCACO, CCCO) to yield 3D experiments (CACON, CBCACON, CCCON) with C′ in the direct acquisition dimension, C^{α} (or $C^{\alpha/\beta}$, or $C^{\alpha/\beta/\gamma\cdots}$) in a second dimension and N in the third (Bermel *et al.* 2006). Finally, inter-residue connectivities are required to perform the sequence specific assignment along the backbone chain. This can be obtained with the CANCO experiment, available in both a 2D and 3D versions (Bertini *et al.* 2004b; Bermel *et al.* 2006), in which coherence transfer from C_i^{α} and C_{i+1}^{α} to N_{i+1} and then to C_i' occurs, giving rise to the two correlations (C_i^{α}–N_{i+1}–C_i' and C_{i+1}^{α}–N_{i+1}–C_i' in the 3D experiments) necessary for sequence specific assignment (Fig. 6).

When dealing with systems characterized by efficient transverse relaxation, the exploitation of ^{13}C–^{13}C dipolar couplings between two directly bound ^{13}C nuclei is an alternative approach to experiments based on coherence transfers via scalar couplings, as suggested already since a decade for large molecules (Fischer *et al.* 1996). With the increase in molecular mass, cross relaxation rates σ_{CC} which originate from dipolar couplings and are at the basis of the NOE effect, increase while the longitudinal relaxation rates decrease. This makes homonuclear ^{13}C–^{13}C NOESY experiments competitive with scalar coupling-based transfer, whose efficiency decreases with increasing the molecular weight (Fischer *et al.* 1996).

The 'protonless' heteronuclear NMR approach has been successfully applied to the monomeric, oxidized, protein Cu(II)Zn superoxide dismutase (SOD) (Bermel *et al.* 2003), on several Ln^{3+}-substituted calcium-binding proteins (Babini *et al.* 2004; Balayssac *et al.* 2006) and on heme

https://doi.org/10.1017/S0033583506004161 Published online by Cambridge University Press

proteins containing high spin Fe^{3+} ions (Caillet *et al.* 2006). In SOD, the presence of a type-II Cu^{2+}, characterized by a relatively long τ_s of $\sim 2{\cdot}2 \times 10^{-9}$ s (Bertini *et al.* 2001f), produces dramatic signal broadening. However, the application of 'protonless' ^{13}C-detected experiments allowed the identification of resonances from all amino-acid residues with the only exception of those directly coordinated to the copper ion. A similar approach was used for the heme protein HasA, which has 176 amino acids and a heme group containing a highly paramagnetic Fe^{3+} (Arnoux *et al.* 1999). In this case, ^{13}C signals, shifted up to 700 ppm downfield, can be observed also for resonances belonging to the axial ligands, one histidine and one tyrosine (Caillet *et al.* 2006).

4.2 Protonless heteronuclear NMR experiments tailored to paramagnetic systems

As outlined at the beginning of this section, protonless heteronuclear experiments are intrinsically less affected than conventional experiments by paramagnetism-induced relaxation. It has been shown that this approach can detect ^{13}C resonances from amino acids which, due to short metal–nucleus distances, are undetectable using ^{1}H-detected experiments, even when they are tailored to fast relaxing resonances (Arnesano *et al.* 2003a; Babini *et al.* 2004; Balayssac *et al.* unpublished observations). For residues in the close proximity of the metal center, which completely escaped signal identification in ^{1}H-detected experiments, the amide HN or backbone CH groups, which cannot be identified via Heteronuclear Single Quantum Coherence (HSQC) can be recovered in one of the experiments described above.

However, ^{13}C-detected experiments for sequential assignments are based on coherence transfers which require relatively long delays. For example, in the CON experiment, the C′ magnetization is kept on the *x,y*-plane for ~ 50 ms, the time needed for the transfer of coherence 'out' to the ^{15}N spin and 'back' to $^{13}C'$ detection (Kostic *et al.* 2002; Bermel *et al.* 2005a). Even the simplest experiment of this class, the CACO experiment, requires ~ 18 ms for the C'–C^{α} coherence transfers. Therefore, like the ^{1}H-detected experiments, the ^{13}C-based approach can be further optimized for paramagnetic systems by selecting the most efficient and least affected by fast relaxation coherence transfer pathways (Bertini *et al.* 2005a).

COSY experiments have been used first for paramagnetic systems, both in the magnitude mode and in the constant time variant (Kolczak *et al.* 1999; Bertini *et al.* 2001e; Machonkin *et al.* 2002, 2004; Arnesano *et al.* 2003a). They have been applied to the oxidized form of the blue copper protein azurin (Kolczak *et al.* 1999) and to study Ln^{3+}-substituted calcium-binding proteins (Bertini *et al.* 2001e), while the constant time (CT) variant of the COSY experiment allowed the detection of further cross peaks in oxidized human Fe_2S_2 ferredoxin (Machonkin *et al.* 2002) and in CopC bound to a type-II Cu^{2+} ion (see Section 6) (Arnesano *et al.* 2003a). Several other experiments based on coherence transfer via the C^{α}–C′ scalar couplings, but also via the smaller N–C′ scalar coupling, exploiting either the single quantum or multiple quantum coherence transfer, have been developed (Kostic *et al.* 2002; Bermel *et al.* 2003; Arnesano *et al.* 2003a; Bertini *et al.* 2005a). Their advantage is that a specific coherence transfer pathway can be selected and optimized. For example, CACO experiments are usually conceived to minimize signal losses due to C′ transverse relaxation, which in general is much more efficient than C^{α}. In the presence of a paramagnetic center, C^{α} may relax faster than the coupled C′ spin, if C^{α} is closer to the metal center than C′. In this case, a CACO experiment recorded with an alternative coherence transfer pathway, optimized for fast relaxing C^{α} spins, would provide a substantial increase of C^{α}–C′ cross-peak intensity (Bertini *et al.* 2005a).

https://doi.org/10.1017/S0033583506004161 Published online by Cambridge University Press

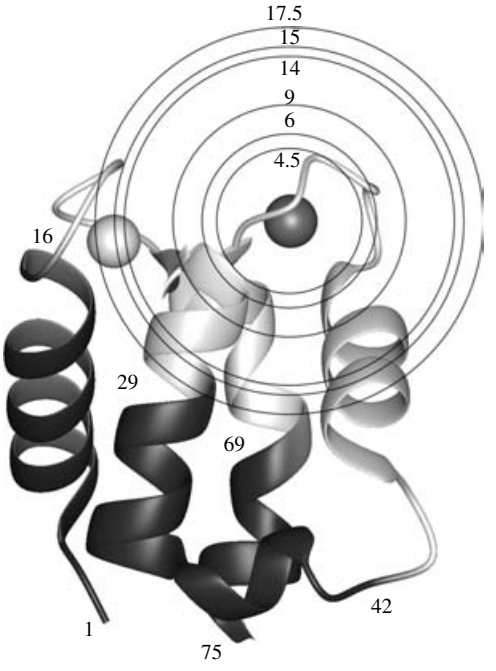


Fig. 7. Spheres within which signals, depending on the type of NMR experiment, cannot be observed in the Tm^{3+}-substituted Calbindin D_{9k}. Radii are as follows: 17·5 Å for standard ^{1}H-detected NMR experiments, 15 Å for ^{1}H experiments optimized to fast relaxing signals, 14 Å for 'standard' ^{13}C-detected experiments, 9 Å for ^{13}C-detected experiments optimized to fast relaxing signals, 6 Å from ^{13}C 1D spectra, 4·5 Å for 1D ^{15}N spectra.

The overall improvement provided by protonless heteronuclear NMR compared to ^{1}H-detected experiments can be summarized by considering a test case in which the paramagnetic center is a metal ion with a very large magnetic susceptibility anisotropy and nuclear relaxation dominated by the CS contribution, like Tm^{3+}. When Tm^{3+} replaces native calcium ion in Calbindin D_{9k}, the effect is such that $\sim$50% of the resonances in the 75 amino-acid protein are significantly affected by paramagnetism and in standard ^{1}H-detected experiments ^{1}H signals at distances shorter than 17·5 Å from the metal center are not detected (Fig. 7). When ^{1}H-detected experiments are optimized to minimize losses due to fast ^{1}H transverse relaxation, the blind sphere around the metal center is reduced to 15 Å, indicating that still complete backbone assignment is not feasible for $\sim$40% of the amino acids, and no sequential assignment is possible. The protonless heteronuclear strategy described in Section 4.1 succeeds to reduce the blind sphere to 14 Å away from the Tm^{3+} while a more significant improvement in signal detectability up to 9 Å is provided when the same protonless heteronuclear experiments are optimized for fast relaxation. Broader ^{13}C signals arising from resonances which are as close as 6 Å from the metal center can be detected in 1D ^{13}C experiments. These resonances cannot be assigned via any 2D experiment, because coherence transfer and NOE effects are dramatically quenched by fast relaxation. However, signals detected through 1D experiments can be assigned on the basis of their pseudocontact shifts. Through ^{15}N 1D experiments, signals could be identified up to 4·5 Å away from the Tm^{3+}. Overall, using the ensemble of these techniques, at least one resonance could be identified for each of the 75 amino

https://doi.org/10.1017/S0033583506004161 Published online by Cambridge University Press

Table 4. *The effect of varying the rotational correlation time (i.e. the molecular mass of the protein) and the electronic correlation time τ_s in the R_{1p}/R_{2p} ratio of ^{13}C nuclei. Only dipolar and Curie contributions were considered at 11·7 T (500 MHz) and 21·1 T (900 MHz)*

	τ_r	τ_s	R_{2p}/R_{1p} at 11·7 T	R_{2p}/R_{1p} at 21·1 T
Cu^{2+}	4 ns	5 ns	3·2	7·8
Cu^{2+}	20 ns	5 ns	7·8	22·7
Cu^{2+}	4 ns	1 ns	1·4	2·0
Cu^{2+}	20 ns	1 ns	1·6	2·5
Dy^{3+}	4 ns	0·5 ps	7·1	21·0
Dy^{3+}	20 ns	0·5 ps	110	393

acids of the protein, including those residues directly bound to the metal center (Balayssac *et al.* 2006).

The applicability of homonuclear ^{13}C–^{13}C NOESY experiments in paramagnetic proteins is strongly dependent on the relative values of R_1 and R_2 (Banci *et al.* 1991). Basically, the larger is the R_2/R_1 ratio, the more the system is suitable to be characterized through R_1-based experiments (i.e. NOESY) rather than through scalar coupling-based experiments. When relaxation is dominated by the electron-nucleus dipolar relaxation, the R_2/R_1 ratio can be relatively low; it is essentially modulated by τ_s, even for proteins with τ_r around 20 ns, and R_1 is still quite large, as shown in Table 4. On the other hand, when CS relaxation is the dominant contribution to R_2 (see Section 2.4), the R_2/R_1 increases dramatically, and the R_1-based experiments becomes useful. For the Tb^{3+}-substituted calcium-binding protein human oncomodulin, ^{13}C–^{13}C NOEs have been shown to be more efficient than CACO or ^{13}C–^{13}C COSY to reduce the blind sphere around the metal center (Babini *et al.* 2004). Twenty-six C^{α}–C' connectivities, which escaped detection in a CACO-type experiment, were observed in a ^{13}C–^{13}C NOESY experiment tailored to fast relaxing systems, in a 12 kDa protein (Babini *et al.* 2004). This reduced the blind sphere around the metal center from 11 Å , as obtained from CACO experiments, down to 8 Å .

5. The use of lanthanides as paramagnetic probes

As extensively discussed in the previous sections, NMR experiments tailored to obtain paramagnetism-based restraints are mandatory to determine structures in solution of paramagnetic metalloproteins with a good precision also in the proximity of the paramagnetic center. The exploitation of paramagnetism-based restraints can be extended to diamagnetic metalloproteins, when the diamagnetic metal ion can be substituted with a suitable paramagnetic metal ion with no significant structure changes. In these conditions the restraints obtained on the paramagnetic derivative can be combined with standard structural restraints obtained on the native diamagnetic form of the protein, to increase structural precision and accuracy. Even in systems without a native metal-binding site, tags have been built to coordinate a Ln^{3+} metal ion. These metal ions, which have been used since decades as shift (Reuben, 1973; Sykes & Lee, 1983; Geraldes & Luchinat, 2003) or relaxing agents (Geraldes & Luchinat, 2003), have high affinity for oxygen and nitrogen donor atoms, preferring high coordination numbers. Therefore, they are an ideal vicariant of Ca^{2+} in calcium-binding proteins.

https://doi.org/10.1017/S0033583506004161 Published online by Cambridge University Press

The f^n configuration of Ln^{3+} ions gives rise to several free-ion terms that, upon spin–orbit coupling, provide, except for the f^7 configuration, several closely spaced energy levels which are further split by crystal field effects (Bertini *et al.* 2001f). As the spin–orbit coupling is strong, the free-ion terms are described by the spin–orbit quantum number J which replaces the purely electron spin quantum number S in all equations of Section 2 (Bleaney, 1972).

The presence of low-lying excited states induces very short electron relaxation times, in the range of $1–7 \times 10^{-13}$ s with the exception of only Gd^{3+} (Bertini *et al.* 2001f). Consequently, line broadening due to DD coupling [Eq. (2.13)] is small and transverse relaxation is dominated by the CS term [Eq. (2.16)], also due to the high J values.

All Ln^{3+} ions (but not Gd^{3+}), each with specific values, have large magnetic susceptibility anisotropy, making them very effective sources of pseudocontact shifts and residual dipolar couplings. The NMR spectra of Ln^{3+}-containing proteins typically show tens of signals which experience shifts larger than 10 ppm and are, therefore, shifted well outside the diamagnetic envelope (Lee & Sykes, 1980; Sykes & Lee, 1983). Because of the large magnetic anisotropy, usually, a few hundreds of δ^{pc} can be safely measured in a range 0·1–80 ppm (Capozzi *et al.* 1993; Balayssac *et al.* 2006). The distance up to which reliable δ^{pc} can be measured and their maximum value depend on the metal ion and on its $\Delta\chi$ values. For Dy^{3+}, Tb^{3+} and Tm^{3+}, which have the largest $\Delta\chi$ values among lanthanides, the effect propagates far in space and measurable δ^{pc} can be observed for nuclei up to 40 Å away from the paramagnetic center (Allegrozzi *et al.* 2000). However, these metal ions also have large J and g_J values and, therefore, induce large CS relaxation, making signals undetectable in a sphere around the metal center with a relatively large radius. ^{1}H signals are lost within 13–15 Å from the metal (Allegrozzi *et al.* 2000; Balayssac *et al.* 2006), while ^{13}C signals cannot be detected within 7–9 Å from the metal and ^{15}N signals can be observed up to 4–5 Å from the metal. On the other hand, metal ions with smaller $\Delta\chi$ values and smaller contributions to relaxation allow the detection of ^{1}H signals even of coordinating residues. A typical example is Ce^{3+}, which provides measurable δ^{pc} shifts up to 15 Å from the metal but for which ^{1}H signals are lost within $\sim$5 Å from the metal (Allegrozzi *et al.* 2000).

The resulting picture is that we can not define *a priori* the 'best lanthanide', but the choice of the metal ion is dictated by the regions in which information are searched for. Ce^{3+} provides information on the immediate proximity of the metal center and, therefore, it is useful to characterize the first coordination sphere, where usually the classical NMR restraints are scarce. δ^{pc} up to 40 Å away, provided by other Ln^{3+} such as Dy^{3+}, Tm^{3+} or Tb^{3+}, are useful to map protein–protein interactions or to address structural/conformational changes far away from the metal center. As for small calcium-binding proteins the 40 Å limit is often larger than the radius of the molecule, therefore, δ^{pc} can be also be measured outside the protein on other molecules interacting with it (Feeney *et al.* 2001). This is an important property which can be successfully exploited for the structure determination of protein–protein complexes.

Furthermore, because of the same structural properties of the various Ln^{3+}-substituted derivatives, a different set of δ^{pc} can be obtained for each different Ln^{3+} and the independent sets of δ^{pc} can be fitted and used together. The available programs for structure calculations can handle different δ^{pc} datasets, each of them depending on its own tensor. Therefore, the use of different lanthanides enlightens the proteins from 0 up to 40 Å away from the metal and dramatically improves the structural resolution, as different sets of data, depending on different tensors, all have to fit to the same structural conformation.

https://doi.org/10.1017/S0033583506004161 Published online by Cambridge University Press

Table 5. *Effect of each class of paramagnetism-based restraints on structure quality. All data have been collected on the Ce^{3+} substituted Calbindin D_{9k} but δ^{pc}, which were collected also on other 10 metal ions of the Ln^{3+} series* (*Bertini* et al. *2001b*)

Restraints used	Number of restraints	r.m.s.d. from the final average structure	Backbone r.m.s.d. for the family of structures	Penalty function (Å^2)	Ramachandram plot statistics (% most favored regions)
Diamagnetic only	2042	1·01	0·69	0·22–0·32	83·1
Diamagnetic and ligands[a]	2052	0·9	0·61	0·22–0·30	84·6
Diamagnetic, ligands and T_1	2078	0·65	0·55	0·23–0·33	83·1
Diamagnetic, ligands and rdc	2116	0·67	0·54	0·61–0·69	87·7
Diamagnetic, ligands and δ^{pc}	3790	0·46	0·33	0·74–0·88	86·2
Diamagnetic, ligands, δ^{pc} and rdc	3854	0·35	0·25	1·19–1·31	89·2
Diamagnetic, ligands, δ^{pc} and T_1	3816	0·40	0·32	1·22–1·45	89·2
Diamagnetic, ligands, T_1 and rdc	2142	0·59	0·30	0·66–0·74	84·6
All	3880	—	0·25	1·74–1·90	92·3

[a] Residues directly bound to the metal center are identified via the analysis of contact shifts and a link between the metal ion and metal donor atoms is used within structure calculations.

The large $\Delta\chi$ values make Ln^{3+} the most suitable probes to induce self-orientation in proteins. Of course, this is especially true for Dy^{3+}, Tb^{3+} and Tm^{3+} which induce, at 700 MHz, rdc up to 18 Hz on HN couplings (Biekofsky *et al.* 1999; Barbieri *et al.* 2002b). These values are of the same order of magnitude as those usually obtained with orienting media (Barbieri *et al.* 2002b). Small calcium-binding proteins have negligible $\Delta\chi^{dia}$ contributions, so that the same $\Delta\chi^{para}$ tensor accounts for both δ^{pc} and rdc (Barbieri *et al.* 2002b). As the $\Delta\chi^{para}$ tensor can be obtained with a high accuracy from δ^{pc}, this is an advantage with respect to the use of orienting media. The independent knowledge of the magnetic susceptibility anisotropy allows one to predict rdc values and to compare them with the experimental values thus providing information, when they do not match, on internal dynamics (Wöhnert *et al.* 2003; Ikegami *et al.* 2004).

The potentialities of lanthanides have been applied to the protein Calbindin D_{9k} as a test case. Calbindin D_{9k} is a small (75 amino-acid) protein which contains two EF-hand motifs separated by a short linker region and which can accommodate two Ca^{2+} ions with different affinity properties (Akke *et al.* 1991). As Ln^{3+} ions have higher affinity for site II than Ca^{2+} (Vogel *et al.* 1985), selective metal substitution can be achieved giving rise to a CaLnCb derivative containing a single paramagnetic center. Simple ^1H–^{15}N and ^1H–^{13}C HSQC experiments, collected on 11 different Ln^{3+} ions, provided 11 different sets of rdc and δ^{pc}. From the analysis of the latter, the $\Delta\chi$ tensor for each metal ion was calculated (Bertini *et al.* 2001c). A set of R_{1p} restraints was obtained for the Ce^{3+} derivative which contributed to define the first coordination sphere. The residues directly bound to Ce^{3+} were identified via ^{13}C NMR experiments (Bertini *et al.* 2001e) and the identified metal-donor bonds were used as structural restraints. This ensemble of 1838 paramagnetism-based restraints, more than 90% of which are δ^{pc}, was used together with a similar number of diamagnetic restraints, 90% of which are NOEs, to calculate the structure (Bertini *et al.* 2001b). The structure obtained using only the diamagnetic restraints has a backbone r.m.s.d. of 0·69 Å, and is, therefore, already relatively well resolved (first line of Table 5). When the diamagnetic restraints are used together

https://doi.org/10.1017/S0033583506004161 Published online by Cambridge University Press

with those arising from paramagnetism, the backbone r.m.s.d. decreases to 0·25 Å, and the quality of the Ramachandram plot substantially improves.

The effect of introducing different classes of restraints into structure calculation can be analyzed with respect to their contributions to precision, accuracy, and agreement among the various classes of constraints. The addition of a large number of paramagnetism-based restraints is accomplished by small increase in penalty function, which originates only from the paramagnetism-based restraints, thus indicating that the classical and the paramagnetism-based restraints are consistent each other. The introduction of coordination bond restraints decreases the r.m.s.d., at no cost for the penalty function and structure quality (Table 5, line 2). δ^{pc} have a high impact on the final quality of the solution structure, as observed when the different classes are used independently in calculations (Table 5, lines 3–5). Pseudocontact shifts determine a decrease in r.m.s.d. from 0·61 to 0·33 Å and provide the dominant contribution to structure precision, according to the fact that $\sim$90% of paramagnetism-based restraints are δ^{pc}. It should also be noted that only 64 rdc, added to 1738 δ^{pc}, provide a remarkable contribution, especially to the quality of the Ramachandran plot, as observed in Table 5 (line 4). This behavior confirms the relevance of the rdc restraints in general, and those arising from the orientation induced by a paramagnetic center in particular. In Table 5 the r.m.s.d. values between each average structure obtained with subsets of restraints and the average final structure are also reported. The addition of a subset of restraints in calculations not only leads to a family with lower r.m.s.d., but also provides a mean structure which can differ from the one obtained with diamagnetic restraints only. Therefore, each subset of restraints affects not only the precision, but also the accuracy of the final family. There is a synergism among the various paramagnetism-based restraints; rdc defines the overall protein structure, δ^{pc} affects a relatively large region far from the metal center, while the first coordination sphere is refined by R_1 restraints and by the links between the metal ion and the ligands, which are unambiguously identified via contact shifts. The deviation of the average structure calculated only with a subset of the available experimental restraints from the final average structure decreases as the number of sets of paramagnetism-based restraints increases and, therefore, the final structure is not only more precise but also more accurate. Figure 8 shows the comparison between the solution structure obtained with NOEs and dihedral angles with that obtained upon addition of the paramagnetism-based restraints.

The number of paramagnetic restraints can be larger than those used in this assessment, as in the example above, δ^{pc} for all atoms were used only for Ce^{3+}, while for all other lanthanides only δ^{pc} of the backbone amide groups were included. Therefore, the complete assignment of each metal-substituted derivative may produce an additional number of δ^{pc}. In a 75 amino-acid protein, such as in the presently reported case, from 300 to 700 δ^{pc} can be obtained for each different Ln^{3+} metal ion. In principle, up to $\sim$5000 δ^{pc} shifts can be obtained.

The use of paramagnetism-based restraints towards solution structure is not focused only on the increase of precision and accuracy, but they can also be used as a tool to perform quick solution structure determination, which can be relevant for structural genome projects. For a number of years, efforts have been made to determine NMR solution structures with experimental restraints which can be quickly determined (Hus *et al.* 2000) and to develop fast methods to identify the backbone fold (Bertini *et al.* 2002b; Banci *et al.* 2005a). δ^{pc} and relaxation rates are easier to obtain than NOEs and dihedral angles, and may, therefore, contribute to this goal. Indeed, a set of paramagnetism-based restraints succeeded, again in the case of CaLnCb, to provide the correct protein fold even in the absence of NOEs (Barbieri *et al.* 2004).

https://doi.org/10.1017/S0033583506004161 Published online by Cambridge University Press

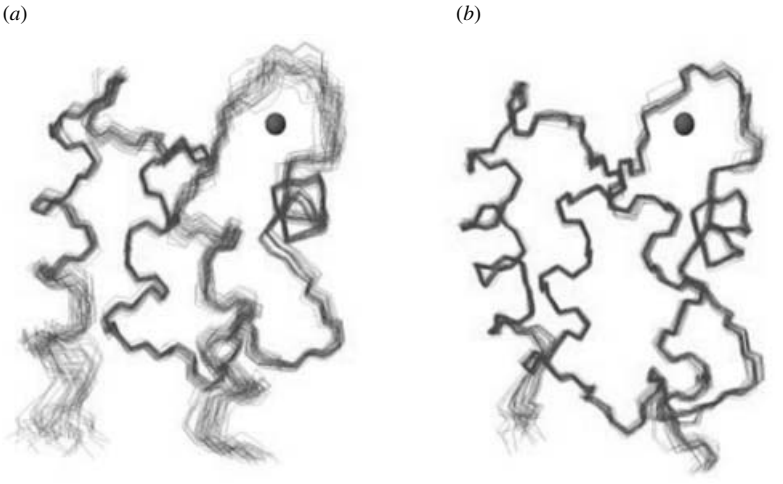


Fig. 8. Family of 30 conformers of Ln^{3+}-substituted Calbindin D_{9k} calculated using only diamagnetic restraints (*a*) and with the inclusion of all the paramagnetism-based restraints (*b*) (see also Table 5).

The interplay between δ^{pc} and rdc can be used to monitor internal dynamics and domain reorientation. Calmodulin is a two-domain calcium-binding protein, capable of binding up to 4 Ca^{2+} ions, which constitutes a paradigm case in structural biology for the characterization of domain reorientation (Chou *et al.* 2001). One of the 4 Ca^{2+} ions, in the N-terminal domain, has been replaced either with Tb^{3+} or with Tm^{3+} ion (Bertini *et al.* 2004a) and δ^{pc} and rdc were measured for both derivatives. The four sets of NMR observables were used to assess domain reorientation. δ^{pc} of the N-terminal domain allows us to determine the $\Delta\chi$ parameters for both Tb^{3+}- and Tm^{3+}-substituted Calmodulin. The δ^{pc} and rdc values measured for the C-terminal domain are, however, completely inconsistent with the values expected on the basis of the $\Delta\chi$ parameters, as the experimental rdc (Fig. 9*b*) are about one order of magnitude smaller than those of the N-term domain (Fig. 9*a*). This behavior is indicative of the presence of internal motions. However, the rdc calculated and averaged over all the sterically allowed conformations are much smaller (Fig. 9*c*) than the experimental ones (Bertini *et al.* 2004a). On the other hand, the experimental rdc can be reproduced with the C-terminal domain sampling a region of space inscribed in an elliptical cone, tilted by 30° with respect to the direction of the N-terminal part of the interdomain helix, as depicted in Fig. 10. Therefore detailed analysis of rdc not only provide hints on the presence of internal motions but also contributes to a detailed description of them.

6. The case of Cu(II) proteins

Copper is an essential metal ion for life (Linder, 1991; Pena *et al.* 1999), as witnessed by the large number of copper-containing proteins and cuproenzymes, that are being continuously discovered, which are involved in a variety of cellular functions (Frausto da Silva & Williams, 2001; Bertini *et al.* 2001h, 2002).

Copper has two magnetically active isotopes ^{63}Cu and ^{65}Cu, both having a spin quantum number $I = 3/2$, and therefore a quadrupole moment. The coupling between the quadrupole

https://doi.org/10.1017/S0033583506004161 Published online by Cambridge University Press

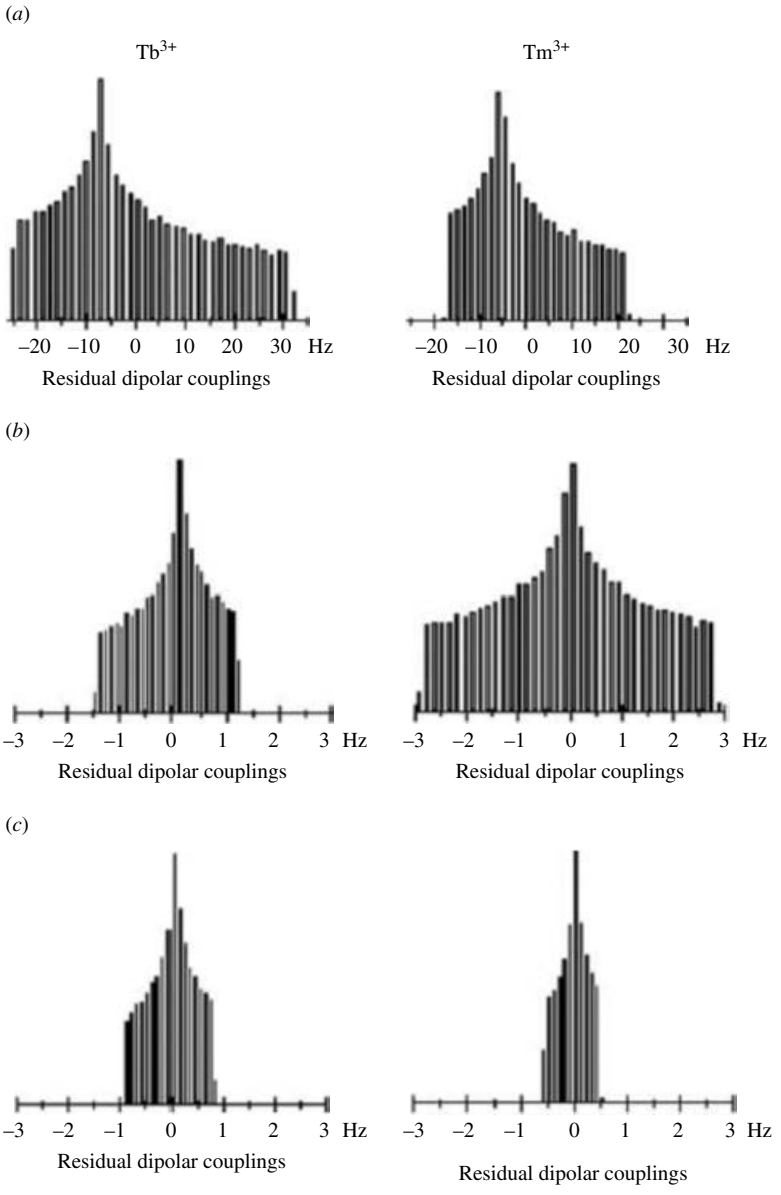


Fig. 9. Distribution of $^{1}H–^{15}N$ rdc values observed in Tb^{3+}- (left) and Tm^{3+}- (right) substituted Calmodulin: (*a*) experimental rdc in the N-terminal domain, (*b*) experimental rdc in the C-terminal domain, (*c*) rdc in the C-terminal domain calculated for the sterically allowed, uniformly sampled, conformations.

moment and the nuclear spin moment of the metal center in a slow-rotating molecule and in an asymmetric environment, such as a protein, increases the nuclear relaxation rates of copper nuclei at such extent to make their linewidths too broad to be detected (Harris & Mann, 1978). Therefore NMR can be applied only to protein nuclei (^{1}H, ^{13}C, ^{15}N).

Copper in proteins can assume two oxidation states, Cu(I) and Cu(II), and in a few cases a mixed valence state (e.g. in multi-copper centers). Cu(I) is a d^{10} metal ion and, as it does

https://doi.org/10.1017/S0033583506004161 Published online by Cambridge University Press

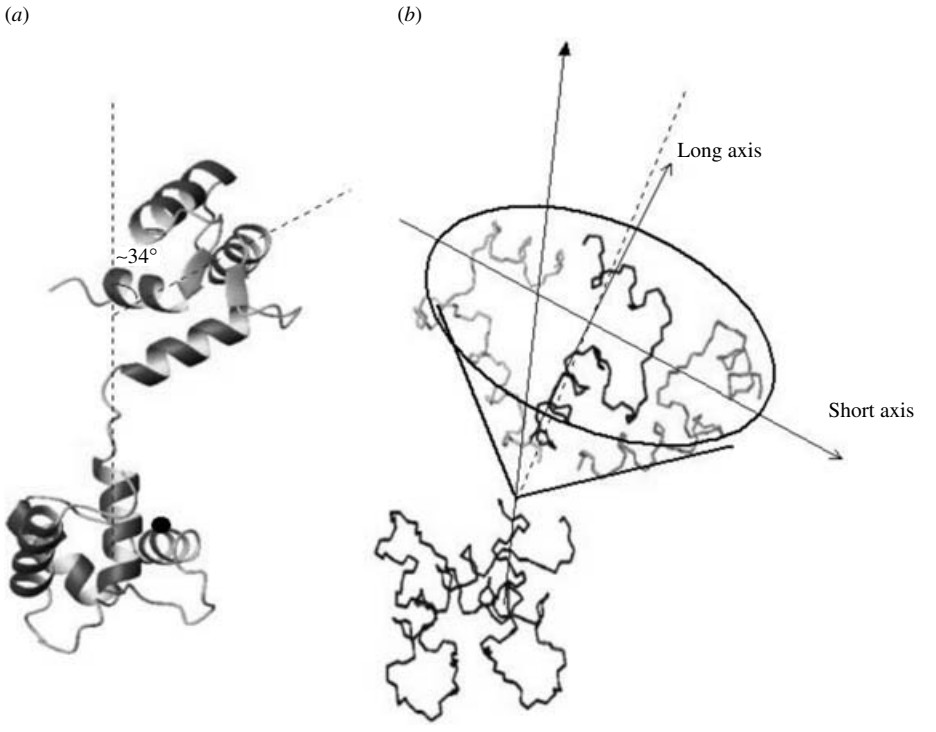


Fig. 10. Domain reorientation in Calmodulin. The axes of the two domains are tilted by $\sim 30^{\circ}$ (*a*). The C-terminal domain may assume an ensemble of different conformations defined in an elliptical cone (*b*). These conformations provide average δ^{pc} and rdc in good agreement with the experimental data.

not have unpaired electrons, it is diamagnetic. In contrast, Cu(II) has a dramatic effect on NMR spectra (Banci *et al.* 1991; Bertini *et al.* 2001f), being a d^9 metal ion with a single unpaired electron, and consequently paramagnetic.

As described in Section 2, the hyperfine coupling between the unpaired electron and nearby nuclei affects both chemical shifts and relaxation rates. Cu(II) has excited electronic states at relatively high energy, which produce small orbital contributions to the electronic spin moment. As a consequence, the magnetic anisotropy of Cu(II) is generally small as is the pseudocontact contribution to chemical shifts. Therefore, signal spreading in NMR spectra is limited and signals of nuclei, broadened due to hyperfine coupling, fall under the diamagnetic envelope, unless they experience contact shifts. The high-energy separation between the ground and the excited electronic levels is also the origin of the relatively slow relaxation rates of Cu(II) with respect to other metal ions (Table 1). In copper proteins where Cu(II) is tetragonally coordinated by nitrogen and oxygen atoms [type-II Cu(II)], the electron relaxation time τ_s, which dominates the correlation time τ_c for slow-rotating systems, is in the order of 10^{-8}–10^{-9} s (Table 1) (Banci *et al.* 1991). In blue copper proteins, where Cu(II) has a trigonal geometry and is coordinated by at least one cysteine [type-I Cu(II)] (Vila & Fernández, 2001; Nersissian & Shipp, 2002), the excited levels are lower in energy due to the interaction between the lone pair of the sulfur of the cysteine with the copper d electrons, and electron relaxation is faster than in type-II copper ions, in the order of 10^{-10} s (Koenig & Brown, 1991; Kroes *et al.* 1996; Bertini *et al.* 2001f).

https://doi.org/10.1017/S0033583506004161 Published online by Cambridge University Press

Table 6. *Dipolar and Curie contributions to R_2 (s^{-1}) and dipolar contribution to R_1 (s^{-1}) of ^1H, ^{13}C and ^{15}N nuclei at 5 Å and at 10 Å from Cu(II), calculated at 21·1 T (900 MHz), at 298 K and assuming $\tau_r = 10^{-8}$ s, and $\tau_s = 1 \times 10^{-10}$ s for type-I Cu(II), and $\tau_s = 5 \times 10^{-9}$ s for type-II Cu(II). The corresponding contributions to linewidth, $\Delta\nu$, are equal to R_2/π*

			21·1 T (900 MHz)[a]					
			$r = 5$ Å			$r = 10$ Å		
Paramagnetic system	τ_s (s)	Nucleus type	R_1^{dip}	R_2^{dip}	R_2^{Curie}	R_1^{dip}	R_2^{dip}	R_2^{Curie}
Type-I Cu^{2+}	1×10^{-10}	^1H	357	491	70	5·6	8	0
		^{13}C	29	34	5	0·4	0·5	0
		^{15}N	5	5	0	0·1	0	0
Type-II Cu^{2+}	5×10^{-9}	^1H	44	10550	70	0·7	165	0
		^{13}C	43	687	5	0·7	11	0
		^{15}N	35	126	0	0·5	2	0

[a] Magnetic field strength and proton Larmor frequency (in parentheses).

The contact contribution to relaxation, which is operative only on nuclei separated by a few chemical bonds from the Cu(II) ion and modulated by τ_s (see Section 2.4), has been observed in blue copper proteins for the β protons of the cysteine ligand (see below). The dipolar coupling, as with the unpaired electron in macromolecular systems, is dominated by τ_s, due to slow protein tumbling (Solomon, 1955), and therefore $\tau_c = \tau_s$. Paramagnetic enhancement of R_2 of nuclei affects their signal linewidth and detectability (Table 6). From the Solomon equations it appears that, in the high field limit, a given nucleus at the same distance from Cu(II) has larger signal linewidth in type-II copper proteins than in blue copper proteins. CS relaxation in Cu(II) proteins does not contribute much, due to the small S value, and, therefore, it can usually be neglected (Bertini *et al.* 2001f). For completeness, one should mention type-III copper proteins, where two Cu(II) ions are antiferromagnetically coupled. Such coupling decreases the overall magnetic susceptibility and decreases the electron relaxation times (Murthy *et al.* 1997; Clementi & Luchinat, 1998), both effects leading to a decrease in linewidths and to a much better detectability of the NMR lines (Holz *et al.* 1998; Salgado *et al.* 1998). For the features discussed above, NMR characterization of type-I and type-II Cu(II) proteins therefore represents a challenge (Banci *et al.* 1991; Bertini *et al.* 2001f).

The structure of a few type-I Cu(II)-containing proteins have been determined in the past years (Bertini *et al.* 2001a; Bertini & Pierattelli, 2004). The identification of ^1H signals (Bertini *et al.* 1999a) arising from residues bound to Cu(II) provided: Cu–S–C–H angles for the coordinated cysteine, R_1 restraints for hyperfine-shifted signals of coordinated histidines and methionine, 1D NOE to establish through space connectivites between protons of the metal-binding groups and those of the second coordination sphere. The exploitation of all the available expertise lead to the obtaining of solution structure with relatively good precision for residues close to the Cu(II) ion (Bertini *et al.* 2001a).

NMR structure determination of proteins containing type-II Cu(II), which experience a variety of structural and coordination environments for the Cu(II) ion (Adman, 1991; Lehnert *et al.* 2001), is more challenging than for type-I Cu(II) proteins. At high magnetic fields the dependence of nuclear R_1 and R_2 values with τ_s, which dominates τ_c (Table 6, Fig. 11) shows that, in type-II Cu(II) proteins, in addition to a more dramatic line broadening than in type-I

https://doi.org/10.1017/S0033583506004161 Published online by Cambridge University Press

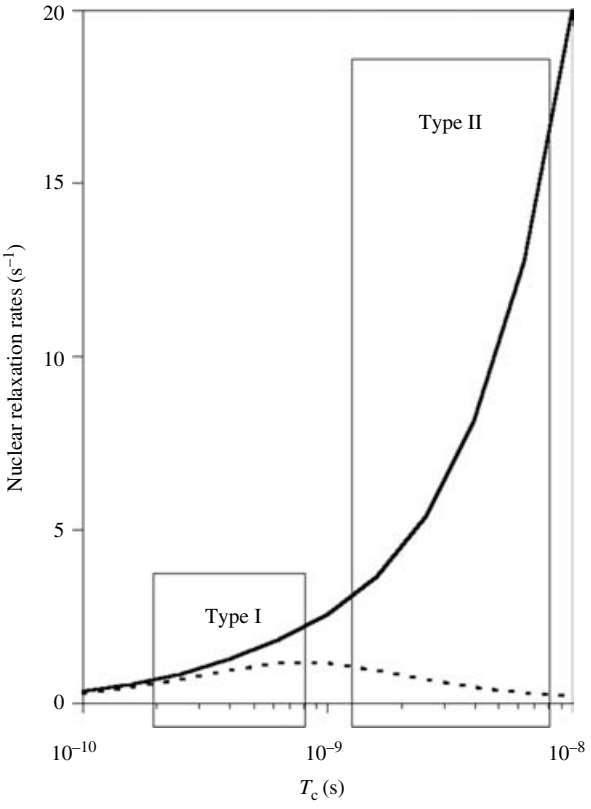


Fig. 11. Plot of the theoretical electron-nucleus dipole–dipole contribution to longitudinal (·····) and transverse (——) relaxation rates as a function of the correlation time τ_c calculated at 16·4 T (176·1 MHz resonating frequency for carbon) (Arnesano *et al.* 2003a).

copper proteins, the longitudinal relaxation rates decrease, thus preventing the use of ^{1}H-based NMR experiments, even if optimized for fast relaxing signals (e.g. fast recycle delays) (Piccioli *et al.* 1995; Bertini *et al.* 1996). For these reasons, until recently, the detection and assignment of signals in the vicinity of type-II Cu(II) was unexplored, being considered impossible.

The recent advancements in NMR experiments based on ^{15}N and/or ^{13}C direct detection have opened new avenues for solution studies of paramagnetic proteins containing unfavorable metal ions, such as type-II Cu(II). The purely heteronuclear approach was originally applied to Cu(II)–CopC, a protein involved in copper trafficking and homeostasis in bacteria (Silver, 1996). CopC is able to bind Cu(I) and Cu(II) at two different sites that are 30 Å apart (Arnesano *et al.* 2003b). Structures of CopC in the apo (Arnesano *et al.* 2002) and in the Cu(I)-bound forms (Arnesano *et al.* 2003b) were solved using standard NMR techniques, with the aid of XAS to define the copper-binding site. The analysis of the Extended X-ray Absorption Fine Structure (EXAFS) region of the XAS describes the coordination sphere of a metal ion, namely the type and number of metal ligands and extremely accurate bond distances (<0·0 Å) (Koningsberger & Prins, 1988). Further information on the electronic structure of the metal ion and its coordination geometry can be obtained from the analysis of the edge and pre-edge regions of the spectrum (Banci *et al.* 2005b). In this way, the EXAFS data provide the missing constraints between the metal ion and the protein frame, which can then be used to

https://doi.org/10.1017/S0033583506004161 Published online by Cambridge University Press

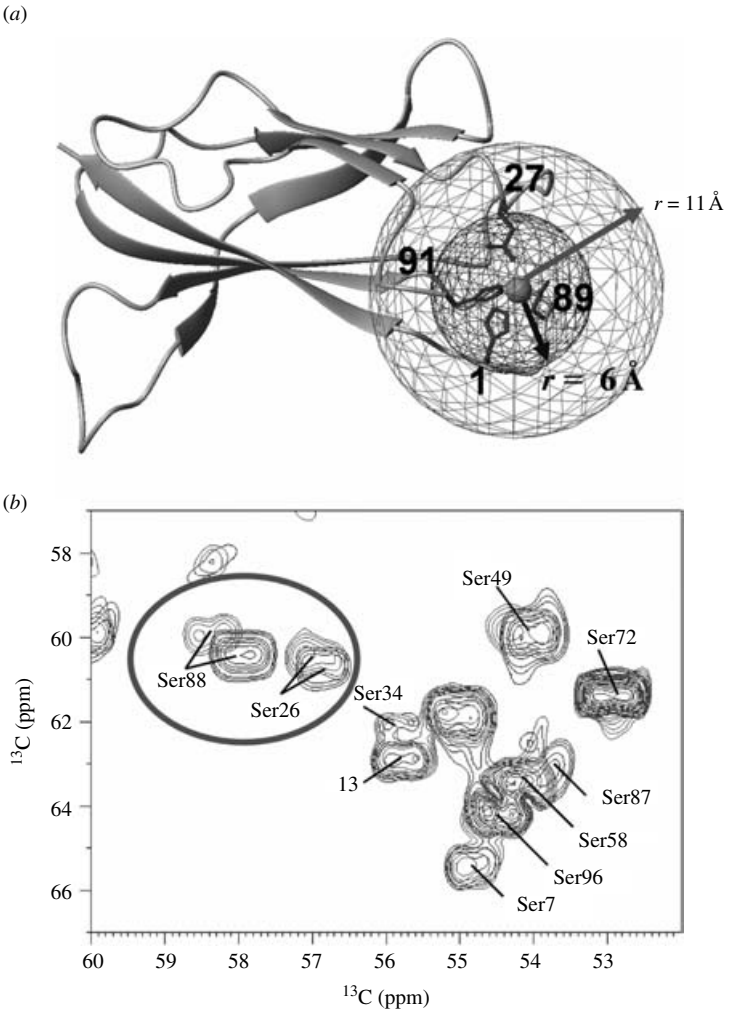


Fig. 12. (*a*) Ribbon drawing of the *Pseudomonas syringae* Cu(II)–CopC structure showing the secondary structure elements. The copper atom is represented as a gray sphere. The four ligands (His1, Glu27, Asp89, and His91) are represented as sticks. The detection limits of NMR are shown as concentric spheres centered on the copper atom. The red sphere represents the blind region when using ^{1}H detection, while using NMR experiments based only on heteronuclei the blind region is restricted to the smaller sphere. (*b*) Region of ^{13}C–^{13}C CT-COSY spectra of apo (dark gray contours) and Cu(II)–CopC (light gray contours) showing C^{α}–C^{β} connectivities of serine residues. The circle indicates serine residues whose amide signals are not detectable in ^{1}H–^{15}N HSQC spectra of Cu(II)–CopC (Arnesano *et al.* 2003a).

complete the structure determination by NMR. In the case of Cu(II)–CopC, extensive broadening of NMR signals occurs around the type-II Cu(II)-binding site. Using standard HSQC experiments recorded on Cu(II)–CopC, no ^{1}H–^{15}N cross peak is detected inside a sphere of ∼11 Å centered on copper. Because of the relatively small R_1 in type-II Cu(II) proteins (Table 6, Fig. 11) little information can be recovered from HSQC experiments optimized for fast relaxing signals. In contrast, using ^{13}C, ^{15}N-tailored experiments, the detection limit is reduced to a sphere of ∼6 Å radius (Fig. 12*a*) (Arnesano *et al.* 2003a). 2D ^{13}C–^{15}N HSQC and ^{13}C–^{13}C CT-COSY

https://doi.org/10.1017/S0033583506004161 Published online by Cambridge University Press

spectra have been used to assign ^{13}C and ^{15}N nuclei of 15 residues that were inaccessible from proton NMR spectroscopy (Arnesano *et al.* 2003a) (Fig. 12*b*). Through the ^{13}C–^{13}C CT-COSY experiment, ^{13}C longitudinal relaxation rates were determined and, therefore, metal–^{13}C distance constraints were obtained. Only residues directly bound to Cu(II), i.e. two histidines and two carboxylate groups, still escaped ^{13}C detection. However, complementary information obtained from EPR, nuclear magnetic relaxation dispersion (NMRD) and EXAFS experiments were fruitfully combined with NMR structural data to structurally define the Cu(II) coordination (Arnesano *et al.* 2003a). Metal–nucleus distance constraints from R_1 measurements, together with pseudocontact shifts, measured for both ^1H and ^{13}C nuclei, have been used to locate the Cu(II) ion in CopC, thus obtaining a refined structural model with a resolution comparable to that of diamagnetic apo and Cu(I) structures (Arnesano *et al.* 2003a). If solvent molecules interact with the Cu(II) ion in the protein and they exchange fast with the bulk ones, the water proton nuclear R_1 contains a contribution due to the dipolar interaction with the unpaired electron. This information is obtained by measuring the water proton longitudinal relaxation enhancement as a function of magnetic field through NMRD (Kroes *et al.* 1996). After best fitting of the NMRD profiles to the Solomon equation, the value of τ_s of the Cu(II) ion is obtained together with the metal–water proton distance (Bertini *et al.* 1995c). For Cu(II)–CopC, NMRD data (Arnesano *et al.* 2003a) indicate a τ_s of 3 ns and indicate the presence of a water molecule at 2·8 Å (Cu–O distance) also consistent with EXAFS data (Arnesano *et al.* 2003b).

The enzyme Cu,Zn SOD, which catalyzes dismutation of superoxide to O_2 and H_2O_2, contains a copper ion which alternates between Cu(II) and Cu(I) during the catalytic cycle (Valentine *et al.* 2004). Cu(II) is coordinated by four histidines, one of which makes a bridge with Zn(II), which in turn is bound to three histidines and an aspartate. For the monomeric analog of SOD (Bertini *et al.* 1994c) it was observed that ^1H NMR signals within a 11 Å sphere centered on Cu(II) are not detectable in standard ^1H–^{15}N HSQC experiments due to paramagnetic broadening induced by type-II Cu(II) (Bermel *et al.* 2003). In this system, τ_s of Cu(II), as measured through NMRD, is 2·2 ns (Banci *et al.* 1988; Bertini *et al.* 1990). Taking into account this value, together with the overall rotational correlation time τ_r obtained through ^{15}N relaxation (9·2 ns), it can be estimated that paramagnetic contributions to ^1H relaxation >20 Hz already occur at 10 Å from the paramagnetic center, whereas a similar contribution to ^{13}C and ^{15}N nuclei occurs only at 6 and 5 Å from the paramagnetic center respectively. For characterizing Cu(II),Zn SOD the ^{13}C-detected NMR experiments, applied for Cu(II)–CopC, were further developed (Bermel *et al.* 2003). Only ^{13}C signals experiencing large contact coupling escaped detection, i.e. the ^{13}C nuclei of the Cu(II)-coordinated histidines (Bermel *et al.* 2003). Otherwise, nuclei as close as 4 Å to Cu(II) could be detected. Most of the signals, broadened beyond detection, have been recovered using both 2D ^{13}C–^{13}C scalar and dipolar correlation experiments (Bertini *et al.* 2004d). These examples represent the most advanced achievement, obtained so far, towards the structural characterization in solution of type-II Cu(II) proteins.

7. Perspectives

Every metal ion has peculiar magnetic properties which are strictly related to its coordination environment and, therefore, in the case of metalloproteins, to the surrounding protein frame. Paramagnetic metal ions, as a consequence of their different electronic structure, are characterized by different electron relaxation times and magnetic anisotropies and, therefore,

https://doi.org/10.1017/S0033583506004161 Published online by Cambridge University Press

the study of paramagnetic systems requires tailored spectroscopic approaches which should be optimized case by case. The effects produced by the presence of a paramagnetic metal ion can be quite deleterious for the NMR spectra. However, in several cases these effects can be turned into sources of structural information. Understanding the hyperfine coupling effects on the NMR parameter is essential both for solution studies of biologically relevant paramagnetic metal ions and to devise new spectroscopic methodologies for solution structure characterization of biological systems, either by substitution of NMR silent metal ions with paramagnetic metal ions into naturally occurring metal sites or by *de novo* design of metal-binding sites in proteins. Hence, paramagnetic metal ions are a source of constraints when the classical ones are not measurable, insufficient, or difficult to obtain. In this regard, the use of lanthanides provides a gamma of versatile paramagnetic probes, but still needs to be fully exploited.

At the methodological level, there is a contact point between the need of characterizing highly paramagnetic systems and some of the future priorities in structural NMR: efficient and standardized protocols for the structure characterization of large molecules, where the rotational correlation time makes ^{1}H relaxation unfavorable, and of membrane proteins. Promising results are provided by the ^{13}C-detected approach which may help to overcome problems of the protein size. Progress is being made in the development of protonless experiments and strategies for complete assignment of heteronuclear protein resonances and are promising in terms of strategies for solution structure determination.

The use of paramagnetic probes is also a promising perspective for structure determination of membrane proteins, especially of those containing α helical structures, which are most common and which present the most serious difficulties through NMR because of the small spreading of the signals and large overlap. With electron relaxation times selecting the most suitable metal ion is also a good strategy when rotational correlation time is slow and then τ_s becomes dominant over τ_r.

Further efforts should be devoted to the optimization of NMR sequences for the identification of novel 'heteronuclear constraints' (constraints based on ^{13}C and ^{15}N) other than longitudinal relaxation rates and pseudocontact shifts (e.g. residual dipolar couplings and cross-correlation rates) and to the integration of NMR data with other spectroscopic techniques (EPR, EXAFS, NMRD).

8. Acknowledgments

We are grateful to Ivano Bertini for valuable suggestions and stimulating discussions. Helpful comments from Claudio Luchinat and Giacomo Parigi are also acknowledged.

9. References

Abragam, A. (1961). *The Principles of Nuclear Magnetism*. Oxford: Oxford University Press.

Abragam, A. & Bleaney, B. (1970). *Electron Paramagnetic Resonance of Transition Metal Ions*. Oxford: Clarendon Press.

Adman, E. T. (1991). Copper protein structures. *Advances in Protein Chemistry* **42**, 144–197.

Akke, M., Forsén, S. & Chazin, W. J. (1991). Molecular basis for co-operativity in Ca^{2+} binding to calbindin D_{9k}. ^{1}H nuclear magnetic resonance studies of (Cd^{2+})1-bovine calbindin D_{9k}. *Journal of Molecular Biology* **220**, 173–189.

Allegrozzi, M., Bertini, I., Choi, S. N., Lee, Y.-M. & Luchinat, C. (2002). Detecting small structural changes

https://doi.org/10.1017/S0033583506004161 Published online by Cambridge University Press

in metalloproteins by the use of NMR pseudocontact shifts. *European Journal of Inorganic Chemistry* **2002**, 2121–2127.

Allegrozzi, M., Bertini, I., Janik, M. B. L., Lee, Y.-M., Liu, G. & Luchinat, C. (2000). Lanthanide induced pseudocontact shifts for solution structure refinements of macromolecules in shells up to 40 A from the metal ion. *Journal of the American Chemical Society* **122**, 4154–4161.

Altieri, A. S. & Byrd, R. A. (2004). Automation of NMR structure determination of proteins. *Current Opinion in Structural Biology* **14**, 547–553.

Andersson, P., Weigelt, J. & Otting, G. (1998). Spin-state selection filters for the measurement of hetero-nuclear one-bond coupling constants. *Journal of Biomolecular NMR* **12**, 435–441.

Andreini, C., Bertini, I. & Rosato, A. (2004). A hint to search for metalloproteins in gene banks. *Bioinformatics* **20**, 1373–1380.

Arnesano, F., Banci, L., Bertini, I., Felli, I. C., Luchinat, C. & Thompsett, A. R. (2003a). A strategy for the NMR characterization of type II copper(II) proteins: the case of the copper trafficking protein CopC from Pseudomonas syringae. *Journal of the American Chemical Society* **125**, 7200–7208.

Arnesano, F., Banci, L., Bertini, I., Mangani, S. & Thompsett, A. R. (2003b). A redox switch in CopC: an intriguing copper trafficking protein which binds copper(I) and copper(II) at different sites. *Proceedings of the National Academy of Sciences USA* **100**, 3814–3819.

Arnesano, F., Banci, L., Bertini, I. & Thompsett, A. R. (2002). Solution structure of CopC: a cupredoxin-like protein involved in copper homeostasis. *Structure* **10**, 1337–1347.

Arnoux, P., Haser, R., Izadi, N., Lecroisey, A., Delepierre, M., Wandersman, C. & Czjzek, M. (1999). The crystal structure of HasA, a hemophore secreted by *Serratia marcescens*. *Nature Structural Biology* **6**, 516–520.

Atreya, H. S. & Szyperski, T. (2004). G/matrix Fourier transform NMR spectroscopy for complete protein resonance assignment. *Proceedings of the National Academy of Sciences USA* **101**, 9642–9647.

Babini, E., Bertini, I., Capozzi, F., Felli, I. C., Lelli, M. & Luchinat, C. (2004). Direct carbon detection in paramagnetic metalloproteins to further exploit pseudocontact shift restraints. *Journal of the American Chemical Society* **126**, 10496–10497.

Baig, I., Bertini, I., Del Bianco, C., Gupta, Y. K., Lee, Y.-M., Luchinat, C. & Quattrone, A. (2004). Paramagnetism-based refinement strategy for the solution structure of human alpha-parvalbumin. *Biochemistry* **43**, 5562–5573.

Bailey/Kellogg, C., Chainraj, S. & Pandurangan, G. (2005). A random graph approach to NMR sequential assignment. *Journal of Computational Biology* **12**, 569–583.

Balayssac, S., Jimenez, B. & Piccioli, M. (2006). Assignment strategy for fast relaxing signals: complete aminoacid identification in Thulium-substituted Calbindin D_{9k}. *Journal of Biomolecular NMR* **34**, 63–73.

Banci, L., Bertini, I., Bren, K. L., Cremonini, M. A., Gray, H. B., Luchinat, C. & Turano, P. (1996). The use of pseudocontact shifts to refine solution structures of paramagnetic metalloproteins: Met80Ala cyano-cytochrome *c* as an example. *Journal of Biological Inorganic Chemistry* **1**, 117–126.

Banci, L., Bertini, I., Bren, K. L., Gray, H. B., Sompornpisut, P. & Turano, P. (1997a). Solution structure of oxidized *Saccharomyces cerevisiae* Iso-1-cyto-chrome *c*. *Biochemistry* 36, 8992–9001.

Banci, L., Bertini, I., Cavallaro, G., Giachetti, A., Luchinat, C. & Parigi, G. (2004). Paramagnetism-based restraints for Xplor-NIH. *Journal of Biomolecular NMR* **28**, 249–261.

Banci, L., Bertini, I., Cavallaro, G. & Luchinat, C. (2002). Chemical shift-based constraints for solution structure determination of paramagnetic low spin heme proteins with bis-His and His-Cn axial ligands. The cases of oxidized cytochrome b5 and Met80Ala cyano-cytochrome c. *Journal of Biological Inorganic Chemistry* **7**, 416–426.

Banci, L., Bertini, I., Cremonini, M. A., Gori Savellini, G., Luchinat, C., Wüthrich, K. & Güntert, P. (1998a). Pseudodyana for NMR structure calculation of paramagnetic metalloproteins using torsion angle molecular dynamics. *Journal of Biomolecular NMR* **12**, 553–557.

Banci, L., Bertini, I., Eltis, L. D., Felli, I. C., Kastrau, D. H. W., Luchinat, C., Piccioli, M., Pierattelli, R. & Smith, M. (1994a). The three dimensional structure in solution of the paramagnetic protein high-potential iron-sulfur protein I from *Ectothiorhodospira halophila* through nuclear magnetic resonance. *European Journal of Biochemistry* **225**, 715–725.

Banci, L., Bertini, I., Felli, I. C. & Sarrou, J. (2005a). Backbone-only restraints for fast determination of the protein fold: the role of paramagnetism-based restraints. Cytochrome b_{562} as an example. *Journal of Magnetic Resonance* **172**, 191–200.

Banci, L., Bertini, I., Gori Savellini, G., Romagnoli, A., Turano, P., Cremonini, M. A., Luchinat, C. & Gray, H. B. (1997b). The pseudocontact shifts as constraints for energy minimization and molecular dynamic calculations on solution structures of paramagnetic metalloproteins. *Proteins: Structure, Function, and Genetics* **29**, 68–76.

Banci, L., Bertini, I., Huber, J. G., Luchinat, C. & Rosato, A. (1998b). Partial orientation of oxidized and reduced cytochrome b_5 at high magnetic fields: magnetic susceptibility anisotropy contributions and consequences for protein solution structure determination. *Journal of the American Chemical Society* **120**, 12903–12909.

https://doi.org/10.1017/S0033583506004161 Published online by Cambridge University Press

Banci, L., Bertini, I. & Luchinat, C. (1990). The ^{1}H NMR parameters of magnetically coupled dimmers – The Fe_2S_2 proteins as an example. *Structure and Bonding* **72**, 113–135.

Banci, L., Bertini, I. & Luchinat, C. (1991). Nuclear and electron relaxation. In *The Magnetic Nucleus – Unpaired Electron Coupling in Solution*. Weinheim: VCH.

Banci, L., Bertini, I. & Luchinat, C. (1994b). 2D NMR spectra of paramagnetic systems. In *Methods in Enzymology* (eds. T. L. James & N. J. Oppenheimer), vol. 239, pp. 485–514. London: Academic Press Inc.

Banci, L., Bertini, I., Luchinat, C., Monnanni, R. & Scozzafava, A. (1988). Water 1H nuclear magnetic relaxation dispersion (NMRD) of Cu_2Zn_2SOD with some anions and ^{1}H NMR spectra of Cu_2Co_2SOD in the presence of CN^{-}. *Inorganic Chemistry* **27**, 107–109.

Banci, L., Bertini, I. & Mangani, S. (2005b). Integration of XAS and NMR techniques for the structure determination of metalloproteins. Examples from the study of copper transport proteins. *Journal of Synchrotron Radiation* **12**, 94.

Banci, L. & Piccioli, M. (1996). Cobalt(II) and Nickel(II) substituted proteins. In *Encyclopedia of Magnetic Resonance* (eds. D. M. Grant & R. K. Harris), pp. 1365–1373. Chichester: J. Wiley & Sons.

Banci, L., Piccioli, M. & Scozzafava, A. (1992). Advancements in NMR investigation of paramagnetic molecules in solution. *Coordination Chemistry Reviews* **120**, 1–28.

Barbieri, R., Bertini, I., Cavallaro, G., Lee, Y.-M., Luchinat, C. & Rosato, A. (2002a). Paramagnetically induced residual dipolar couplings for solution structure determination of lanthanide-binding proteins. *Journal of the American Chemical Society* **124**, 5581–5587.

Barbieri, R., Bertini, I., Lee, Y.-M., Luchinat, C. & Velders, A. H. (2002b). Structure-independent cross-validation of residual dipolar couplings originating from internal and external orienting media. *Journal of Biomolecular NMR* **22**, 365–368.

Barbieri, R., Luchinat, C. & Parigi, G. (2004). Backbone-only protein solution structures with a combination of classical and paramagnetism-based constraints: a method that can be scaled to large molecules. *ChemPhysChem* **21**, 797–806.

Battiste, J. L. & Wagner, G. (2000). Utilization of site-directed spin labelling and high-resolution heteronuclear nuclear magnetic resonance for global fold determination of large proteins with limited nuclear *Overhauser effect data*. *Biochemistry* **39**, 5355–5365.

Bax, A., Kontaxis, G. & Tjandra, N. (2001). Dipolar couplings in macromolecular structure determination. *Methods in Enzymology* **339**, 127–174.

Bax, A. & Tjandra, N. (1997). Are proteins even floppier than we thought? *Nature Structural Biology* **4**, 254–256.

Bentrop, D., Bertini, I., Cremonini, M. A., Forsén, S., Luchinat, C. & Malmendal, A. (1997). The solution structure of the paramagnetic complex of the N-terminal domain of calmodulin with two Ce^{3+} ions by 1H NMR. *Biochemistry* **36**, 11605–11618.

Bermel, W., Bertini, I., Duma, L., Emsley, L., Felli, I. C., Pierattelli, R. & Vasos, P. (2005a). Complete assignment of heteronuclear protein resonances by protonless NMR spectroscopy. *Angewandte Chemie International Edition* **44**, 3089–3092.

Bermel, W., Bertini, I., Felli, I. C., Kümmerle, R. & Pierattelli, R. (2003). ^{13}C direct detection experiments on the paramagnetic oxidized monomeric copper, zinc superoxide dismutase. *Journal of the American Chemical Society* **125**, 16423–16429.

Bermel, W., Bertini, I., Felli, I. C., Kümmerle, R. & Pierattelli, R. (2006). Novel ^{13}C direct detection experiments, including extension to the third dimension, to perform fhe complete assignment of proteins. *Journal of Magnetic Resonance* **178**, 56–64.

Bermel, W., Bertini, I., Felli, I. C., Piccioli, M. & Pierattelli, R. (in press). ^{13}C-detected protonless NMR spectroscopy of proteins in solution. *Progress in Nuclear Magnetic Resonance Spectroscopy*.

Bermel, W., Bertini, I., Felli, I. C., Pierattelli, R. & Vasos, P. R. (2005b). A selective experiment for the sequential protein backbone assignment from 3D heteronuclear spectra. *Journal of Magnetic Resonance* **172**, 324–328.

Bertini, I., Capozzi, F., Ciurli, S., Luchinat, C., Messori, L. & Piccioli, M. (1992). Identification of the iron ions of HiPIP from *Chromatium vinosum* within the protein frame through 2D NMR experiments. *Journal of the American Chemical Society* **114**, 3332–3340.

Bertini, I., Capozzi, F., Luchinat, C., Piccioli, M. & Vila, A. J. (1994a). The Fe_4S_4 centers in ferredoxins studied through proton and carbon hyperfine coupling. Sequence specific assignments of cysteines in ferredoxins from *Clostridium acidi urici* and *Clostridium pasteurianum*. *Journal of the American Chemical Society* **116**, 651–660.

Bertini, I., Cavallaro, G., Cosenza, M., Kümmerle, R., Luchinat, C., Piccioli, M. & Poggi, L. (2002a). Cross correlation rates between Curie spin and dipole-dipole relaxation in paramagnetic proteins: the case of cerium substituted calbindin D_{9k}. *Journal of Biomolecular NMR* **23**, 115–125.

Bertini, I., Cavallaro, G., Luchinat, C. & Poli, I. (2003). A use of Ramachandran potentials in protein solution structure determinations. *Journal of Biomolecular NMR* **4**, 355–366.

Bertini, I., Ciurli, S., Dikiy, A., Fernández, C. O., Luchinat, C., Safarov, N., Shumilin, S. & Vila, A. J. (2001a). The first solution structure of an oxidized paramagnetic copper (II) protein: the case of plastocyanin from the cyanobacterium *Synechocystis* PCC6803. *Journal of the American Chemical Society* **123**, 2405–2413.

Bertini, I., Ciurli, S., Dikiy, A., Gasanov, R., Luchinat, C., Martini, G. & Safarov, N. (1999a). High-field

https://doi.org/10.1017/S0033583506004161 Published online by Cambridge University Press

NMR studies of oxidized blue copper proteins: the case of spinach plastocyanin. *Journal of the American Chemical Society* **121**, 2037–2046.

Bertini, I., Couture, M. M. J., Donaire, A., Eltis, L. D., Felli, I. C., Luchinat, C., Piccioli, M. & Rosato, A. (1996). The solution structure refinement of the paramagnetic reduced HiPIP I from *Ectothiorhodospira halophila* by using stable isotope labeling and nuclear relaxation. *European Journal of Biochemistry* **241**, 440–452.

Bertini, I., Del Bianco, C., Gelis, I., Katsaros, N., Luchinat, C., Parigi, G., Peana, M., Provenzani, A. & Zoroddu, M. A. (2004a). Experimentally exploring the conformational space sampled by domain reorientation in calmodulin. *Proceedings of the National Academy of Sciences, USA* **101**, 6841–6846.

Bertini, I., Dikiy, A., Luchinat, C., Macinai, R. & Viezzoli, M. S. (1998a). ^{1}H NMR study of the reduced cytochrome c′ from *Rhodopseudomonas palustris* containing a high spin iron(II) heme moiety. *Inorganic Chemistry* **37**, 4814–4821.

Bertini, I., Donaire, A., Feinberg, B. A., Luchinat, C., Piccioli, M. & Yuan, H. (1995a). Solution structure of the oxidized 2[Fe_4S_4] ferredoxin from *Clostridium pasteurianum*. *European Journal of Biochemistry* **232**, 192–205.

Bertini, I., Donaire, A., Jiménez, B., Luchinat, C., Parigi, G., Piccioli, M. & Poggi, L. (2001b). Paramagnetism-based versus classical constraints: an analysis of the solution structure of Ca Ln calbindin D_{9k}. *Journal of Biomolecular NMR* **21**, 85–98.

Bertini, I., Donaire, A., Luchinat, C. & Rosato, A. (1997). Paramagnetic relaxation as a tool for solution structure determination: *Clostridium pasterianum* ferredoxin as an example. *Proteins: Structure, Function, and Genetics* **29**, 348–358.

Bertini, I., Duma, L., Felli, I. C., Fey, M., Luchinat, C., Pierattelli, R. & Vasos, P. (2004b). A heteronuclear direct detection NMR experiment for protein backbone assignment. *Angewandte Chemie International Edition* **43**, 2257–2259.

Bertini, I., Eltis, L. D., Felli, I. C., Kastrau, D. H. W., Luchinat, C. & Piccioli, M. (1995b). The solution structure of oxidized HiPIP I from *Ectothiorhodospira halophila*, can NMR probe rearrangements associated to electron transfer processes? *Chemistry – A European Journal* **1**, 598–607.

Bertini, I., Felli, I. C., Kümmerle, R., Luchinat, C. & Pierattelli, R. (2004c). ^{13}C-^{13}C NOESY: a constructive use of ^{13}C-^{13}C spin-diffusion. *Journal of Biomolecular NMR* **30**, 245–251.

Bertini, I., Felli, I. C., Kümmerle, R., Moskau, D. & Pierattelli, R. (2004d). ^{13}C-^{13}C NOESY: an attractive alternative to study large macromolecules. *Journal of the American Chemical Society* **126**, 464–465.

Bertini, I., Felli, I. C. & Luchinat, C. (1998b). High magnetic field consequences on the NMR hyperfine shifts in solution. *Journal of Magnetic Resonance* **134**, 360–364.

Bertini, I., Fernández, C. O., Karlsson, B. G., Leckner, J., Luchinat, C., Malmström, B. G., Nersissian, A. M., Pierattelli, R., Shipp, E., Valentine, J. S. & Vila, A. J. (2000a). Structural information through NMR hyperfine shifts in blue copper proteins. *Journal of the American Chemical Society* **122**, 3701–3707.

Bertini, I., Galas, O., Luchinat, C. & Parigi, G. (1995c). A computer program for the calculation of paramagnetic enhancements of nuclear relaxation rates in slowly rotating systems. *Journal of Magnetic Resonance Series A* **113**, 151–158.

Bertini, I., Janik, M. B. L., Lee, Y.-M., Luchinat, C. & Rosato, A. (2001c). Magnetic susceptibility tensor anisotropies for a lanthanide ion series in a fixed protein matrix. *Journal of the American Chemical Society* **123**, 4181–4188.

Bertini, I., Jiménez, B. & Piccioli, M. (2005a). ^{13}C direct detected experiments: optimisation to paramagnetic signals. *Journal of Magnetic Resonance* **174**, 125–132.

Bertini, I., Kowalewski, J., Luchinat, C. & Parigi, G. (2001d). Cross-correlation between the dipole–dipole interaction and the Curie spin relaxation. The effect of anisotropic magnetic susceptibility. *Journal of Magnetic Resonance* **152**, 103–108.

Bertini, I., Lanini, G., Luchinat, C., Messori, L., Monnanni, R. & Scozzafava, A. (1985). Investigation of Cu_2Co_2SOD and its anion derivatives. ^{1}H NMR and electronic spectra. *Journal of the American Chemical Society* **107**, 4391–4396.

Bertini, I., Lee, Y.-M., Luchinat, C., Piccioli, M. & Poggi, L. (2001e). Locating the metal ion in calcium-binding proteins by using cerium(III) as a probe. *ChemBioChem* **2**, 550–558.

Bertini, I. & Luchinat, C. (1996). *NMR of Paramagnetic Substances*. Coordination Chemistry Reviews, vol. 150. Amsterdam: Elsevier.

Bertini, I., Luchinat, C., Banci, L. & Viezzoli, M. S. (1990). ^{1}H NMR and relaxometry of copper-containing dimers in proteins. *Biology of Metals* **3**, 146–150.

Bertini, I., Luchinat, C. & Parigi, G. (2001f). *Solution NMR of Paramagnetic Molecules*. Amsterdam: Elsevier.

Bertini, I., Luchinat, C. & Parigi, G. (2002b). Paramagnetic constraints: an aid for quick solution structure determination of paramagnetic metalloproteins. *Concepts in Magnetic Resonance* **14**, 259–286.

Bertini, I., Luchinat, C., Parigi, G. & Pierattelli, R. (2005b). NMR of paramagnetic metalloproteins. *ChemBioChem* **6**, 1536–1549.

Bertini, I., Luchinat, C., Parigi, G. & Walker, F. A. (1999b). Heme methyl ^{1}H chemical shifts as structural parameters in some low spin ferriheme proteins. *Journal of Biological Inorganic Chemistry* **4**, 515–519.

Bertini, I., Luchinat, C. & Piccioli, M. (2001g). Paramagnetic probes in metalloproteins. turning

https://doi.org/10.1017/S0033583506004161 Published online by Cambridge University Press

limitations into advantages. *Methods in Enzymology* **339**, 314–340.

Bertini, I., Luchinat, C., Piccioli, M. & Tarchi, D. (1994b). COSY spectra of paramagnetic macromolecules, observability, scalar effects, cross correlation effects, relaxation allowed coherence transfer. *Concepts in Magnetic Resonance* **6**, 307–335.

Bertini, I., Luchinat, C. & Tarchi, D. (1993). Are true scalar proton-proton connectivities ever measured in COSY spectra of paramagnetic macromolecules? *Chemical Physics Letters* **203**, 445–449.

Bertini, I., Luchinat, C. & Turano, P. (2000b). ^{15}N chemical shift changes in cytochrome b5: redox-dependent vs. guanidinium chloride-induced changes. *Journal of Biological Inorganic Chemistry* **5**, 761–764.

Bertini, I., Piccioli, M., Viezzoli, M. S., Chiu, C. Y. & Mullenbach, G. T. (1994c). A spectroscopic characterization of a monomeric analog of copper-zinc superoxide dismutase. *European Journal of Biophysics* **23**, 167–176.

Bertini, I. & Pierattelli, R. (2004). Copper(II) proteins are amenable for NMR investigation. *Pure and Applied Chemistry* **76**, 321–333.

Bertini, I., Sigel, A. & Sigel, H. (2001h). *Handbook on Metalloproteins*. New York: Marcel Dekker.

Biekofsky, R. R., Martin, S. R., Browne, J. P., Bayley, P. M. & Feeney, J. (1998). Ca^{2+} coordination to backbone carbonyl oxygen atoms in Calmodulin and other EF-hand proteins: ^{15}N chemical shifts as probes for monitoring individual-site Ca^{2+} coordination. *Biochemistry* **37**, 7617–7629.

Biekofsky, R. R., Muskett, F. W., Schmidt, J. M., Martin, S. R., Browne, J. P., Bayley, P. M. & Feeney, J. (1999). NMR approaches for monitoring domain orientations in calcium-binding proteins in solution using partial replacement of Ca^{2+} by Tb^{3+}. *FEBS Letters* **460**, 519–526.

Bleaney, B. (1972). Nuclear magnetic resonance shifts in solution due to lanthanide ions. *Journal of Magnetic Resonance* **8**, 91–100.

Bleaney, B., Dobson, C. M., Levine, B. A., Martin, R. B., Williams, R. J. P. & Xavier, A. V. (1972). Origin of lanthanide nuclear magnetic resonance shifts and their uses. *Journal of the Chemical Society, Chemical Communications* **791**.

Bloembergen, N. (1957). Proton relaxation times in paramagnetic solutions. *Journal of Chemical Physics* **27**, 572–573.

Bodenhausen, G. & Freeman, R. (1977). Correlation of proton and carbon-13 NMR spectra by heteronuclear two-dimensional spectroscopy. *Journal of Magnetic Resonance* **28**, 471.

Boisbouvier, J., Brutscher, B., Pardi, A., Marion, D. & Simorre, J. P. (2000). NMR determination of sugar puckers in nucleic acids from CSA-dipolar cross-correlated relaxation. *Journal of the American Chemical Society* **122**, 6779–6780.

Boisbouvier, J., Gans, P., Blackledge, M., Brutscher, B. & Marion, D. (1999). Long-range structral information in NMR studies of paramagnetic molecules from electron spin-nuclear spin cross-correlated relaxation. *Journal of the American Chemical Society* **121**, 7700–7701.

Bothner-By, A. A., Domaille, J. P. & Gayathri, C. (1981). Ultra high-field NMR spectroscopy: observation of proton-proton dipolar coupling in paramagnetic bis[tolyltris(pyrazolyl)borato]cobalt(II). *Journal of the American Chemical Society* **103**, 5602–5603.

Boyd, J., Dobson, C. M., Morar, A. S., Williams, R. J. P. & Pielak, G. J. (1999). ^{1}H and ^{15}N hyperfine shifts of cytochrome c. *Journal of the American Chemical Society* **121**, 9247–9248.

Boyd, J., Domene, C., Redfield, C., Ferraro, M. & Lazzeretti, P. (2003). Calculation of dipole/shielding polarizabilities ($\sigma^{1}_{\alpha\beta\gamma}$) the influence of uniform electric field effects on the shielding of backbone nuclei in proteins. *Journal of the American Chemical Society* **125**, 9556–9557.

Bren, K. L., Gray, H. B., Banci, L., Bertini, I. & Turano, P. (1995). Paramagnetic ^{1}H NMR spectroscopy of the cyanide derivative of Met80Ala-iso-1-cytochrome *c*. *Journal of the American Chemical Society* **117**, 8067–8073.

Brunger, A. T., Adams, P. D., Clore, G. M., Delano, W. L., Gros, P., Grosse-Kunstleve, R. W., Jiang, J. S., Kuszewski, J., Nilges, M., Pannu, N. S., Read, R. J., Rice, L. M., Simonson, T. & Warren, G. L. (1998). Crystallography & NMR system: A new software suite for macromolecular structure determination. *Acta Crystallographica Section D – Biological Crystallography* **54**, 905–921.

Brunner, E. (2001). Residual dipolar couplings in protein NMR. *Concepts in Magnetic Resonance* **13**, 238–259.

Caillet, C., Delepierre, M., Lecroisey, A., Bertini, I., Piccioli, M. & Turano, P. (2006). Direct detected ^{13}C NMR to investigate the iron(III) hemophone HasA. *Journal of the American Chemical Society* **128**, 150–158.

Capozzi, F., Cremonini, M. A., Luchinat, C. & Sola, M. (1993). Assignment of pseudo-contact-shifted ^{1}H NMR resonances in the EF-site of Yb^{3+}-substituted rabbit parvalbumin through a combination of 2D techniques and magnetic susceptibility tensor determination. *Magnetic Resonance in Chemistry* **31**, S118–S127.

Cavagnero, S., Dyson, H. J. & Wright, P. E. (1999). Improved low pH bicelle system for orienting macromolecules over a wide temperature range. *Journal of Biomolecular NMR* **13**, 387–391.

Chance, M. R., Fiser, A., Sali, A., Pieper, U., Eswar, N., Xu, G., Fajardo, J. E., Radhakannan, T. & Marinkovic, N. (2004). High-throughput computational and experimental techniques in structural genomics. *Genome Research* **14**, 2145–2154.

https://doi.org/10.1017/S0033583506004161 Published online by Cambridge University Press

Chou, J. J., Li, S., Klee, C. B. & Bax, A. (2001). Solution structure of Ca^{2+} calmodulin reveals flexible hand-like properties of its domains. *Nature Structural Biology* **8**, 990–997.

Clementi, V. & Luchinat, C. (1998). NMR and spin relaxation in dimers. *Accounts of Chemical Research* **31**, 351–361.

Clore, G. M. & Gronenborn, A. M. (1998). New methods of structure refinement for macromolecular structure determination by NMR. *Proceedings of the National Academy of Sciences USA* 95, 5891–5898.

Clore, G. M., Gronenborn, A. M., Brunger, A. T. & Karplus, M. (1985). The solution conformation of a heptadecapeptide comprising the DNA binding helix F of the cyclic AMP receptor protein of *Escherichia coli*: combined use of ^{1}H-nuclear magnetic resonance and restrained molecular dynamics. *Journal of Molecular Biology* **186**, 435–455.

Dayie, K. T. & Wagner, G. (1997). Carbonyl carbon probe of local mobility in ^{13}C, ^{15}N-enriched proteins using high-resolution nuclear magnetic resonance. *Journal of the American Chemical Society* **119**, 7797–7806.

Degtyarenko, K. N. (2000). Bioinorganic motifs: towards functional classification of metalloproteins. *Bioinformatics* **16**, 851–864.

Degtyarenko, K. N., North, A. C. T. & Findlay, J. B. C. (1999). PROMISE: a database of bioinorganic motifs. *Nucleic Acids Research* **27**, 233–236.

Desvaux, H. & Gochin, M. (1999). Coherence transfer between nuclear spins in paramagnetic systems: effects of nucleus-electron dipole–dipole cross-correlation. *Molecular Physics* **96**, 1317–1333.

Desvaux, H., Kümmerle, R., Kowalewski, J., Luchinat, C. & Bertini, I. (2004). Direct measurement of dynamic frequency shift of cross-correlation in ^{15}N enriched proteins. *ChemPhysChem* **5**, 959–965.

Donaire, A., Jiménez, B., Fernandez, C. O., Pierattelli, R., Niizeki, T., Moratal, J. M., Hall, J. F., Kohzuma, T., Hasnain, S. S. & Vila, A. J. (2002). Metal-ligand interplay in blue copper proteins studied by ^{1}H NMR spectroscopy: Cu(II)-pseudoazurin and Cu(II)-rusticyanin. *Journal of the American Chemical Society* **124**, 13698–13708.

Donaire, A., Salgado, J. & Moratal, J. M. (1998). Determination of the magnetic axes of cobalt(II) and nickel(II) azurins from ^{1}H NMR data: influence of the metal and axial ligands on the origin of magnetic anisotropy in blue copper proteins. *Biochemistry* **37**, 8659–8673.

Duma, L., Hediger, S., Lesage, A. & Emsley, L. (2003). Spin-state selection in solid-state NMR. *Journal of Magnetic Resonance* **164**, 187–195.

Dunham, S. U. & Lippard, S. J. (1995). Long-range distance constraints in platinated nucleotides: structure determination of the 5′ orientational isomer of *cis*-[Pt(NH_3) (4-aminoTEMPO)[d(GpG)]]$^{+}$ from combined paramagnetic and diamagnetic NMR constraints with molecular modeling. *Journal of the American Chemical Society* **117**, 10702–10712.

Eghbalnia, H. R., Bahrani, A., Wang, L., Assadi, A. & Markley, J. L. (2005). Probabilistic identification of spin systems and their assignments including coil/helix inference as output (PISTACHIO). *Journal of Biomolecular NMR* **32**, 219–233.

Emerson, S. D. & La Mar, G. N. (1990). NMR determination of the orientation of the magnetic susceptibility tensor in cyanometmyoglobin: a new probe of steric tilt of bound ligand. *Biochemistry* **29**, 1556–1566.

Ernst, R. R., Bodenhausen, G. & Wokaun, A. (1987). *Principles of Nuclear Magnetic Resonance in One and Two Dimensions*. London: Oxford University Press.

Feeney, J., Birdsall, B., Bradbury, A. F., Biekofsky, R. R. & Bayley, P. M. (2001). Calmodulin tagging provides a general method of using lanthanide induced magnetic field orientation to observe residual dipolar couplings in proteins in solution. *Journal of Biomolecular NMR* **21**, 41–48.

Fermi, E. (1930). Uber die magnetischen Momente der AtomKerne. *Zeitschrift fur Physik* 60, 320.

Fiaux, J., Bertelsen, E. B., Horwich, A. L. & Wüthrich, K. (2002). NMR analysis of a 900 kDa GroEL GROES complex. *Nature* **418**, 207–211.

Fischer, M. W. F., Zeng, L. & Zuiderweg, E. R. P. (1996). Use of ^{13}C-^{13}C NOE for the assignmetn of NMR lines of larger labeled proteins at larger magnetic fields. *Journal of the American Chemical Society* **118**, 12457–12458.

Fitzgerald, R. J. & Drago, R. S. (1967) Contact-shift studies and delocalization mechanisms of nickel(II)-benzylamine complexes. *Journal of the American Chemical Society* **89**, 2879.

Fossi, M., Linge, J., Labudde, D., Leitner, D., Nilges, M. & Oschkinat, H. (2005). Influence of chemical shift tolerances on NMR structure calculations using ARIA protocols for assigning NOE data. *Journal of Biomolecular NMR* **31**, 21–34.

Frausto Da Silva, J. J. R. & Williams, R. J. P. (2001). *The Biological Chemistry of the Elements: The Inorganic Chemistry of Life*. New York: Oxford University Press.

Fushman, D. & Cowburn, D. (2001). Nuclear magnetic resonance relaxation in determination of residue-specific ^{15}N chemical shift tensors in proteins in solution: protein dynamics, structure, and applications of transverse relaxation optimized spectroscopy. *Methods in Enzymology* **339**, 109–126.

Gaponenko, V., Altieri, A. S., Li, J. & Byrd, R. A. (2002). Breaking symmetry in the structure determination of (large) symmetric protein dimers. *Journal of Biomolecular NMR* **24**, 143–148.

Gaponenko, V., Dvoretsky, A., Walsby, C., Hoffman, B. M. & Rosevear, P. R. (2000a). Calculation of

https://doi.org/10.1017/S0033583506004161 Published online by Cambridge University Press

z-coordinates and orientational restraints using a metal binding tag. *Biochemistry* **39**, 15217–15224.

Gaponenko, V., Howarth, J. W., Columbus, L., Gasmi-Seabrook, G., Yuan, J., Hubbell, W. L. & Rosevear, P. R. (2000b). Protein globl fold determination using site-directed spin and isotope labeling. *Protein Science* **9**, 302–309.

Gaponenko, V., Sarma, S. P., Altieri, A. S., Horita, D. A., Li, J. & Byrd, R. A. (2004). Improving the accuracy of NMR structures of large proteins using pseudocontact shifts as long/range restraints. *Journal of Biomolecular NMR* **28**, 205–212.

Gayathri, C., Bothner-By, A. A., Van Zijl, P. C. M. & Maclean, C. (1982). Dipolar magnetic field effects in NMR spectra of liquids. *Chemical Physics Letters* **87**, 192–196.

Geraldes, C. F. G. C. & Luchinat, C. (2003). Lanthanides as shift and relaxation agents in elucidating the structure of proteins and nucleic acids. *Metal Ions in Biological Systems* **40**, 513–588.

Ghose, R., Huang, K. & Prestegard, J. H. (1998). Measurement of cross correlation between dipolar coupling and chemical shift anisotropy in the spin relaxation of ^{13}C, ^{15}N-labeled proteins. *Journal of Magnetic Resonance* **135**, 487–499.

Ghose, R. & Prestegard, J. H. (1997). Electron spin-nuclear spin cross-correlation effects on multiplet splittings in paramagnetic proteins. *Journal of Magnetic Resonance* **128**, 138–143.

Goasdoue, N., Riviere, D. G., Correia, I., Convert, O. & Piccioli, M. (2000). Multiple selective excitation as a tool for NMR studies of paramagnetic proteins. *Magnetic Resonance in Chemistry* **38**, 827–832.

Gochin, M. (2000). A high-resolution structure of a DNA-chromycin-Co(II) complex determined from pseudocontact shifts in nuclear magnetic resonance. *Structure with Folding and Design* **8**, 441–452.

Griffith, J. S. (1961). *The Theory of Transition-metal Ions*. Cambridge: Cambridge University Press.

Grishaev, A. & Llinas, M. (2005). Protein structure elucidation form minimal NMR data: the CLOUDS approach. *Methods in Enzymology* **394**, 261–295.

Grzesiek, S. & Bax, A. (1992a). An efficient experiment for sequential backbone assignment of medium-sized isotopically enriched proteins. *Journal of Magnetic Resonance* **99**, 201–207.

Grzesiek, S. & Bax, A. (1992b). Correlating backbone amide and side chain resonances in larger proteins by multiple relayed triple resonance NMR. *Journal of the American Chemical Society* **114**, 6291–6293.

Gueron, M. (1975). Nuclear relaxation in macromolecules by paramagnetic ions: a novel mechanism. *Journal of Magnetic Resonance* **19**, 58–66.

Guntert, P. (2004). Automatd NMR structure calculation with CYANA. *Methods in Molecular and Cellular Biology* **278**, 353–378.

Güntert, P., Braun, W. & Wüthrich, K. (1991). Efficient computation of three-dimensional protein structures in solution from Nuclear Magnetic Resonance data using the program DIANA and the supporting programs CALIBA, HABAS and GLOMSA. *Journal of Molecular Biology* **217**, 517–530.

Güntert, P., Mumenthaler, C. & Wüthrich, K. (1997). Torsion angle dynamics for NMR structure calculation with the new program DYANA. *Journal of Molecular Biology* **273**, 283–298.

Harris, R. K. & Mann, B. E. (1978). *NMR and the Periodic Table*. London: Academic Press.

Hasnain, S. S. (2004). Synchrotron techniques for metalloproteins and human disease in a post genome era. *Journal of Synchrotron Radiation* **11**, 7–11.

Heller, C. & McConnell, H. M. (1960). Radiation damage in organic crystals. II. Electron spin resonance of $(CO_2H)CH_2CH(CO_2H)$ in β-succinic acid. *Journal of Chemical Physics* **32**, 1535–1539.

Herrmann, T., Güntert, P. & Wüthrich, K. (2002a). Protein NMR structure determination with automated NOE assignment using the new software CANDID and the torsion angle dynamics algorithm DYANA. *Journal of Molecular Biology* **319**, 209–227.

Herrmann, T., Guntert, P. & Wüthrich, K. (2002b). Protein NMR structure determination with automated NOE-identification in the NOESY spectra using the new software ATNOS. *Journal of Biomolecular NMR* **24**, 171–189.

Holz, R. C., Bennet, B., Chen, G. J. & Ming, L. J. (1998). Proton NMR spectroscopy as a probe of dinuclear copper(II) active sites in metalloproteins. Characterization of hyperactive copper(II)-substituted amonipeptidase from *Aeromonas proteolytica*. *Journal of the American Chemical Society* **120**, 6329–6335.

Holz, R. C., Que, Jr., L. & Ming, L.-J. (1992). NOESY Studies on the Fe(III) Co(II) active site of the purple acid phosphatase uteroferrin. *Journal of the American Chemical Society* **114**, 4434–4436.

Hu, K., Vögeli, B. & Pervushin, K. (2005). Side-chain H and C resonance assignment in protonated/partially deuterated proteins using an improved 3D ^{13}C-detected HCC-TOCSY. *Journal of Magnetic Resonance* **174**, 200–208.

Hus, J. C., Marion, D. & Blackledge, M. (2000). *De novo* determination of protein structure by NMR using orientational and long-range order restraints. *Journal of Molecular Biology* **298**, 927–936.

Hyberts, S. G. & Wagner, G. (2003). IBIS: a tool for automated sequebntial assignment of protein spectra from triple resonance experiments. *Journal of Biomolecular NMR* **26**, 335–344.

Ikegami, T., Verdier, L., Sakhaii, P., Grimme, S., Pescatore, P., Saxena, K., Fiebig, K. M. & Griesinger, C. (2004). Novel techniques for weak alignment of proteins in solution using chemical tags

https://doi.org/10.1017/S0033583506004161 Published online by Cambridge University Press

coordinating lanthanide ions. *Journal of Biomolecular NMR* **29**, 339–349.

Jung, Y. S. & Zweckstetter, M. (2004). Mars: robust automatic backbone assignment of proteins. *Journal of Biomolecular NMR* **30**, 11–23.

Karplus, M. (1959). Contact electron-spin coupling of nuclear magnetic moments. *Journal of Chemical Physics* **30**, 11–15.

Karplus, M. & Fraenkel, G. K. (1961). Theoretical interpretation of Carbon-13 hyperfine interactions in Electron Spin Resonance Spectra. *Journal of Chemical Physics* **35**, 1312–1323.

Kateb, F. & Piccioli, M. (2003). New routes to the detection of relaxation allowed coherence transfer in paramagnetic molecules. *Journal of the American Chemical Society* **125**, 14978–14979.

Kay, L. E. (2005). NMR studies of protein structure and dynamics. *Journal of Magnetic Resonance* **173**, 193–207.

Kay, L. E., Ikura, M., Tschudin, R. & Bax, A. (1990). Three-dimensional triple-resonance NMR spectroscopy of isotopically enriched proteins. *Journal of Magnetic Resonance* **89**, 496–514.

Kay, L. E., Nicholson, L. K., Delaglio, F., Bax, A. & Torchia, D. A. (1992). Pulse sequences for removal of the effects of cross correlation between dipolar and chemical-shift anisotropy relaxation mechanisms on the measurement of heteronuclear T_1 and T_2 values in proteins. *Journal of Magnetic Resonance* **97**, 359–375.

Koenig, S. H. & Brown III, R. D. (1991). The dynamics of water-protein interactions. Results from measurements of nuclear magnetic relaxation dispersion. *Progress in Nuclear Magnetic Resonance Spectroscopy* **22**, 487–567.

Koenig, S. H., Prodell, A. G. & Kusch, P. (1952). The anomalous magnetic moment of the electron. *Physical Review* **88**, 191.

Kolczak, U., Salgado, J., Siegal, G., Saraste, M. & Canters, G. W. (1999). Paramagnetic NMR studies of blue and purple copper proteins. *Biospectroscopy* **5**, S19–S32.

Koningsberger, D. C. & Prins, R. (1988). *X-ray Absorption, Principles, Techniques of EXAFS, SEXAFS and XANES*. New York: John Wiley and Sons.

Kostic, M., Pochapsky, S. S. & Pochapsky, T. C. (2002). Rapid recycle ^{13}C, ^{15}N and ^{13}C,^{13}C heteronuclear and homonuclear multiple quantum coherence detection for resonance assignments in paramagnetic proteins: example of Ni^{2+}-containing acireductone dioxygenase. *Journal of the American Chemical Society* **124**, 9054–9055.

Kovacs, H., Moskau, D. & Spraul, M. (2005). Cryogenically cooled probes – a leap in NMR technology. *Progress in Nuclear Magnetic Resonance Spectroscopy* **46**, 131–155.

Krizek, B. A. & Berg, J. M. (1992). Complexes of zinc finger peptides with Ni(II) and Fe(II). *Inorganic Chemistry* **31**, 2984–2986.

Kroes, S. J., Salgado, J., Parigi, G., Luchinat, C. & Canters, G. W. (1996). Electron relaxation and solvent accessibility of the metal site in wild-type and mutated azurins as determined from nuclear magnetic relaxation dispersion experiments. *Journal of Biological Inorganic Chemistry* **1**, 551–559.

Kumar, A., Grace, R. C. R. & Madhu, P. K. (2000). Cross correlations in NMR. *Progress in Nuclear Magnetic Resonance Spectroscopy* **37**, 191–319.

Kurland, R. J. & McGarvey, B. R. (1970). Isotropic NMR shifts in transition metal complexes: calculation of the Fermi contact and pseudocontact terms. *Journal of Magnetic Resonance* **2**, 286–301.

Lee, L. & Sykes, B. D. (1980). Nuclear magnetic resonance determination of metal-proton distances in the EF site of carp parvalbumin using the susceptibility contribution to the line broadening of lanthanide-shifted resonances. *Biochemistry* **19**, 3208–3214.

Lehmann, T. E., Luchinat, C. & Piccioli, M. (2002). Redox-related chemical shift perturbations on backbone nuclei of high-potential iron sulfur proteins. *Inorganic Chemistry* **41**, 1679–1683.

Lehnert, N., George, S. D. & Solomon, E. I. (2001). Recent advances in bioinorganic spectroscopy. *Current Opinion in Chemical Biology* **5**, 176–187.

Lemaster, D. (1990). Deuterium labeling in NMR structural analysis of larger proteins. *Quarterly Reviews of Biophysics* **23**, 133–174.

Lemaster, D. M. (1994). Isotope Labeling in solution protein assignment and structural analysis. *Progress in Nuclear Magnetic Resonance Spectroscopy* **26**, 371–419.

Lewin, A. C., Hill, J. P., Boetzel, R., Georgiou, T., James, R., Kleanthous, C. & Moore, G. R. (2002). Site-specific labeling of proteins with cyclen-bound transition metal ions. *Inorganica Chimica Acta* **331**, 123–130.

Linder, M. C. (1991). *Biochemistry of Copper*. New York: Plenum Press.

Ma, C. & Opella, S. J. (2000). Lanthanide ions bind specifically to an added 'EF-hand' and orient a membrane protein in micelles for solution NMR spectroscopy. *Journal of Magnetic Resonance* **146**, 381–384.

Ma, L., Jørgensen, A. M. M., Sorensen, G. O., Ulstrup, J. & Led, J. J. (2000). Elucidation of the paramagnetic R1 relaxation of heteronuclei and protons in Cu(II) plastocyanin from *Anabaena variabilis*. *Journal of the American Chemical Society* **122**, 9473–9485.

Machonkin, T. E., Westler, W. M. & Markley, J. L. (2002). ^{13}C-^{13}C 2D NMR: a novel strategy for the study of paramagnetic proteins with slow electronic relaxation times. *Journal of the American Chemical Society* **124**, 3204–3205.

Machonkin, T. E., Westler, W. M. & Markley, J. L. (2004). Strategy for the study of paramagnetic proteins with slow electronic relaxation rates by NMR spectroscopy application to oxidized human [2Fe-2S]

https://doi.org/10.1017/S0033583506004161 Published online by Cambridge University Press

ferredoxin. *Journal of the American Chemical Society* **126**, 5413–5426.

Madhu, P. K., Mandal, P. K. & Muller, N. (2002). Cross-correlation effects involving Curie spin relaxation in methyl groups. *Journal of Magnetic Resonance* **155**, 29–38.

Malmodin, D., Papavoine, C. H. & Billeter, M. (2003). Fully automated sequence/specific resonance assignment of hetero/nuclear protein spectra. *Journal of Biomolecular NMR* **27**, 69–79.

Mandal, P. K., Grandori, R., Hohenthanner, K. & Muller, N. (2001). Geometry dependent two-dimensional heteronuclear multiplet effects in paramagnetic proteins. *Journal of Biomolecular NMR* **20**, 31–37.

Mandal, P. K., Madhu, P. K. & Muller, N. (2000). Nuclear magnetic relaxation of methyl protons in a paramagnetic protein: cross correlation effects. *Chemical Physics Letters* **320**, 269–276.

McConnell, H. M. (1956). Indirect hyperfine interactions in paramagnetic resonance spectra of aromatic free radicals. *Journal of Chemical Physics* **24**, 764–766.

McConnell, H. M. & Chesnut, D. B. (1958). Theory of isotropic hyperfine interactions in π-electron radicals. *Journal of Chemical Physics* **28**, 107–117.

Mcconnell, H. M. & Robertson, R. E. (1958). Isotropic nuclear resonance shifts. *Journal of Chemical Physics* **29**, 1361–1365.

Meiler, J., Prompers, J. J., Peti, W., Griesinger, C. & Bruschweiler, R. (2001). Model-free approach to the dynamic interpretation of residual dipolar couplings in globular proteins. *Journal of the American Chemical Society* **123**, 6098–6107.

Moura, I., Teixeira, M., Legall, J. & Moura, J. J. G. (1991). Spectroscopic studies of cobalt and nickel substituted rubredoxin and desulforedoxin. *Journal of Inorganic Biochemistry* **44**, 127–139.

Mullinger, R. N., Cammack, R., Rao, K. K., Hall, D. O., Dickson, D. P. E., Johnson, C. E., Rush, J. D. & Simonopulos, A. (1975). Physicochemical characterization of the four-iron, four-sulphide ferredoxin from *Bacillus stearothermophilus*. *Biochemical Journal* **151**, 75–83.

Murthy, N. N., Karlin, K. D., Bertini, I. & Luchinat, C. (1997). NMR and electronic relaxation in paramagnetic Dicopper(II) compounds. *Journal of the American Chemical Society* **119**, 2156–2162.

Nersissian, A. M. & Shipp, E. (2002). Blue-copper binding domain. *Advances in Protein Chemistry* **60**, 271–340.

Oh, B.-H. & Markley, J. L. (1990). Multinuclear magnetic resonance studies of the 2Fe-2S* ferredoxin from Anabaena species strain PCC 7210. 3. Detection and characterization of hyperfine-shifted nitrogen-15 and hydrogen-1 resonances of the oxidized form. *Biochemistry* **29**, 4012–4017.

Ösapay, K. & Case, D. A. (1991). A new analysis of proton chemical shifts in proteins. *Journal of the American Chemical Society* **113**, 9436–9444.

Ottiger, M., Delaglio, F. & Bax, A. (1998). Measurement of J and dipolar couplings from simplified two-dimensional NMR spectra. *Journal of Magnetic Resonance* **131**, 373–378.

Palmer III, A. G., Skelton, N. J., Chazin, W. J., Wright, P. E. & Rance, M. (1992). Suppression of the effects of cross-correlation between dipolar and anisotropic chemical shift relaxation mechanisms in the measurements of spin-spin relaxation rates. *Molecular Physics* **75**, 699–711.

Pellecchia, M., Pang, Y., Wang, L., Kurochkin, A. V., Kumar, A. & Zuiderweg, E. R. P. (1999). Quantitative measurement of cross-correlations between ^{15}N and ^{13}CO chemical shift anisotropy relaxation mechanisms by multiple quantum NMR. *Journal of the American Chemical Society* **121**, 9165–9170.

Pena, M. M. O., Lee, J. & Thiele, D. J. (1999). A delicate balance: homeostatic control of copper uptake and distribution. *Journal of Nutrition* **129**, 1251–1260.

Pervushin, K. (2000). Impact of transverse relaxation optimized spectroscopy (TROSY) on NMR as a technique in structural biology. *Quarterly Reviews of Biophysics* **33**, 161–197.

Pervushin, K. & Eletsky, A. (2003). A new strategy for backbone resonance assignment in large proteins using a MQ-HACACO experiment. *Journal of Biomolecular NMR* **25**, 147–152.

Pervushin, K., Riek, R., Wider, G. & Wüthrich, K. (1997). Attenuated T_2 relaxation by mutual cancellation of dipole-dipole coupling and chemical shift anisotropy indicates an avenue to NMR structures of very large biological macromolecules in solution. *Proceedings of the National Academy of Sciences USA* **94**, 12366–12371.

Piccioli, M., Luchinat, C., Mizoguchi, T. J., Ramirez, B. E., Gray, H. B. & Richards, J. H. (1995). Paramagnetic NMR spectroscopy and coordination structure of cobalt(II) Cys112Asp azurin. *Inorganic Chemistry* **34**, 737–742.

Pintacuda, G., Hohenthanner, K., Otting, G. & Muller, N. (2003). Angular dependence of dipole-dipole-Curie-spin cross-correlation effects in high-spin and low-spin paramagnetic myoglobin. *Journal of Biomolecular NMR* **27**, 115–132.

Pintacuda, G., Keniry, M. A., Huber, T., Park, A. Y., Dixon, N. E. & Otting, G. (2004). Fast structure/based assignment of ^{15}N HSQC spectra of selectively ^{15N} labeled paramagnetic proteins. *Journal of the American Chemical Society* **126**, 2963–2970.

Poe, M., Phillips, W. D., Mcdonald, C. C. & Lovenberg, W. (1970). Proton magnetic resonance study of ferredoxin from *Clostridium pasteurianum*. *Proceedings of the National Academy of Sciences USA* 65, 797–804.

Prestegard, J. H., Bougault, C. M. & Kishore, A. I. (2004). Residual dipolar couplings in structure determination of biomolecules. *Chemical Reviews* **104**, 3519–3540.

https://doi.org/10.1017/S0033583506004161 Published online by Cambridge University Press

Prestegard, J. H., Mayer, K. L., Valafar, H. & Benison, G. C. (2005). Determination of protein backbone structures from residual dipolar couplings. *Methods in Enzymology* **394**, 175–209.

Prudencio, M., Rohovec, J., Peters, J. A., Tocheva, E., Boulanger, M. J., Murphy, M. E., Hupkes, H. J., Koster, W., Impagliazzo, A. & Ubbink, M. (2004). A caged lanthanide complex as a paramagnetic shift agent for protein NMR. *Chemistry – A European Journal* **5**, 3252–3260.

Ramos, A. & Varani, G. (1998). A new method to detect long-range protein-RNA contacts: NMR detection of electron-proton relaxation induced by nitroxide spin-labeled RNA. *Journal of the American Chemical Society* **120**, 10992–10993.

Reuben, J. (1973). On the origin of chemical shifts in lanthanide complexes and some implications thereof. *Journal of Magnetic Resonance* **11**, 103–104.

Ried, A., Gronwald, W., Trenner, J. M., Brunner, K., Neidig, K. P. & Kalbitzer, H. R. (2004). Improved simulation of NOESY spectra by RELAX-JT2 including effects of J-coupling, transverse relaxation and chemical shift anisotropy. *Journal of Biomolecular NMR* **30**, 121–131.

Salgado, J., Warmerdam, G., Bubacco, L. & Canters, G. W. (1998). Understanding the electronic properties of the CuA site from the soluble domain of cytochrome c oxidase through paramagnetic ^{1}H NMR. *Biochemistry* **37**, 7378–7389.

Sattler, M., Schleucher, J. & Griesinger, C. (1999). Heteronuclear multidimensional NMR experiments for the structure determination of proteins in solution employing pulsed field gradients. *Progress in Nuclear Magnetic Resonance Spectroscopy* **34**, 93–158.

Schubert, M., Labudde, D., Leitner, D., Oschkinat, H. & Schmieder, P. (2005). A modified strategy for sequence specific assignment of protein NMR spectra based on amino acid type selective experiments. *Journal of Biomolecular NMR* **31**, 115–128.

Schwieters, C. D., Kuszewski, J., Tjandra, N. & Clore, G. M. (2003). The Xplor-NIH NMR molecular structure determination package. *Journal of Magnetic Resonance* **160**, 65–73.

Silver, S. (1996). Bacterial resistances to toxic metal ions – a review. *Gene* **179**, 9–19.

Slupsky, C. M., Boyko, R. F., Booth, V. K. & Sykes, B. D. (2003). Smartnotebook: a semi-automated approach to protein sequential NMR resonance assignments. *Journal of Biomolecular NMR* **27**, 313–321.

Solomon, I. (1955). Relaxation processes in a system of two spins. *Physical Review* **99**, 559–565.

Sørensen, M. D., Meissner, A. & Sørensen, O. W. (1997). Spin-state-selective coherence transfer via intermediate states of two-spin coherence in IS spin systems: application to E.COSY-type measurement of J coupling constants. *Journal of Biomolecular NMR* **10**, 181–186.

Stevens, K. W. H. (1976). Exchange interactions in magnetic insulators. *Physics Reports* **24c**, 1–75.

Stone, E. W. & Maki, A. H. (1962). Hindered internal rotation and ESR spectroscopy. *Journal of Chemical Physics* **37**, 1326–1333.

Sykes, B. D. & Lee, L. (1983). Use of lanthanide-induced nuclear magnetic resonance shifts for determination of protein structure in solution: EF calcium binding site of carp parvalbumin. *Biochemistry* **22**, 4366–4373.

Szupnar, J. (2004). Metallomics: a new frontier in analytical chemistry. *Analytical and Bioanalytical Chemistry* **378**, 54–56.

Tessari, M., Vis, H., Boelens, R., Kaptein, R. & Vuister, G. W. (1997). Quantitative measurement of relaxation interference effects between $^{1}H_{N}{}^{1}$ CSA and ^{1}H-^{15}N dipolar interaction: cross correlation with secondary structure. *Journal of the American Chemical Society* **119**, 8985–8990.

Tjandra, N. & Bax, A. (1997). Direct measurement of distances and angles in biomolecules by NMR in a dilute liquid crystalline medium. *Science* **278**, 1111–1114.

Tjandra, N., Omichinski, J. G., Gronenborn, A. M., Clore, G. M. & Bax, A. (1997). Use of dipolar ^{1}H-^{15}N and ^{1}H-^{13}C couplings in the structure determination of magnetically oriented macromolecules in solution. *Nature Structural Biology* **4**, 732–738.

Tjandra, N., Szabo, A. & Bax, A. (1996). Protein backbone dynamics and N-15 chemical shift anisotropy from quantitative measurement of relaxation interference effects. *Journal of the American Chemical Society* **118**, 6886–6891.

Tolman, J. R., Flanagan, J. M., Kennedy, M. A. & Prestegard, J. H. (1995). Nuclear magnetic dipole interactions in field-oriented proteins: information for structure determination in solution. *Proceedings of the National Academy of Sciences USA* **92**, 9279–9283.

Tugarinov, V., Choy, W. Y., Orekhov, V. Y. & Kay, L. E. (2005). Solution NMR-derived global fold of a monomeric 82-kDa enzyme. *Proceedings of the National Academy of Sciences USA* **102**, 622–627.

Tugarinov, V., Hwang, P. M. & Kay, L. E. (2004). Nuclear Magnetic Resonance spectroscopy of high/molecular/weight proteins. *Annual Review of Biochemistry* **73**, 107–146.

Turano, P., Battaini, G. & Casella, L. (2003). Validation of paramagnetic cross correlation rates for solution structure determination of high spin iron(III) heme proteins. *Chemical Physics Letters* **373**, 460–463.

Turner, D. L., Brennan, L., Chamberlin, S. G., Louro, R. O. & Xavier, A. V. (1998). Determination of solution structures of paramagnetic proteins by NMR. *European Biophysics Journal* **27**, 367–375.

https://doi.org/10.1017/S0033583506004161 Published online by Cambridge University Press

VALENTINE, J. S., DOUCETTE, P. A. & POTTER, S. Z. (2005). Copper-zinc superoxide dismutase and amyotrophic lateral sclerosis. *Annual Review of Biochemistry* **74**, 563–593.

VATHYAM, S., BYRD, R. A. & MILLER, A. F. (2000). Mapping the effects of metal ion reduction and substrate analog binding to Fe-superoxide dismutase by NMR spectroscopy. *Magnetic Resonance in Chemistry* **38**, 536–542.

VILA, A. J. & FERNÁNDEZ, C. O. (2001). Copper in electron-transfer proteins. In *Handbook on Metalloproteins* (eds. I. Bertini, A. Sigel & H. Sigel), pp. 813–880. New York: Marcel Dekker.

VOGEL, H. J., DRAKENBERG, T., FORSÉN, S., O'NEIL, J. D. & HOFMANN, T. (1985). Structural differences in the two calcium binding sites of the porcine intestinal calcium binding protein: a multinuclear NMR study. *Biochemistry* **24**, 3870–3876.

VRANKEN, W. F., BOUCHER, W., STEVENS, T. J., FOGH, R. H., PAJON, A., LLINAS, M, ULRICH, E. L., MARKLEY, J. L., IONIDES, J. & LAUE, E. D. (2005). The CCPN data model for NMR spectroscopy: development of a software pipeline. *Proteins* **59**, 687–696.

WALKER, F. A. (1999). Magnetic spectroscopic (EPR, ESEEM, Mossbauer, MCD and NMR) studies of low-spin ferriheme centers and their corresponding heme proteins. *Coordination Chemistry Reviews* **185–186**, 471–534.

WERBELOW, L. G. (1996). Cross-correlation and interference terms. In *Encyclopedia of Nuclear Magnetic Resonance* (eds. D. M. Grant & R. K. Harris), pp. 4072–4079. Chichester: Wiley.

WILKENS, S. J., XIA, B., VOLKMAN, B. F., WEINHOLD, F., MARKLEY, J. L. & WESTLER, W. M. (1998a). Inadequacies of the point-dipole approximation for describing electron-nuclear interactions in paramagnetic proteins: hybrid density functional calculations and the analysis of NMR relaxation of high spin iron(III) rubredoxin. *Journal of Physical Chemistry* (*B*) **102**, 8300–8305.

WILKENS, S. J., XIA, B., WEINHOLD, F., MARKLEY, J. L. & WESTLER, W. M. (1998b). NMR Investigations of Clostridium pasteurianum Rubredoxin. Origin of hyperfine ^{1}H, ^{2}H, ^{13}C and ^{15}N NM chemical shifts in iron-sulfur proteins as determined by comparison of experimental data with hybrid density functional calculations. *Journal of the American Chemical Society* **120**, 4806–4814.

WIMPERIS, S. & BODENHAUSEN, G. (1987). Relaxation-allowed transfer of coherence in NMR between spins which are not scalar coupled. *Chemical Physics Letters* **140**, 41–45.

WIMPERIS, S. & BODENHAUSEN, G. (1989). Relaxation-allowed cross-peaks in two-dimensional NMR correlation spectroscopy. *Molecular Physics* **66**, 897–919.

WISHART, D. S. & CASE, D. A. (2001). Use of chemical shifts in macromolecular structure determination. *Methods in Enzymology* **338**, 3–34.

WÖHNERT, J., FRANZ, K. J., NITZ, M., IMPERIALI, B. & SCHWALBE, H. (2003). Protein alignment by a coexpressed lanthanide-binding tag for the measurement of residual dipolar couplings. *Journal of the American Chemical Society* **125**, 13338–13339.

XIA, B., WESTLER, W. M., CHENG, H., MEYER, J., MOULIS, J.-M. & MARKLEY, J. L. (1995). Detection and classification of hyperfine-shifted ^{1}H, ^{2}H, and ^{15}N resonances from the four cysteines that ligate iron in oxidized and reduced *Clostridium pasteurianum* rubredoxin. *Journal of the American Chemical Society* **117**, 5347–5350.

YANG, D., MOK, Y., MUHANDIRAM, D. R., FORMAN-KAY, J. D. & KAY, L. E. (1999). ^{1}H-^{13}C dipole-dipole cross-correlated spin relaxation as a probe of dynamics in unfolded proteins: application to the DrkN SH3 domain. *Journal of the American Chemical Society* **121**, 3555–3556.

YAO, J., DYSON, H. J. & WRIGHT, P. E. (1997). Chemical shift dispersion and secondary structure prediction in unfolded and partly folded proteins. *FEBS Letters* **419**, 285–289.

ZENG, L., FISCHER, M. W. F. & ZUIDERWEG, E. R. P. (1996). Study of protein dynamics in solution by measurement of $^{13}C^{\alpha}$-^{13}CO NOE adn ^{13}CO longitudinal relaxation. *Journal of Biomolecular NMR* **7**, 157–162.

ZWECKSTETTER, M. & BAX, A. (2001). Single-step determination of protein substructures using dipolar couplings: aid to structural genomics. *Journal of the American Chemical Society* **123**, 9490–9491.

https://doi.org/10.1017/S0033583506004161 Published online by Cambridge University Press